Hailes, R., Oliver, A., Gwyther, J., Whittell, G., & Manners, I. (2016). Polyferrocenylsilanes: synthesis, properties, and applications. *Chemical Society Reviews*, *45*, 5358-5407. https://doi.org/10.1039/c6cs00155f

Polyferrocenylsilanes: Synthesis, Properties, and Applications

Rebekah L. N. Hailes[a], Alex M. Oliver[a], Jessica Gwyther[b], George R. Whittell[b], and Ian Manners*

[a,b] School of Chemistry, University of Bristol, Bristol, BS8 1TS, UK. E-mail: ian.manners@bristol.ac.uk

[a,b] These authors contributed equally

This in-depth review covers progress in the area of polyferrocenylsilanes (PFS), a well-established, readily accessible class of main chain organosilicon metallopolymer consisting of alternating ferrocene and organosilane units. Soluble, high molar mass samples of these materials were first prepared in the early 1990's by ring-opening polymerisation (ROP) of silicon-bridged [1]ferrocenophanes ([1]silaferrocenophanes). Thermal, transition metal-catalysed, and also two living different anionic ROP methodologies have been developed: the latter permit access to controlled polymer architectures such as monodisperse PFS homopolymers and block copolymers. Depending on the substituents, PFS homopolymers can be amorphous or crystalline, and soluble in organic solvents or aqueous media. PFS materials have attracted widespread attention as high refractive index materials, electroactuated redox-active gels, fibres, films, and nanoporous membranes, as precursors to nanostructured magnetic ceramics, and as etch resists to plasmas and other radiation. PFS block copolymers form phase-separated iron-rich, redox-active and preceramic nanodomains in the solid state with applications in nanolithography, nanotemplating, and nanocatalysis. In selective solvents functional micelles with core-shell structures are formed. Block copolymers with a crystallisable PFS core-forming block were the first to be found to undergo "living crystallisation-driven self-assembly" in solution, a controlled method of assembling block

copolymers into 1D or 2D structures that resembles a living covalent polymerisation but on a longer length scale of 10 nm - 10 μm.

1. Introduction

Metals centres plays a crucial role in the functions of biological polymers and many solid state compounds, such as state of the art magnetic materials used in data storage, electrical conductors and superconductors, electrochromics, and catalysts. Metal-containing polymers (metallopolymers), in which the facile processing typical of organic polymers is combined with the worthwhile properties of the metal centre, have therefore been long regarded as a desirable target. However, synthetic access to soluble, well-characterised metallopolymers with a molar mass above the critical entanglement molecular weight has proven to be a significant challenge. Although pioneering studies in the metallopolymer field were initiated shortly after the 2nd World War, examples of well-characterised truly macromolecular materials (with molar masses above 10,000 g mol^{-1}) that exhibit chain entanglement were not reported until in the 1970s. However, only since the mid 1990s has much more rapid progress has been made and metallopolymers now play an increasingly important role in terms of complementing the vast and impressive array of functional organic polymers that are now available.[1]

Polyferrocenylsilanes (**PFS**s) represent one of the most well-developed classes of metallopolymer and possess a main chain consisting of alternating ferrocene and organosilane units. Poorly characterised examples were first described in patents in the 1960s as discoloured, very low molecular weight materials formed in step-growth polycondensation reactions.[2, 3] The use of ring-opening polymerisation (ROP) of strained silicon-bridged [1]ferrocenophane precursors was first described in 1992 and represents a chain-growth route.[4] The ROP method affords amber, high molar mass, soluble **PFS** materials that have been well-characterised by a wide range of techniques (Scheme 1). The initial ROP approach

involved thermal treatment of the monomer (*ca.* 130 – 150°C) but the synthetic toolbox has rapidly expanded with the development of alternative, more convenient ambient temperature routes and also "living" polymerisation approaches. This has permitted molar mass control, access to materials with narrow molecular weight distributions and desired end-group functionalisation, and also the formation of **PFS** block copolymers and other controlled architectures. **PFS** materials are readily processed from solution or the melt (see Figure 1) and studies of their properties and applications by numerous workers over the past 25 years have created a field that continues to flourish.[5, 6]

Developments concerning **PFS** homopolymers and/or block copolymers and their properties and applications have been previously reviewed.[4-7] This article, while aiming to be comprehensive, has a particular focus on more recent developments over the past decade although key work from earlier is also discussed.

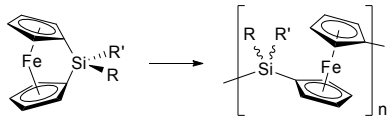

Scheme 1. Synthesis of **PFS**s by the ROP of Silicon-Bridged [1]ferrocenophanes

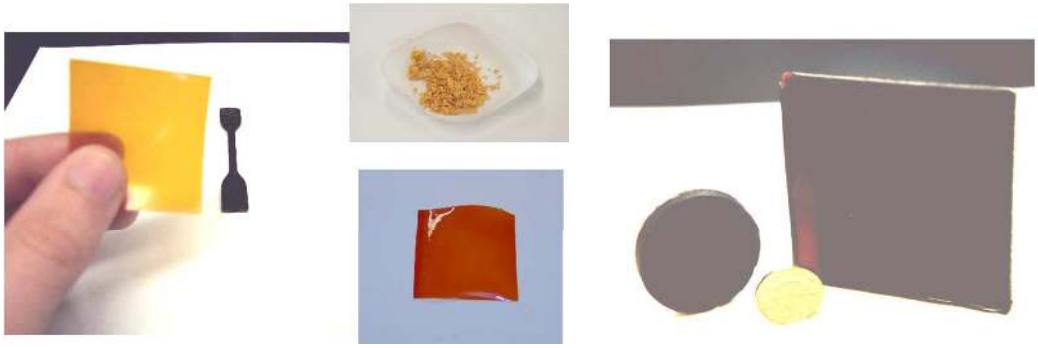

Figure 1. **PFS**s isolated as a powder and after fabrication into films and shapes by solution- of melt-processing.

2. Synthetic Routes to Polyferrocenylsilane Homopolymers

2.1 Monomer Synthesis

Silicon-bridged [1]ferrocenophanes were first prepared in the mid 1970s by Osborne *et al.*,[8] and are now readily available on a significant scale. In solution, each of the cyclopentadienyl (Cp) rings of ferrocene can be lithiated by a strong Li-containing base such as *n*-butyllithium, catalysed by *N*,*N*,*N*′,*N*′-tetramethylethylenediamine (TMEDA).[9] The orange crystalline solid isolated after work up has been shown to have the bulk formula of $(\eta^5\text{-}C_5H_4Li)_2Fe\cdot$TMEDA although single crystal X-ray analysis has shown that other compositions are possible.[10, 11] Reactions between the dilithioferrocene-TMEDA complex and dichloroorganosilanes give a wide range of sila[1]ferrocenophanes with symmetrically and unsymmetrically substituted silicon atoms bearing alkyl or aryl groups (Scheme 2[A]).[12-14] Alternatively, chlorine has been introduced as a substituent through the reaction of $Fe(\eta^5\text{-}C_5H_4Li)_2\cdot$TMEDA with $SiCl_4$ or $RSiCl_3$, which, *via* subsequent nucleophilic substitution reactions at the $SiCl_2$- or SiClR-bridge, provides a facile route to [1]ferrocenophanes with alkoxy, aryloxy, and amino substituents at silicon.[15] Hypercoordinate silicon-bridged [1]ferrocenophanes can also be synthesised from chlorosila[1]ferrocenophanes $Fe(\eta^5\text{-}C_5H_4)_2SiRR'$ (R = R' = Cl or R = Me, R' = Cl) and $Li[2\text{-}C_6H_4CH_2NMe_2]$ or $Fe(\eta^5\text{-}C_5H_4)_2SiCl(CH_2Cl)$ and N-methyl-N-(trimethylsilyl)acetamide.[16, 17] These pentacoordinate species show a pronounced Si-N or Si-O interaction with a pseudo trigonal bipyramidal geometry at the bridging silicon atom in the solid state.[17, 18] In addition, spirocyclic sila[1]ferrocenophanes can be prepared in a similar manner to that already described: for example the reaction of $Fe(\eta^5\text{-}C_5H_4Li)_2\cdot$TMEDA with $Cl_2Si(CH_2)_3$ gives silacyclobutyl[1]ferrocenophane (Scheme 2[B]).[19] These species are of

importance in the preparation of **PFS** materials as they function as crosslinkers during polymerisation reactions.

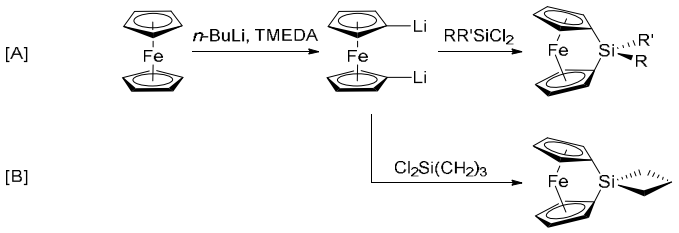

Scheme 2. Synthesis of sila[1]ferrocenophanes from ferrocene.

The introduction of an *ansa*-bridge can result in a loss of the coplanar cyclopentadienyl ring arrangement of ferrocene. The angle, α, measured between the two tilted cyclopentadienyl rings relative to when they are parallel (α = 0°), can be taken as an indication of the strain present. Typical values of α for sila[1]ferrocenophanes lie between 16 - 21°.[12, 20] For example, the cyclopentadienyl rings in dimethylsila[1]ferrocenophane are tilted by 20.8(5)° with respect to one another, and the corresponding strain energy for the complex was measured to be 80 kJ mol^{-1}.[21] Increasing methylation of the Cp rings leads to a decreased ring tilt, increased angles between the Cp ring planes and the exocyclic Cp–Si bonds (β), and decreased Fe–Si distances: the permethylated analogue of dimethylsila[1]ferrocenophane analogue has an α angle of 16.1(3)°,[22] due to the greater energetic penalty in deforming the octamethylferrocenediyl unit the potential energy of the ferrocenediyl unit is increased compared to the substituted case.[23] Other angles that are used to describe the structure of [1]metallocenophanes include: δ, the $Cp_{centroid}$–M–$Cp'_{centroid}$ angle; and θ, the C_{ipso}–E–C'_{ipso} angle (Figure 2).

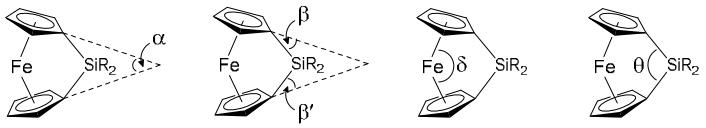

Figure 2. Geometric parameters used to describe the structure of [1]ferrocenophanes.

In addition to loss of planarity, another consequence of the *ansa* bridge in [1]ferrocenophanes is that the iron centre lies in closer proximity to the Cp ipso-carbons than to the two carbons that lie on the opposite side of the ring. Thus, the C–C bond opposite the ipso-carbons is shortened. Furthermore, the angle θ is far lower than is expected compared to that of ideal hybridisation at the bridging atom, E.[23]

Silicon-bridge [1]ferrocenophanes are isolated as red, crystalline solids or liquids. As a result of their ring strain, they can readily undergo ring-opening polymerisation (ROP) reactions to give polyferrocenylsilanes (**PFS**s). It is noteworthy that even [1]silaferrocenophanes with highly sterically-demanding substituents at silicon such as $Si(SiMe_3)_3$ still undergo ROP.[14] Reported synthetic methods to prepare high molecular weight PFSs involve: thermal, transition metal-catalysed, γ-irradiation-induced, cationic, and living anionic and photocontrolled living anionic ROP, and these methods are now discussed.

2.2 ROP Routes to PFS Homopolymers

2.2.1 Thermal Ring-Opening Polymerisation

A thermal method of synthesising high-molecular weight **PFS**s from silicon-bridged [1]ferrocenophanes was first reported in 1992,[21] with the release of ring-strain (60 - 80 kJ mol^{-1}) driving the reaction. Due to its relatively high functional group tolerance, a wide range

of strained ferrocenophanes have been used to access alkyl, alkoxy, aryl, aryloxy, amino, and chloro functionalised **PFS**s (Scheme 3) *via* this route. [4, 7, 14, 24, 25] Interestingly, a cyclic dimer in addition to high molecular weight polymer was isolated from dichlorosila[1]ferrocenophane when attempting thermal ROP.[26, 27] The thermal ROP reactions can be performed in either high boiling point solvents or the melt, and although high molecular weight polymers are formed, there is no control over the molecular weight and the molecular weight distributions are broad (PDI > 1.5).

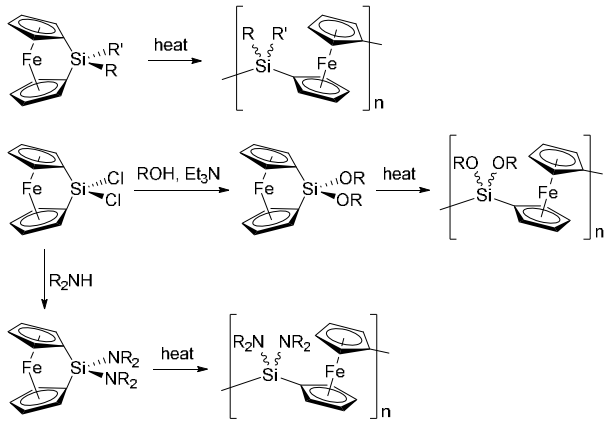

Scheme 3. Thermal ring-opening polymerisation of sila[1]ferrocenophanes to give **PFS**s.

Thermal ROP of silicon-bridged [1]ferrocenophanes has been shown to proceed *via* cleavage of the Cp–Si bond; in the case of Cp rings with the a different degree of methylation, nonselective cleavage of the Si–Cp bonds occurs.[28] Increasing the degree of methylation of the Cp rings resulted in increasing onset temperatures for the polymerisation but did not appreciably affect the enthalpy of polymerisation, ΔH_p, as measured by DSC.[29] Although attempts have been made to deduce the mechanism of thermal polymerisation, neither this nor the nature of the propagating species is known with certainty. A carbanionic mechanism appears unlikely however, because the ROP of monomers bearing Si–Cl substituents results

in high molecular weight polymers.[5] Radicals also do not appear to be involved, and the most likely mechanism appears to be a nucleophilically-assisted process.[30, 31]

2.2.2 Catalytic ROP

In 1995 it was discovered that a variety of late transition metal complexes catalysed the ROP of sila[1]ferrocenophanes, to yield high molecular weight **PFS**s both in solution and at room temperature.[32, 33] Complexes used as precatalysts feature platinum (Pt^0, Pt^{II}),[34] for example Karstedt's catalyst (platinum divinyltetramethyldisiloxane complex),[35] palladium (Pd^0, Pd^{II}), and rhodium (Rh^I).[36] Catalytic amounts of $[Rh(1,5\text{-cod})_2]A$ (cod = 1,5-cyclooctadiene, A = $[OTf]^-$, $[PF_6]^-$) initiated the ROP of [1]silaferrocenophanes with quantitative conversion within 2 minutes. In the case of Pt, it has been reported that heterogeneous metal colloids form as the active catalysts, and postulated that oxidative-addition and reductive-elimination reactions at the metal surface resulted in formation of the polymer.[37] For silicon-bridged ferrocenophanes in which one Cp ring is methylated, Pt^{II}-catalysed ROP proceeds solely by selective cleavage of the Si–Cp^H ($Cp^H = C_5H_4$)bond to yield a regioregular, crystalline **PFS**, unlike thermal ROP which affords a regioirregular amorphous material.[38]

Transition metal-catalysed ROP is advantageous in that it does not require high monomer and solvent purity unlike anionic ROP (Section 2.2.4.1), or the high temperatures used in thermal ROP.[39] The method therefore allows the use of many monomers that would otherwise decompose under more aggressive reaction conditions. However, in contrast to **PFS** prepared by anionic ROP, polydispersities remain typically in excess of 1.4. When transition metal catalysed ROP of sila[1]ferrocenophanes is carried out in the presence of a termination agent

containing an Si–H bond, the molecular weight of **PFS** can be controlled by variation of the initial ratio of the monomer to the silane. The mechanism is believed to involve competition between the Si–H and strained Si–C bonds for oxidative-addition at the metal centre.[37, 40] Use of such materials with Si–H groups has allowed the preparation of regioregular, comb-shaped graft copolymers, star-shaped polymers, and block copolymer architectures.[38] Chlorosilanes such as ClMePhSiH are more effective terminating agents than Et_3SiH due to steric considerations, and also introduce a Si–Cl end functionality on telechelic polyferrocenylsilanes. These can then be used in a variety of post-polymerisation reactions to yield block copolymers.[40] Alternatively if **PFS** is synthesised from a monomer containing chlorine at silicon, a wide range of substitution reactions on the polymer backbone can be performed,[27, 41] (Scheme 4). However, broad molecular weight distributions result with all terminating agents.

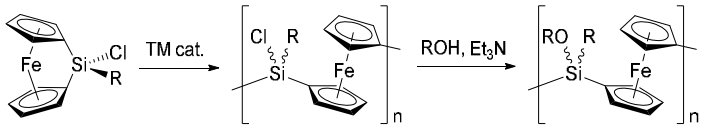

Scheme 4. Transition metal catalysed ROP of a strained sila[1]ferrocenophane, and subsequent main chain functionalisation.

2.2.3 ROP Induced by γ-Irradiation and Cationic Initiators

PFDMS (**PFDMS**: Poly(ferrocenyldimethylsilane)) can be synthesised from the crystalline monomer in the solid state, with the use of γ-irradiation at elevated temperature (60 °C). It was reported that as the dose of initiating radiation rose, the weight average molar mass increased, indicating a greater degree of polymerisation.[42] Higher radiation rates are expected to yield more reaction centres, which typically, and contrary to that observed, would be

expected to afford lower molar mass polymers. Solid state polymerisation of crystalline [Fe(η^5-C_5H_4)$_2$SiMePh] yielded stereoregular **PFMPS** (**PFMPS**: poly(ferrocenylmethylphenylsilane)), in a topotactic process based on NMR analysis.[43] Thus, the tacticity of the polymer was inherited from the arrangement of substituents in the monomer of the crystal were inherited as the tacticity of the polymer. However, as sources of γ-radiation are inconvenient to access, this is not a commonly used method.

Cationic ROP of a hypercoordinate [1]silaferrocenophane has been reported in the presence of a silyl cation as an initiator.[17] The resulting PFS appears to retain the pentacoordinate Si centres but the molar mass was low (M_w = *ca*. 9000 Da).

2.2.4 Living Anionic ROP Routes to Homopolymers

2.2.4.1 Living Anionic ROP Involving Cleavage of the Cp-Si Bond

Living anionic ROP of sila[1]ferrocenophanes was developed in the mid 1990s,[44, 45] and allows access to **PFS**s with molecular weight control and predetermined chain end function, provided that low levels of impurity are present.[45, 46] For this reason, high purity monomer is required and this is generally achieved by multiple recrystallisation and sublimation steps to remove ring-opened or cyclic and linear oligomeric contaminants. Induced by nucleophilic attack of an anionic initiator at the bridging silicon atom, ROP proceeds *via* Si–Cp bond cleavage generating a basic iron-coordinated cyclopentadienyl anion. Fast initiation is followed by rapid chain propagation, which occurs with minimal chain transfer or termination, and therefore yields polymers of controlled molecular weight (Figure 3) and with narrow molecular weight distributions (PDI < 1.2). Thus, this process is an example of a

living polymerisation which, when discovered, represented the first of its kind to afford polymers with transition metal atoms in the main chain. Since the initial report, the living anionic ROP of sila[1]ferrocenophanes has been extended to other monomers with both symmetrical (R = R' = Me)[45] and unsymmetrical (R, R' = Me, Et; Me, Ph; Me, iPr)[47-50] substitution at silicon (Scheme 5). Studies on silicon-bridged [1]ferrocenophanes $Fe(\eta^5\text{-}C_5H_4)_2SiRR'$ with bulky substituents have shown that if R = H, R'= $N(SiMe_3)_2$ does not undergo anionic ROP, despite forming a polymer under thermal ROP conditions. It was proposed that this was due to a lack of propagation at the hindered Cp-based sp^2 carbanion, presumably due to steric protection of the silicon centre by the bulky $N(SiMe_3)_2$ substituent.[14] Generally the rate of living anionic ROP decreases as the size of the substituents on silicon increases.[50]

Subsequent end functionalisation can occur at the lithiated site on the polymer using a variety of reagents to modify the polymer properties or yield block and graft copolymers.[51,52] In addition, sequential polymerisation of different monomers can occur to produce a range of block copolymers.[53] If post-polymerisation, 4-[(trimethylsilyl)ethynyl]-benzaldehyde is used to trap the living chain, a terminal alkyne is generated. Diblock copolymers can then be constructed *via* a Cu(I)-catalysed alkyne/azide cycloaddition with azide end-capped polymers.[54] Anionic initiators used comprise alkyl, aryl, and ferrocenyl lithiates, and can include other polymers prepared by anionic polymerisation.[45] *tert*-Butyldimethylsilyloxy-1-propyllithium has also been used as an initiator for the polymerisation of dimethylsila[1]ferrocenophane, as this provides a convenient route to hydroxyl-terminated **PFS**s.[55] Unfortunately, monomers with base sensitive side groups are incompatible with this method of polymerisation.

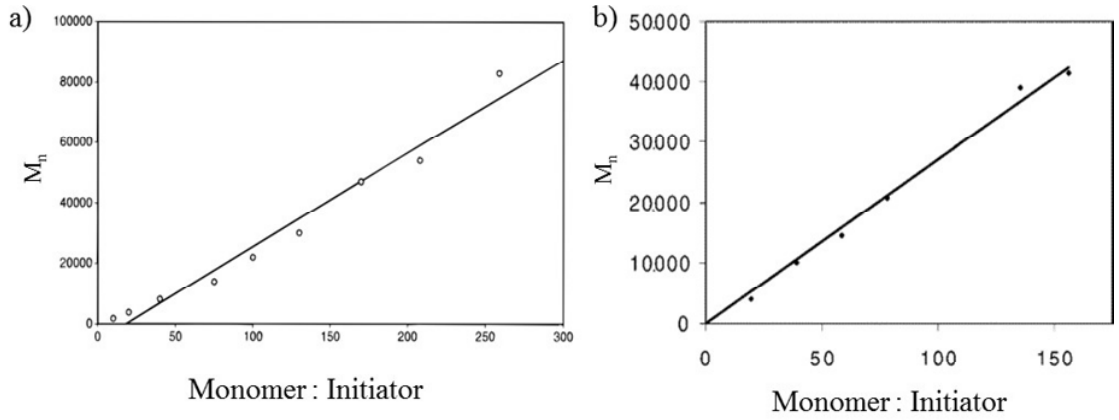

Figure 3. A plot of the mole ratio of monomer : initiator versus M_n for a) the *n*-BuLi initiated synthesis of **PFDMS** (R = *n*-Bu, E = H, Scheme 5); b) the *n*-BuLi initiated synthesis of **PFEMS** (**PFEMS**: poly(ferrocenylethylmethylsilane)) (R = *n*-Bu, E = H). Reproduced with permission from references 45 and 48.

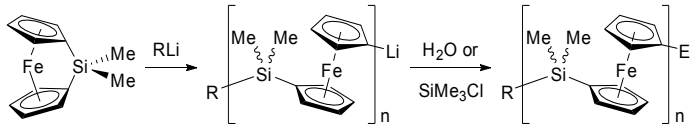

Scheme 5. Living anionic ring opening polymerisation of sila[1]ferrocenophanes. R = Fc, Ph, or *n*-Bu; E = H or $SiMe_3$.

2.2.4.2 Living "Photocontrolled" Anionic ROP Involving Cp-Fe Bond Cleavage

An alternative living anionic polymerisation method was reported in the mid 2000s, involving the photoactivation of sila[1]ferrocenophanes.[56, 57] In this case, ROP proceeds with irradiation of the monomer by the Pyrex-filtered emission from a mercury lamp ($\lambda > 310$ nm) in a donor solvent, such as THF. The subsequent, presumably solvated, ring-slipped structure reacts with the anionic initiator, sodium cyclopentadienide ($Na[C_5H_5]$).[56] Cleavage of the Fe–η^1-cyclopentadienyl bond in the photoexcited monomer affords a ring-opened species

possessing a free silyl-substituted Cp anion that can propagate *via* attack on another ring-slipped monomer. The living polymer chain can then be capped with, for example, methanol to give **PFS**s (Scheme 6).[58] This method contrasts with the previously reported living anionic ROP, which proceeds in the absence of UV irradiation and uses organolithium initiators to induce Si–Cp(ipso) bond cleavage.[56] Nevertheless, both anionic ROPs generate polymers of controlled molecular weight and with narrow molecular weight distributions. Crucially for "photocontrolled" anionic ROP, the delocalised free cyclopentadienyl initiating and propagating sites are far less basic than the charge localised iron-coordinated alternative that occurs in the classical anionic ROP.[59] This reaction is therefore more tolerant of sensitive functional monomers; for example, it has allowed the preparation of a **PFS** with pendant alkynyl,[60] amino,[61] and fluoroalkyl groups.[59] Also, **PFS** with a pendant ruthenocenyl group was prepared *via* "photocontrolled" anionic ROP to give monodisperse, soluble polymers, where the use of thermal ROP had failed.[62] As this polymerisation can be controlled by switching the light source on and off, sequential addition of different monomers is facile. Diblock copolymers have also been produced by the use of **PS** (**PS**: polystyrene) homopolymers end-capped with a cyclopentadienyl group, and used as macroinitiators for the PROP of sila[1]ferrocenophanes.[63] *t*Bu$_3$terpy (4,4',4''-tri-*tert*-butyl-2,2':6',2''-terpyridine) was evaluated as another initiator, but displayed far less molecular weight control and gave lower polymer yields than Na[C_5H_5].[58] Remarkably, photolysis of a solution containing dimethylsila[1]ferrocenophane, Na[C_5H_5], and *t*Bu$_3$terpy resulted in dissociation of both ferrocenophane Cp rings.

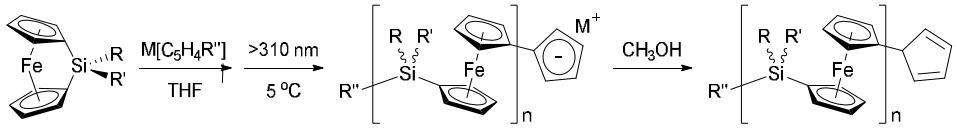

Scheme 6. Photocontrolled living anionic ring opening polymerisation of sila[1]ferrocenophanes.

Irradiation of [Fe(η^5-C_5H_4)$_2$SiMe$_2$] in the presence of 4,4′-dimethyl-2,2′-bipyridine, a substitutionally more labile ligand than Cp, initiated ROP to give a distribution of cyclic **PFS**s and linear oligomers.[64] Temperature and concentration were reported to influence the molecular weight distribution and the ratio of cyclic to linear products, thus enabling the formation of cyclic **PFS**s with molecular weights greater than 100 kDa.[65]

Although the mechanism of photocontrolled anionic ROP has not been completely elucidated, the presence of a sila-bridge in a [1]ferrocenophane causes the cyclopentadienyl rings to tilt, and, presumably as a consequence, weakens the Fe–Cp bond. Metal-ligand charge transfer occurs due to photoirradiation, and is suggested to further weaken this bond and to increase the electrophilicity at iron and, probably, to induce Cp ring-slippage in the presence of a donor solvent (such as THF). These effects all combine to favour polymerisation when an anionic initiator is present. Kinetic studies of the photopolymerisation at various temperatures demonstrated that the reaction was a living process (PDI < 1.1).[57] While the photoactivation of the monomer is independent of temperature, deactivation of the photoexcited system, or the subsequently formed ring-slipped product (M*) to the ground state monomer (M) is favoured at higher temperatures (Scheme 7). As a consequence, at elevated temperatures the rates of initiation and propagation are decreased, and ROP is slower. Moreover, the polymers obtained have a broader molecular weight distribution (PDI = 1.2 – 1.3).[57]

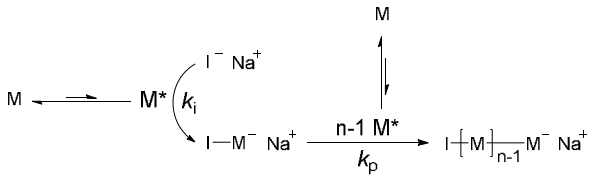

Scheme 7. Upon irradiation some monomers (M) are promoted to a photoexcited state (M*). The photoexcited monomer M* reacts with the initiator (I) with rate constant k_i to form a ring-opened monomer, which undergoes chain propagation (with rate constant k_p) in the presence of more photoexcited monomer.[57] The photoexcited monomer M* is presumed to possess a ring-slipped structure.[66]

2.2.5 Post-polymerisation Functionalisation

Modification of the properties of **PFS** materials is most commonly achieved by varying the substituents on the silicon atom of the organosilyl spacer. This can be performed either on the monomer, as described in Scheme 3, or with post-polymerisation reactions on the **PFS** backbone (Scheme 8). Certain reaction conditions, such as the presence of low pH, should be avoided generally, as **PFS** can be sensitive towards chain cleavage.

PFSs with chlorine substituents at silicon undergo nucleophilic substitution reactions to give a variety of products, including hydrophilic **PFS**s with organic substituents that promote water solubility.[27, 35, 67] The first of these was reported in 2000, through the treatment of poly(ferrocenylchloromethylsilane) with oligo(ethylene glycol) monomethylether or $Me_2NCH_2CH_2OH$.[35] Cationic polyelectrolytes were subsequently prepared *via* quaternisation of the dimethylamino groups in the latter. Further water soluble polyelectrolytes were synthesised from **PFS** (R = Me, R' = C≡CCN$(Me_2SiCH_2)_2$), which itself was readily obtained *via* a substitution reaction from poly(ferrocenylchloromethylsilane).[68] These polyelectrolytes

remained stable in water even after a period of several months. The **PFS**, $[Fe(\eta^5\text{-}C_5H_4)_2SiMe(N(CH_2)_3SiMe_2(CH_2)_2SiMe_2)]_n$ was prepared by the ROP of a ferrocenophane precursor with a cyclic silylamino substituent *via* an unexpected rearrangement/ring expansion process.[68] Alternatively, the water soluble cation, poly(ferrocenyl(3-ammoniumpropyl)methylsilane) was produced by the ROP of $[Fe(\eta^5\text{-}C_5H_4)_2SiCH_3(CH_2)_3Cl]$ and subsequent amination of the chloropropyl moieties using potassium 1,1,3,3-tetramethylsilazide followed by protonation (Scheme 8).[69] Water-soluble **PFS** polyanions and polycations have also been synthesised by reaction of poly(ferrocenyl(3-halopropyl)methylsilanes) (halo = Cl, Br, or I) with a variety of nucleophiles, including alkali metal amides, neutral amines, and ester enolate anions. [69-71]

With a hydrogen or olefinic substituent at silicon, hydrosilation chemistry is possible. Reaction of poly(ferrocenylmethylvinylsilane) with Et_3SiH allowed for facile functionalisation, giving an example of a hexane soluble **PFS** material.[72] Hydrosilylation reactions have also proved useful in attaching mesogenic groups to **PFS**s containing Si–H functionalities, which allow access to thermotropic side chain liquid crystalline (LC) materials.[73]

Thiol–ene click provides a versatile approach to **PFS** functionalisation. The reaction of a range of thiols with vinyl-containing **PFS** scaffolds gave hydrothiolated **PFS**s, which displayed interesting solubility and functionality.[74] As a diverse range of thiols are available, and the thiol-ene reaction is tolerant to most functional groups, this post-polymerisation route is useful for the preparation of **PFS** materials with a range of properties from the same homopolymer precursor.

Highly metallised **PFS**s: $[Fe(\eta^5\text{-}C_5H_4)_2Si(Me)(Co_2(CO)_6C_2Ph)]_n$ (Co-**PFS**), $[Fe(\eta^5\text{-}C_5H_4)_2Si(Me)(Mo_2Cp_2(CO)_4C_2Ph)]_n$ (Mo-**PFS**), and $[Fe(\eta^5\text{-}C_5H_4)_2Si(Me)(Ni_2Cp_2C_2Ph)]_n$ (Ni-**PFS**), were synthesised by the clusterisation of carbon-carbon triple bonds in an acetylide substituted **PFS**.[75, 76] By varying the chain length of the parent acetylide-substituted **PFS** or by changing the extent of clusterisation, the molecular weight and metal content of the **PFS**, respectively, could be controlled.[76] The materials were all air- and moisture-stable and they have been shown to serve as resists for electron-beam and UV photolithography (Section 3.9).

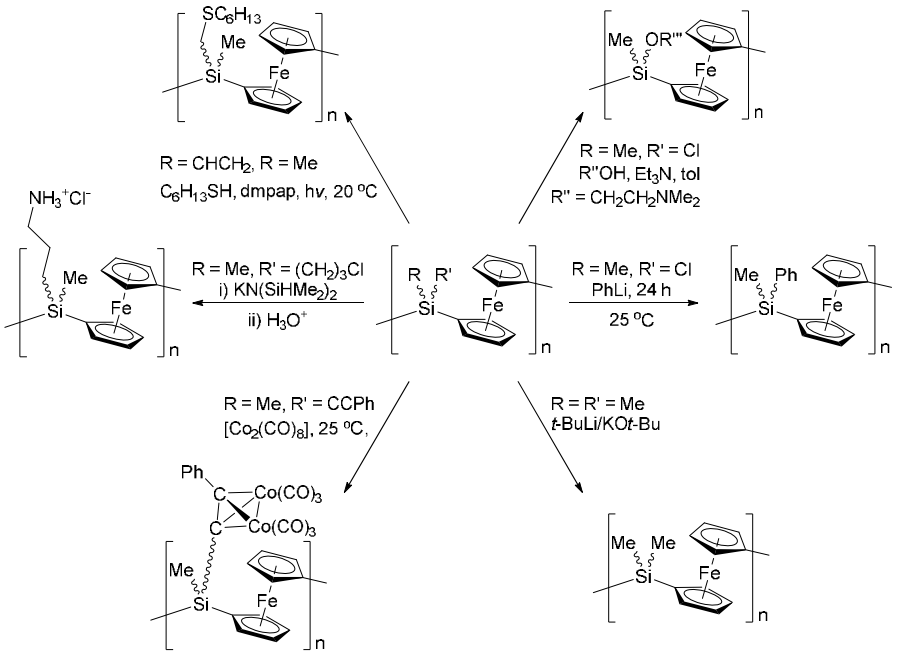

Scheme 8. Examples of post-polymerisation functionalisation methods for polyferrocenylsilanes.

Another distinct route of modification involves using Cp-substituted sila[1]ferrocenophane monomers to undergo ROP, but the syntheses of such species are multi-step and often low yielding.[77] Functional groups directly attached to the cyclopentadienyl rings are appealing as

the redox properties of the iron centres can be directly influenced. In response to the above problems, successful functionalisation of the Cp groups of **PFDMS** was reported using low temperature metalation with *t*-BuLi/KO*t*-Bu in THF, followed by reaction with Me_3SiCl. The degree of substitution varied between 0.59 and 1.82 per ferrocendiyl, the maximum of which was achieved with a mixture of polymer and KO*t*-Bu (8 equivalents), and *t*-BuLi (16.5 equivalents). Notably, lithiation occurred regioselectively on the β-carbon.[78] The substitution of the Cp ring led to a loss of crystallinity, solubility in alkanes, and a large increase in glass transition temperatures.

3. Polyferrocenylsilane Homopolymers: Properties and Applications

3.1 Solution Characterisation

Multiple methods for determining the molecular weights and molecular weight distributions have been used for soluble **PFS**s, the most common of which is gel permeation chromatography (GPC). To characterise the solution behaviour of **PFS** in tetrahydrofuran (THF), **PFDMS**s spanning a molecular weight range of *ca* 10,000-100,000 g mol^{-1}, with narrow polydispersities, were synthesised by anionic polymerisation. The molecular weight was determined by GPC versus monodisperse polystyrene standards, GPC with a triple detection system (refractive index, viscometry, and light-scattering), and static light scattering.[79] Whilst the latter two techniques produced molecular weights that were in good agreement, conventional GPC versus **PS** standards gave a 30% underestimation. In THF, **PFDMS** retains a more compact random coil conformation than for **PS** of the same molecular weight, due to less favourable **PFDMS**-solvent interactions. The Mark–Houwink parameter for high molar mass **PFDMS** in THF at 23 °C, $a = 0.62$ ($k = 2.5 \times 10^{-4}$), is typical of flexible chains in a fairly marginal solvent.[79] Earlier studies of other **PFS**s by low angle laser light scattering in THF revealed that conventional GPC with **PS** standards for column calibration also gave a substantial molar mass underestimation.[80, 81]

The solubility parameter of a polymer (δ) is often estimated by measuring the degree of swelling of a lightly crosslinked polymer network in different solvents. Thus, from the swelling characteristics of a **PFDMS** network containing 4 mol% of a spirocyclic crosslinker, a δ value of 18.7 $MPa^{1/2}$ was established.[82] Maximum swelling of the gel is therefore observed for solvents with δ values of 18.0 to 19.4 $MPa^{1/2}$ (xylenes (18.0), toluene (18.2),

THF (18.6), dichloromethane (18.6), chloroform (19.0), methyl ethyl ketone (19.0), styrene (19.0), chlorobenzene (19.4)).

Small-angle neutron scattering (SANS) in solution has also been employed to calculate the radius of gyration, weight-averaged molecular weight, and polydispersity index of **PFS**s, but in the absence of the column effects present in GPC.[83] Fitting the scattered intensity to a model based on a Schultz–Zimm distribution of isolated chains with excluded volume, yielded molecular weight and size data that was in acceptable agreement with values determined by GPC. However, the assumed shape of the molecular weight distribution had a small influence on the polydispersity index values.

Solution state ^{1}H, ^{13}C, and ^{29}Si NMR spectroscopy is readily applicable for structural characterisation of **PFS**s, due to the presence of these NMR active nuclei in the polymer backbone or side-group structure. For example, NMR analysis has been used to investigate the tacticity of **PFS**s: ethylmethylsila[1]ferrocenophane underwent living anionic ROP to give an atactic **PFS** as determined from the integration of the triad methyl peaks (*mm*, *mr*, and *rr*) in the ^{1}H NMR spectrum.[48] Thermal ROP also appears to give atactic materials and this has been evidenced by ^{29}Si NMR spectroscopy.[27] In addition, post-polymerisation functionalisation can be monitored by NMR spectroscopy. A LC polymer brush with a mesogenic phenyl benzoate group was characterised by ^{1}H and ^{13}C NMR spectroscopy, and compared to the spectra of the poly[6-(4'-butyloxyphenyl 4''-benzoyl)hexyl acrylate] to determine when side chain grafting was complete.[84]

3.2 Morphology in the Solid State: Crystalline and Amorphous Materials

In the case of **PFS**s, their physical properties are largely determined by the substituents on silicon and the Cp rings. **PFS**s symmetrically substituted at silicon with small alkyl groups (Me, Et, *n*-Pr, *n*-Bu, and *n*-Pentyl) are able to crystallise, as evidenced by a variety of analytical methods.[7] The degree of crystallinity has been observed to increase with time, particularly once the selected polymer has been annealed above its T_g. With longer substituents such as di(*n*-hexyl), or unsymmetrical side groups at silicon, however, **PFS**s are usually amorphous. One exception to this is atactic **PFMS** (**PFMS**: poly(ferrocenylmethylsilane)) which has Me and H substituents at silicon and was found to be semicrystalline in nature.[85] Apparently the reduced steric demand of hydrogen compared to methyl still enables the ordered packing of polymer chains even in this unsymmetrically-substituted case, despite the irregular arrangement of substituents along the backbone. The presence of two melting points (87 and 102 °C) for **PFMS** were assigned to reorganisation of the crystals during the heating process.[85] **PFS**s with long flexible substituents at silicon (e.g. $OC_{18}H_{37}$) have been found to undergo side-chain crystallisation.[15]

Generally, for **PFS**s with hydrogen substituents on the Cp rings, T_g values can range from -51 °C with long, flexible substituents at silicon, such as R=R'=OC_6H_{13}, to 99 °C for materials with ferrocenyl and methyl substituents, demonstrating the substantial influence of the side group structure. For a comprehensive illustration, Table 1 contains thermal transition and molecular weight data for **PFS** homopolymers determined by differential scanning calorimetry (DSC) and gel permeation chromatography (GPC), respectively.[6, 50, 59, 67, 70, 74, 77] A significant increase in T_g also occurs when the hydrogens on the cyclopentadienyl ligands are replaced with more sterically demanding methyl groups.[77]

One notable property of these materials is their high thermal stabilities to weight loss; for example, **PFS** with two hydrogen substituents retained 90% of its initial mass when heated to 600 °C.[86] **PFDMS**, is an amber thermoplastic with a glass transition temperature (T_g) of 33 °C, and a melt transition temperature (T_m) between 122-145 °C depending on the thermal history of the polymer.[46] Experimental T_m comprises a range of values as each of the varying sizes of crystallite present melt at minutely different temperatures.[87] O'Driscoll's equation: $T_g = T_{g,\infty} - KM_n^{-2/3}$,[88] describes the relationship between the glass transition temperature at infinite chain length, $T_{g,\infty}$, and T_g which reaches a maximum value when the polymer comprises *ca* 90 repeat units. A detailed study of the crystallisation behaviour of **PFDMS** attributed the slow rate of crystallisation to the low melt enthalpy.[89] Moreover, using the Gibbs-Thomson approach resulted in the prediction of an equilibrium melting temperature of *ca.* 215 °C.[89] This value corresponds to a 100 % perfect crystallite of infinite size, which cannot be obtained experimentally.

A LC polymer brush of **PFS** with poly[6-(4'-butyloxyphenyl-4"-benzoyl)hexyl acrylate] side chains (Figure 4) was synthesised by atom transfer radical polymerisation.[84] It was demonstrated to form a thermotropic nematic phase in the high temperature region and smectic A phase in the low temperature region. When compared to the molecular LC, poly[6-(4'-butyloxyphenyl-4'-benzoyl)hexyl acrylate], the **PFS** brush material exhibited a lower glass transition temperature (46 °C vs. 48 °C) and clearing point (118 °C vs. 125 °C).

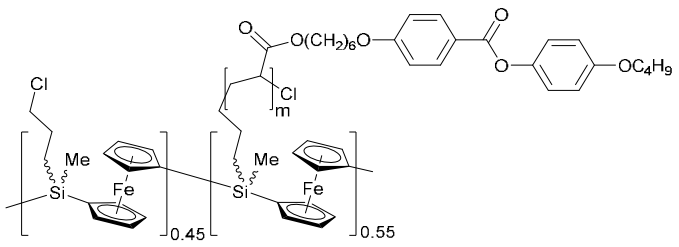

Figure 4. A LC **PFS** with poly[6-(4'-butyloxyphenyl-4"-benzoyl)hexyl acrylate] side chains.

Table 1. Thermal transition and gel permeation chromatography (GPC) molecular weight data **PFS** homopolymers, $Fe(\eta^5\text{-}C_5H_4)_2SiRR'$.

R	R'	$T_g(T_m)$[b]/°C	M_n[a]	PDI[c]	Ref.
H	H	16(165)	[d]	[d]	6
Me	Me	33(122-143)	3.4×10^5	1.5	6
Et	Et	22 (108)	4.8×10^5	1.6	6
Pr^n	Pr^n	24 (98)	8.5×10^5	2.7	6
Bu^n	Bu^n	3 (116, 129)	3.4×10^5	2.6	6
n-C_5H_{11}	*n*-C_5H_{11}	-11 (80-105)	3.0×10^5	1.6	6
n-C_6H_{13}	*n*-C_6H_{13}	-26	7.6×10^5	1.5	6
Me	H	9 (87,102)	4.2×10^5	2.0	6
Me	Et	15	2.9×10^5	1.7	6
Me	$CH_2CH_2CF_3$	59	8.1×10^5	3.3	6
Me	$CH{=}CH_2$	28	7.7×10^5	2.1	6
Me	$CH_2CH{=}CH_2$	7	1.1×10^5	1.2	6
Me	*n*-$C_{18}H_{37}$	1 (16)	5.6×10^5	2.5	6
Me	Ph	90	1.5×10^5	2.0	6
Me	$(\eta^5\text{-}C_5H_4)Fe(\eta^5\text{-}C_5H_5)$	99	7.1×10^5	2.3	6
Me	5-Norbornyl	81	1.1×10^5	1.5	6
OMe	OMe	19	1.5×10^5	1.9	6
OEt	OEt	0	3.8×10^5	2.1	6
OCH_2CF_3	OCH_2CF_3	16	2.2×10^5	1.2	6
OBu	OBu	-43	3.9×10^5	2.1	6
OC_6H_{13}	OC_6H_{13}	-51	0.9×10^5	2.4	6
$O(CH_2)_{11}CH_3$	$O(CH_2)_{11}CH_3$	(-30)	1.9×10^5	2.5	6
$O(CH_2)_{17}CH_3$	$O(CH_2)_{17}CH_3$	(32)	2.3×10^5	2.2	6
OPh	OPh	54	2.3×10^5	2.0	6
$OC_6H_4Bu^t$-*p*	$OC_6H_4Bu^t$-*p*	89	1.9×10^5	1.9	6
OC_6H_4Ph-*p*	OC_6H_4Ph-*p*	97	5.4×10^5	2.4	6
Me	$OCH_2CH{=}CH_2$	8	2.8×10^5	2.1	6
Me	$OCH_2CH_2OCOC{=}CH_2(Me)$	16	3.0×10^5	2.7	6
Me	*i*Pr	60	2.9×10^4	1.3	50
Me	$(CH_2)_3Cl$	38	1.9×10^5	1.6	70
Me	$(CH_2)_3I$	45	1.9×10^5	1.6	70
Me	$(CH_2)_3Br$	41	1.5×10^5	1.9	70
Me	$(CH_2)_2SC_6H_{13}$	-28	1.5×10^4	1.0	74
Me	$(CH_2)_2SC_9H_{19}$	-36	1.7×10^4	1.0	74
Me	$(CH_2)_2SC_{12}H_{25}$	-43	1.9×10^4	1.0	74
Me	$(CH_2)_2SC_{18}H_{37}$	(42)	2.1×10^4	1.0	74
Me	$CH_2CH_2(CF_2)_7CF_3$	16	1.8×10^4	1.0	59
Me	$CH_2CH_2CH_2C_6F_5$	35	1.8×10^4	1.1	59
Me	$CH_2CH_2CF_3$	56	1.5×10^4	1.0	59
Me	$OCH_2CH_2NMe_3COOC_6H_2(O(CH_2)_{12}CH_3)_3$	16 (64)	[e]	[e]	67
Me	$OCH_2CH_2NMe_3COOC_6H_2(O(CH_2)_{14}CH_3)_3$	15 (78)	[e]	[e]	67
Me	$OCH_2CH_2NMe_3COOC_6H_2(O(CH_2)_{16}CH_3)_3$	13 (85)	[e]	[e]	67
Me[f]	Me[f]	73	7.3×10^4	1.9	77
Ph[g]	Ph[g]	212	1.7×10^6	1.4	77

[a] GPC data obtained from the analysis of THF polymer solutions which contained 0.1% $[Bu_4N][Br]$ and molecular weight values are relative to polystyrene standards. Although in

this case GPC provides only molecular weight estimates, absolute determinations of M_w by static light scattering for several polymers have indicated that GPC underestimates the real values by 30%.
[b] DSC data collected at a heating rate of at 10 °C/min.
[c] PDI = M_w/M_n.
[d] Insoluble polymer.
[e] Not reported.
[f] $[Fe(\eta^5\text{-}C_5H_3Me)_2SiMe_2]_n$
[g] $[Fe(\eta^5\text{-}C_5H_3tBu_2)_2SiPh_2]_n$

An understanding of the conformations of **PFS** polymer chains in the solid state is primarily based again on the study of **PFDMS**. Molecular mechanics calculations of the possible conformations of well-defined oligomeric species, both as isolated molecules and in the solid state, have been compared to single crystal X-ray diffraction data.[90-92] The diffraction pattern of the pentamer was found to display a broad peak with a similar *d*-spacing to that of high molecular weight **PFDMS**, thus providing evidence of a close relationship between the two structures. With reference to the pentamer, a single-crystal X-ray diffraction study showed parallel packing of *trans*-planar zig-zag polymer chains, with the terminal ferrocene twisted approximately perpendicular to the plane (Figure 5).[92] Calculations showed the the polymer chains in **PFDMS** to be conformationally flexible. Intermolecular interactions were found to be significant and the lowest energy conformation displayed twisted ferrocene units with favourable Fe-Cp electrostatic interactions between neighbouring polymer chains.[90]

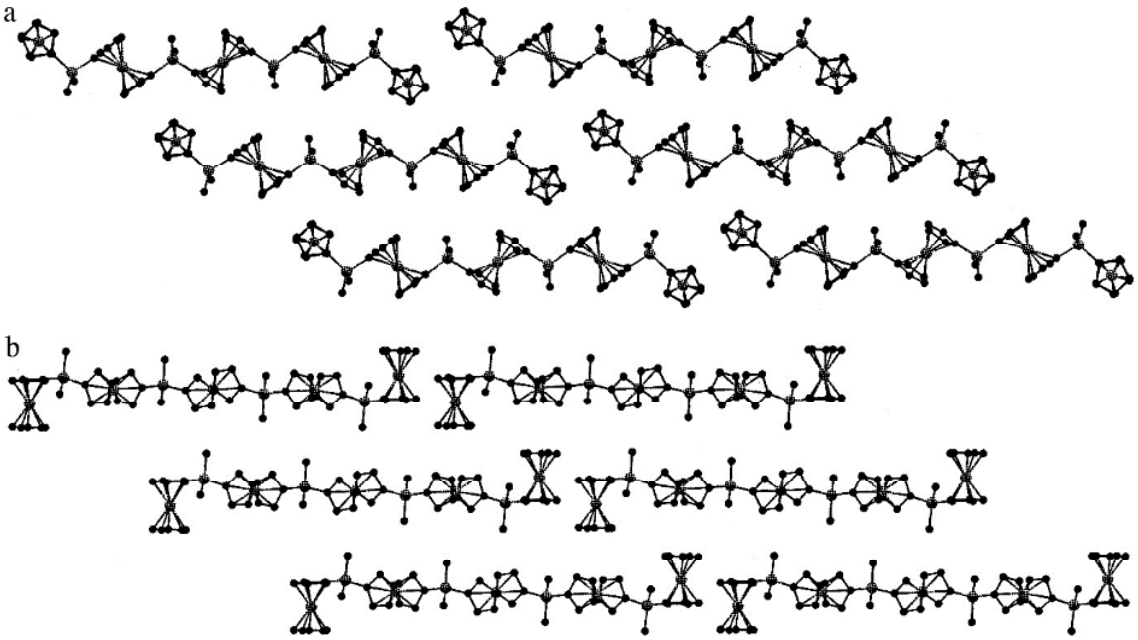

Figure 5. The crystal packing arrangement of the **PFDMS** pentamer, showing three pairs of molecules. The terminal ferrocenyl groups are twisted in opposite directions perpendicularly to the interior, trans-planar, zig-zag units. Reproduced with permission from reference 92.

Studies of films and fibres using X-ray diffraction revealed that crystalline **PFDMS** contains coexisting 2-D mesophases, crystals with a hexagonal or tetragonal packing of macromolecules, and 3-D monoclinic crystalline phases.[93] The formation of partially disordered crystalline phases was attributed to small energy differences between the various polymer conformations. Electrospun nanofibres of **PFDMS** have also been studied and in this case using electron diffraction.[94] The data obtained were consistent with the assignment of a monoclinic unit cell for the crystals in the nanofibre. Furthermore, the c-axes of the crystals were found to lie along the fibre axis but both the a- and b-axes of a multitude of crystals were found to be randomly distributed in the azimuthal directions. Studies of other **PFS**s, including amorphous materials that were unsymmetrically substituted at silicon, have also been reported.[95] In comparison to the semicrystallinity of **PFDMS** and symmetrically substituted analogs with small alkyl groups at silicon, *n*-hexyl substituted **PFS** has been

isolated as an amorphous gum with a T_g of -26 °C. Apparently, for these materials once the length of the alkyl chain exceeds five carbon atoms regular packing of the polymer chains cannot be achieved.[7] Alkoxy-substituted **PFS**s are also generally amorphous, however, the incorporation of long alkoxy chains at silicon, such as *n*-octadecyloxy, yields **PFS**s that exhibit side-chain crystallisation to form lamellar structures with interdigitated side groups.[15]

The polymer backbone motions of deuterium-labelled **PFS**s over a range of temperatures were studied by solid-state ^{2}H NMR spectroscopy, and the nature and rates of molecular motions were determined from the shape of the spectral line and the spin-lattice relaxation time (T_1). Symmetrically substituted **PFS**s with methyl, methoxy, hexyloxy substituents at silicon were studied where the Cp rings were fully deuterated (Figure 6). Interestingly, when the Cp rings were deuterium-labelled, a lack of motion in the backbone was observed below the T_g.[96] This was unexpected because Cp ligand rotation in ferrocene is facile due to the low barrier of rotation about the iron-Cp bonds (3.34 kJ mol^{-1}).[97] At temperatures just above the T_g, small-angle oscillations of the Cp groups were noted which increased in rate with temperature. Above 50-70 °C, the spectra indicated the presence of rapid isotropic movements. Studies of **PFS**s with $-CD_3$ or $-OCD_3$ groups at silicon provided insight into the motions of side groups as a function of temperature. For example, **PFDMS** side groups showed fast methyl rotation about the Si–CD_3 bond even at temperatures below the glass transition.[98] With methoxy substituents, fast methyl rotation was observed about the O–CD_3 bond alongside a discrete jumping motion displayed by the Si–O bond.[98] In a separate study, solid state ^{13}C NMR spectra of **PFDMS** and poly(ferrocenyldibutylsilane) allowed the structure and segmental motions of these semicrystalline polymers to be examined. Polymer main chain rigidity on the time scale of the cross-polarisation time between protons and carbons, T_{CH}, was confirmed at room temperature although some libration of ferrocenyl

groups was possible in the latter case.[99] In addition, the butyl substituents were found to be significantly disordered.

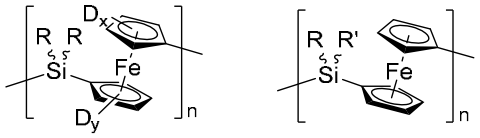

$R = CH_3$, x+y = 2
$R = OCH_3$, x+y = 4
$R = OC_6H_{13}$, x+y = 4

$R_1 = CD_3$, $R_2 = CH_3$
$R_1 = R_2 = OCD_3$

Figure 6. The polymer backbone motions of polyferrocenylsilanes over a range of temperatures were studied by solid-state ^2H NMR spectroscopy. Either symmetrical methyl and methoxy substituents at silicon or the Cp rings were fully deuterated, and the resultant polymers studied.

3.3 High Refractive Index Materials

Organic polymers possess a relatively narrow range of refractive indices (RIs), commonly between 1.35 and 1.65,[100] which limits their application. [101] To resolve this, RIs can be increased through molecular tailoring of polymers with functional groups that vary in electronic polarisation, such as incorporating conjugated double bonds or aromatic heterocyclic rings directly on the polymer backbone.[102] However, the device applications of these highly conjugated, organic polymers are often limited by unfavourable optical properties and insolubility.[103] An alternative approach incorporates high refractive index inorganic clusters into a polymer matrix.[104] For example, RIs reported for nanocomposites containing **PEO** (**PEO**: poly(ethylene oxide)) and PbS range between 2.9 and 3.4.[105] These polymers, however, suffer from optical inhomogeneities, poor processability, and increased Rayleigh scattering at critical diameters.[104] Notably, the inclusion of highly polarisable atoms

(Si, Ge, Sn, S), substituents with low molar volumes and high molar refractions (aromatic rings, halogens excluding F), or metallic elements into macromolecules increases the RI exhibited by the material without significantly increasing the optical dispersion.[106, 107] Frequently, as several components are combined in a polymer, the refractive index of the material is increased further by synergistic effects.

High molecular weight **PFS**s have been found to possess relatively high RI values (up to *ca.* 1.70), as expected from the high concentration of polarisable iron and silicon atoms in the polymer backbone.[108] The refractive indices at λ = 589 nm of **PFS**s with various substituents are displayed in Table 2. These **PFS**s also possess significantly lower optical dispersion than organic polymers for the same values of refractive index.[109]

Table 2.[108, 109] The refractive indices at λ = 589 nm of **PFS**s with various substituents.

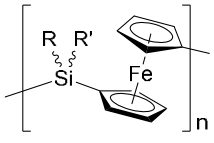

R	**R'**	***n* (589 nm)**
CH_3	$CH_2CH_2CF_3$	1.599
CH_3	CH_2CH_3	1.663
CH_3	CH_3	1.678
CH_3	C_6H_5	1.681
CH_3	*p*-OC_6H_4Br	1.682
CH_3	Ferrocenyl	1.696
CH_3	Thienyl	1.691

Tapered optical fibres coated with **PFS** (R = Me, R' = Ph) have been explored as gas sensing devices for NH_3 and CO_2. When a gas interacted with the polymer coating, the resulting small variations in refractive index caused significant changes in the transmitted optical signal.[110] However, while the device was highly sensitive to other changes in environment, the magnitude of the response was (qualitatively) not concentration dependent.

3.4 Redox and Charge Transport Properties

Unlike ferrocene containing side-chain polymers, which generally only exhibit a single oxidation wave for the Fe(II)/Fe(III) redox couple, **PFS**s display cyclic voltammograms with two reversible oxidation waves of equal intensity. [21, 92, 111-113] This is indicative of a stepwise process where initial oxidation at alternating iron centres occurs, because as one iron centre is oxidised ($^1E_{1/2}$), the neighbouring sites become more difficult to oxidise (Scheme 9). Thus a higher potential is required ($^2E_{1/2}$), resulting in the two oxidation waves with redox coupling, $\Delta E_{1/2} = {}^2E_{1/2} - {}^1E_{1/2}$ (≈ 250 mV for **PFS**s).[92] When identical experimental conditions are used for the electrochemical experiments (including the use of the same solvent and supporting electrolyte) the separation of the two waves, $\Delta E_{1/2}$, provides an approximate measure of the electronic interaction between iron centres along the polymer backbone.[114] Studies of isolated linear and cyclic oligomers has shown that the equal intensity, two redox-wave pattern characteristic of **PFS** materials corresponds to the limiting case of an infinite chain.[65, 92] Functionalisation of the Cp rings with electron donating groups lowers the oxidation potential of the ferrocene center in the neutral species. For example the cyclic voltammetric halfwave oxidation potentials of **PFS** are reduced by *ca.* 55 mV per Cp methyl substituent relative to the non-methylated polymer.[29]

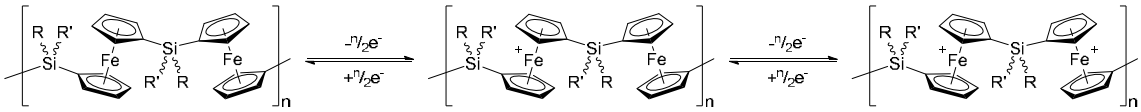

Scheme 9. The stepwise oxidation and reduction of **PFS**.

The redox properties of **PFS**s have been exploited for a wide range of studies and applications. **PFS** homopolymers with a thiol end group have been self-assembled as monolayers on a gold surface, and probed to determine the morphology and volume changes upon oxidation and reduction.[115] Surface plasmon resonance spectroscopy and spectroscopic ellipsometry measurements showed a reversible 15% increase in thickness of the polymer monolayers upon electrochemical oxidation, confirmed by X-ray reflectivity measurements. The authors attributed this change to both stretching of the polymer backbone upon oxidation, as a result of an increase in charge density, and the attraction of counter-ions and associated solvent molecules. These processes were reversed when the polymer monolayer was reduced to a neutral state. Furthermore, in a separate study, changes in elasticity of individual **PFS** chains on a surface was also induced by a change in oxidation state,[116] such that the oxidised polymer had an increased segment elasticity (45 nN nm^{-1}) and Kuhn length (0.65 nm) compared to its neutral analogue (30 nN nm^{-1} and 0.40 nm, respectively).[117] This change was reversible and has been used as the basis for a single (macro)molecular motor. **PFS** was operated in a controlled cyclic fashion to perform mechanical movement (output) as a consequence of an electrochemical potential (input) (Figure 7).[117] For **PFS** homopolymers (degree of polymerisation = 80) 3.4 x 10^{-19} J of work was achieved at an efficiency of 5%, as estimated from the experimental data. Closed mechanoelectrochemical cycles of individual **PFS** chains have also been studied using electrochemical AFM-based single-molecule force spectroscopy, and a quantitative analysis of the efficiency of the closed cycles has been performed as a function of extension. A maximum value of 26 % was observed experimentally.[118] Atomic force microscopy (AFM) was used to study the force interactions

between the tip and a **PFS** grafted gold surface subjected to external potential in $NaClO_4$ solution.[119] The physisorption of the **PFS** chains to the tip dominated the total interaction force, regardless of a subsequently applied surface charge, if the tip was in contact with the polymer surface prior to electrochemical induced redox chemistry.

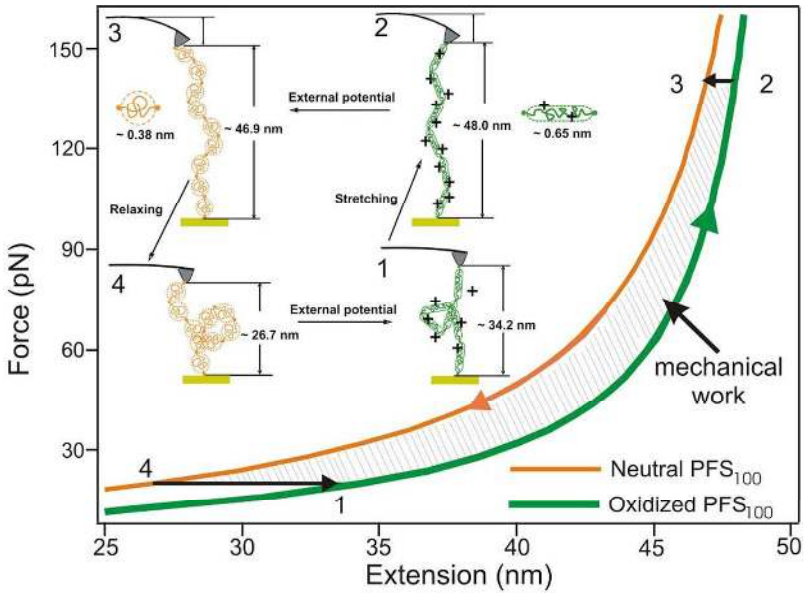

Figure 7. Single molecule operating cycle of **PFS** macromolecules (degree of polymerisation = 80) powered by an electrochemical potential; (inset) schematic illustration of a single molecule operating cycle with redox-active macromolecules. Reproduced with permission from reference 117.

Although neutral **PFS**s are classed as insulators, with an intrinsic conductance (σ) of 10^{-14} Ω^{-1} cm^{-1}, oxidative doping can increase this by several orders of magnitude to values in the range of 10^{-8} to 10^{-4} Ω^{-1} cm^{-1}, typical of p-type semiconductors.[120] The hole transport properties have been shown to be appreciable.[120] Vapour-phase chemical oxidation of **PFS** thin films was achieved using iodine, *via* irreversible electron transfer to form ferrocenium ion centres with $[I_3]^-$ counter-ions.[121, 122] Further doping with I_2 saw the reversible formation of $[I_5]^-$ ions.[123] Treatment of the iodine-doped films with NH_3 resulted in reformation of the

insulating material. Significantly, chemical oxidation under these conditions resulted in considerable cleavage of the polymer backbone. Oxidation can also occur with ferric chloride, $[Et_4][NBF_4]$, tris(4-bromophenyl)ammoniumyl hexachloroantimonate,[124, 125] tetracyanoethylene, or 2,3-dichloro-5,6-dicyanoquinone.[41] Tris(4-bromophenyl)ammoniumyl hexachloroantimonate, however, can also act as an oxidant in radical cation chemistry and a Lewis acid in carbocation mediated transformations, as aminium hexachloroantimonates can release antimony pentachloride.[126] On the other hand, tris(4-bromophenyl)amminium hexafluorophosphate, a one electron oxidant, cleanly oxidises ferrocene derivatives as the counterion is relatively inert.[127] Decamethylferrocene was found to be a good reducing agent for oxidised **PFS**.[125]

Photo-oxidation of amorphous **PFMPS** thin films either cast from chloroform solution or in the presence of chloroform vapour, was achieved by irradiation with near-UV light.[128] The photo-oxidised films displayed a significant increase in conductivity in the absence of light relative to pristine samples; moreover, a significant photoconductive response was also measured under illumination. However, a substantial reduction in the molecular weight of the polymer was detected after the photo-oxidation/reduction process which is believed to be caused by the highly reactive chlorinated photoproducts derived from $CHCl_3$.

Significant chain cleavage has been noted to be facile when the degree of oxidation of **PFS** exceeded 10%, even with mildly nucleophilic species, as the highly labile ferrocenium centres readily undergo Fe–Cp bond cleavage.[77] As oxidised **PFS**s are generally insoluble in non-nucleophilic organic solvents these materials are difficult to process and study. Introducing bulky electron-donating substituents to the Cp rings has been used in an attempt to resolve these issues. Thus, the oxidation potentials of poly(*tert*-

butylferrocenyldiphenylsilane) (Figure 8) were more negative than those of the methylated or non-methylated analogues due to the electron donating effect of the *tert*-butyl group on the iron centre.[77] Substantial redox coupling ($\Delta E_{1/2}$ = 0.33 V) was also detected. Significantly, the presence of *tert*-butyl groups markedly decreased the propensity for the polymer to undergo chain cleavage on oxidation. Furthermore, soluble (e.g. in CH_2Cl_2) **PFS**s salts were achieved up to high degrees of oxidation (*ca.* 50 %).[77]

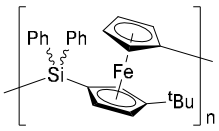

Figure 8. Poly(ferrocenyldiphenylsilane) with a *tert*-butyl substituent per ferrocenediyl.

PFSs have also been investigated as host materials for CdSe nanocrystals.[129] It was noted that **PFS** caused quenching of the band edge photoluminescence of the quantum dots in films and in solution, although in the latter case the quenching effects were solvent dependent. As the emission properties of the CdSe nanocrystals can be controlled *via* the controlled oxidation of **PFS**, there are potential applications in electrochromics or optical switching in which the response of the nanocrystal is altered by the redox chemistry of the polymer.

PFDMS and **PFMPS** have also shown potential as charge dissipation coatings for dielectric poly(ethylene terephthalate) (Mylar) films.[130] In this study, a 50 mm thick Mylar layer was coated with **PFS** and then exposed to an electron beam. It was noted that the **PFS**s imparted a high degree of immunity to the dielectric films with respect to high energy arc discharges brought about by negative charge accumulation. This was rationalised by the explanation that the **PFS**s were acting as a semiconductor: the charge formed at the surface of the coated sample was drained slowly to the ground.

PFS nanocontainers prepared by a miniemulsion/solvent evaporation protocol by hydrogen peroxide were found to release hydrophobic material over a period of time when oxidised by H_2O_2.[131] The release was also coupled to the enzymatic oxidation of glucose with oxygen by the enzyme glucose oxidase.

3.5 Redox-Active Gels

Stimuli responsive materials rapidly alter their structure and properties in response to changes in environment, such as pH, temperature, applied stress, and electromagnetic fields.[132] While responses to such traditional stimuli have been well documented, redox responsive gels are much less studied.[133] Organic solvent swellable gels based on crosslinked **PFS** were reported in 1996 and their preparation involved thermal copolymerisation of dimethylsila[1]ferrocenophane with a small quantity of spirocyclic [1]ferrocenophane.[19, 134] As noted earlier (Section 3.1), the best solvents for **PFDMS** are tetrahydrofuran, chloroform, and dichloromethane; these resulted in the maximum degree of swelling.[82] Analogous crosslinked **PFS** materials have also been produced *via* photo-crosslinking of pendant methacrylate groups,[34] hydrolysis of **PFS** with ethoxy side groups,[135] and thiol-ene addition reactions.[136]

As a result of the low polarity of **PFS** in the neutral Fe(II) state and the higher polarity of oxidised Fe(III) materials, **PFS** gels show tunable swelling based on the degree of oxidation in the selected solvent. Based on this concept, a redox-responsive colloidal photonic crystal was reported that consisted of an unconnected array of silica spheres embedded in a swellable crosslinked **PFS** matrix. Monodisperse silica microspheres were organised into planar silica

colloidal crystals by evaporative deposition, surface-modified with chloromethylsila[1]ferrocenophane, and infiltrated with ethylmethylsila[1]ferrocenophane (an unsymmetrically substituted monomer was used to prevent microcrystallisation of the resulting **PFS** within the network) and a silacyclobutyl-substituted [1]ferrocenophane crosslinker.[127] Thermal polymerisation then yielded a silica-**PFS** composite colloidal crystal film (Figure 9). A later study investigated the effect of exposing a similar photonic crystal to solvent vapour, deducing that the subsequent swelling changed the refractive index and increased the lattice spacing of the photonic crystal at higher vapour pressures.[137] The degree of swelling of the **PFS** chains in the photonic crystal was noted to depend on oxidation state of the iron centres, and the solvent system used. This response was used to develop a device in which the reflected colour was voltage tunable through the whole visible range, *via* reversible expansion and contraction of the photonic lattice.[138] Thin films of monodisperse silica spheres were deposited onto glass plates coated with indium tin oxide. The voids between the spheres were infiltrated by low molecular weight **PFMVS** (**PFMVS**: poly(ferrocenylmethylvinylsilane)), a small amount of multifunctional thiol, and a radical photo-initiator, then irradiated with ultra-violet light to give a **PFS** polymeric network *via* a thiol-ene addition reaction. However, it was noted that electrolyte diffusion through the silica packed polymer matrix impeded electron and ion transport, slowed switching times, and increased the voltage required to power the device.[138]

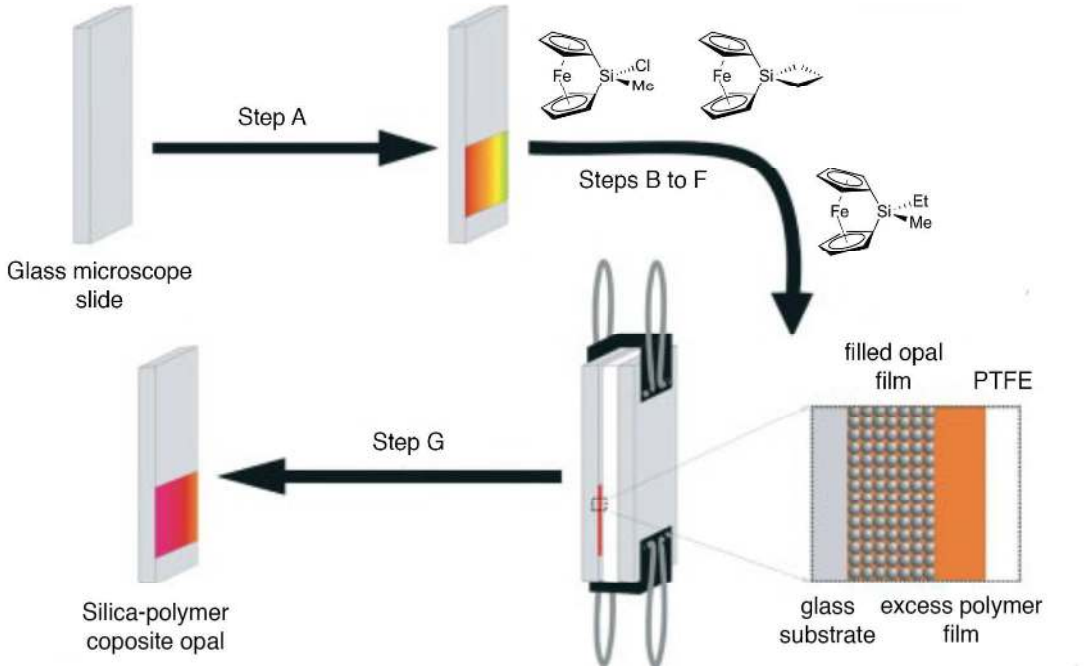

Figure 9. Schematic of steps in fabrication of a silica-**PFS** composite opal. A) Evaporation deposition of silica colloids. B) 200 °C, 12 h, vacuum. C) Treatment with capping agent (chloromethylsila[1]ferrocenophane). D) Infiltration of ethylmethylsila[1]ferrocenophane and a cyclobutyl-substituted [1]ferrocenophane crosslinker, solvent removal. E) Sample covered with PTFE sheet, glass slide, and bound. F) 190 °C, 13 h, N_2. G) Removal of clips, PTFE, and glass cover. Reproduced with permission from reference 127.

Electroactive *inverse* polymer gel opals based on **PFS** were reported in 2009. Silica spheres were deposited on glass and infiltrated as before with well-defined **PFMVS** or **PFDVS** (**PFDVS**: poly(ferrocenyldivinylsilane)), however after crosslinking and removal of the polymer over-layer, the spheres were removed with hydrofluoric acid.[136] This yielded a free-standing inverse polymer-gel opal in which electrolyte could freely infuse the nanoporous lattice. When an oxidative potential was applied the reflected optical diffraction peak was red-shifted, as the influx of ions and solvent caused the polymer to swell. When a reducing potential was applied the reverse occurred. Thus, full colour was afforded at low drive

voltages with wavelength shifts across the ultraviolet, visible, and near infrared spectral range (Figure 10).

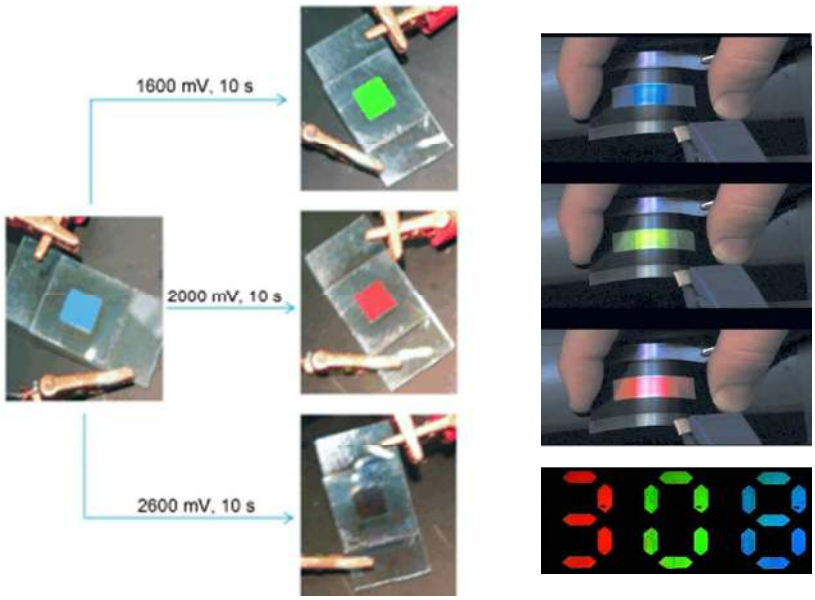

Figure 10. A) Proof of full colour tuning by photographs of the first electroactive inverse polymer-gel opal. The cross-linker concentration in this sample was 10 mol %. B) Extracted frames from a video taken when a flexible P-Ink device was simultaneously switched and flexed. Reproduced with permission of reference 136.

Hydrogels based on water soluble **PFS**s have also been developed.[139] The incorporation of ionic side groups into the **PFS**, or the linking the polymer chains with water soluble polymers such as **PEG** (**PEG**: poly(ethyleneglycol)), has allowed for hydrogel formation.[140] For example, two distinct types of **PFS** polyanion networks with either permanently positively or negatively charged side groups have been prepared (Figure 11).[141] The reaction of poly[ferrocenyl(3-iodopropyl)methylsilane] with *N*,*N*,*N*′,*N*″,*N*″-pentamethyldiethylenetriamine gave a lightly crosslinked network. The remaining iodopropyl side groups were then converted into positively charged moieties by quaternisation using *N*,*N*-dimethylethylamine, which resulted in a permanently charged cationic network. An

anionic **PFS** hydrogel was obtained from poly(ferrocenyl(3-iodopropyl)methylsilane) and α-lithio isobutyl methanesulfonate *via* intermolecular alkylation, followed by cleavage of the isobutylsulfonate side groups using tetrabutylammonium iodide, and exchange of counterions. The **PFS** hydrogels showed reversible hydration and dehydration in water, the extent of which was controlled by the redox voltage. An obvious change in mechanical behaviour occurred upon the oxidation of the anionic hydrogel: the elastic nature was lost and the gel collapsed. However, the network reswelled and regained its elasticity upon subsequent reduction and reestablishment of charge balance.[141] Water-solubility was also achieved by cross-linking **PFS** containing acrylic side groups with PEG-dithiol using the thiol-ene addition click reaction.[142] The redox state, and hence swelling and mechanical properties of the **PFS**, could be reversibly tuned. The **PFS-PEG** hydrogel was thought to have potential use as a redox controlled drug release carrier where release is based on hydrophobic–hydrophilic switching. A dual thermo- and redox-responsive poly(*N*-isopropylacrylamide)–**PFS** based hydrogel was synthesised as a precursor for the redox-induced formation of hydrogel silver composites.[143] These composites were reported to have a good biocompatibility with cells and display high antimicrobial activity. Dual-responsive **PFS** bottlebrushes with poly(N-isopropylacrylamide) side chains have also been studied.[144]

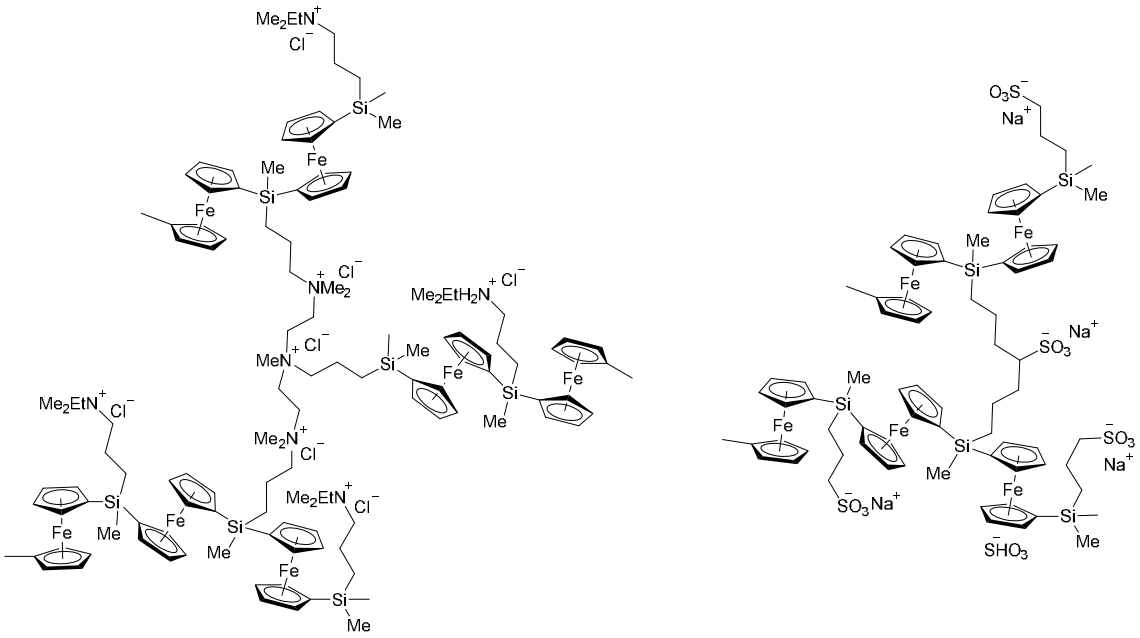

Figure 11. Permanently charged cationic and anionic **PFS** networks.

Redox responsive **PFS**-based poly(ionic liquids) (PILs) have been reported to form water swellable, redox-active gels. Poly[ferrocenyl(3-iodopropyl)methylsilane] was reacted with 1-vinylimidazole, before the iodide counterions were exchanged for chloride to improve solubility.[145] At low concentrations, the PIL self-cross-linked into nanogels, and at higher concentrations macroscopic hydrogel networks were formed. Chemical oxidation of the iron centres in **PFS** by H_2O_2 was accompanied by a distinct colour change from amber to blue/green.[139] Upon oxidation the hydrogel collapsed, whist subsequent reduction allowed the **PFS** chains to reswell. A current use of **PFS**-PIL is as a stabiliser for micro emulsion polymerisation, due to the amphiphilic nature of the polymer chain. Redox-responsive porous membranes have been formed by electrostatic complexation between **PFS**-based PILs with vinylimidazolium bis(trifluoromethylsulfonyl)imide side groups (VImTf_2N), and **PAA** (**PAA**: poly(acrylic acid)).[146] The **PFS**-VImTf_2N/PAA membrane displayed redox responsive behaviour, which enabled reversible switching between open and closed porous structures with associated changes in permeability (Figure 12). The authors noted that such a system

could have uses in selective filtration, the preparation of enzyme-entrapped membranes for bio-sensing, controlled loading and release, and catalysis in microfluidic reactors.

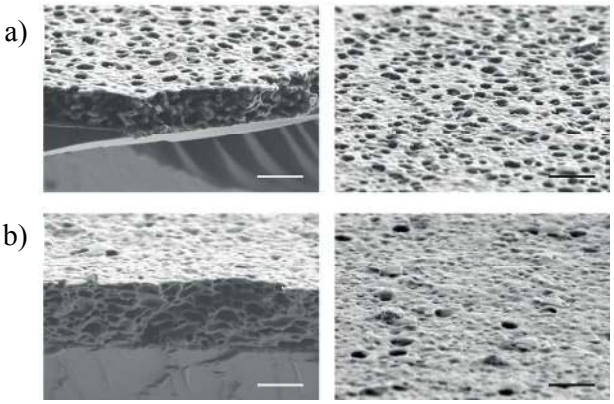

Figure 12. Cross-sectional and surface SEM images of **PFS**-VImTf_2N/PAA porous membranes after oxidation at 0.6 V for 10 min (a), and then reduction at −0.2 V for 10 min (b). Scale bars are 1 μm. Reproduced with permission from reference 146.

A comb copolymer consisting of a **PFS** backbone with *N*-dimethylethyl and *N*-dimethyldecyl ammonium substituents (Figure 13) was reported for use in the redox triggered release of molecular payloads. The amphiphilic behaviour of the comb polymer allowed the formation of micellar assemblies with hydrophobic pockets that displayed redox induced morphology changes in water.[147] When Paclitaxel and Nile Red were encapsulated in the micelles, oxidation of the polymer chains caused a shift to a less compact structure that allowed the controlled release of the compounds.

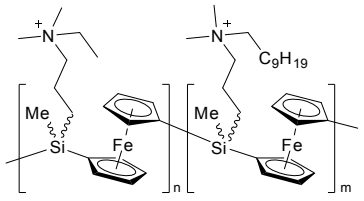

Figure 13. A comb-copolymer consisting of a **PFS** backbone with *N*-dimethylethyl and *N*-dimethyldecyl ammonium substituents.

3.6 Magnetic Ceramic Precursors

Ceramic materials have traditionally been prepared from powders in a sequence of synthesis, processing, shaping, and sintering steps that require exact stoichiometries and afford little control over ceramic morphology.[148] Moreover, the very high temperatures (> 1500 °C) required mean that processing is both difficult and expensive. Synthesis from polymers has been explored as it allows for homogeneous ceramics, better control over morphology, and enhanced physical properties, in addition to easy fabrication into fibers, films and shaped objects.[149] The incorporation of iron into polymer precursors has the potential to introduce magnetic, conductive, and catalytic properties.[150] **PFS**s are a well-studied class of organometallic polymers for the preparation of Fe/Si/C ceramics with the first studies reported in 1993.[151]

Pyrolysis of **PFS**s at temperatures above 400 °C under a flow of nitrogen yielded α-Fe crystallites embedded in a C/SiC/Si_3N_4 matrix.[151-153] Various substituents on silicon were investigated and **PFS**s with Si–H and vinyl groups gave the highest ceramic yields at 600 °C, whilst a 1:1 blend of both was highest at 1000 °C. Nonetheless, these ceramic yields (17-56%) were still too low to afford good shape retention. Subsequent work demonstrated that a crosslinked matrix obtained from the thermal ROP of **PFDMS** with a spirocyclic crosslinker formed well-defined ceramics when pyrolysed at 600 - 1000 °C, in greater than 90% ceramic yield (Scheme 10).[154] Within this temperature range it was found that the magnetic properties of the ceramics could be tuned. When prepared at temperatures below 900 °C, small, single domain iron nanoclusters were formed that displayed virtually no hysteresis at 100 or 300 K, characteristic of superparamagnetic ceramics (Young's modulus = 29.4 GPa). Ceramics

prepared at higher temperatures (Young's modulus = 15.4 GPa), however, contained larger ferromagnetic, multi-domain iron nanoparticles. This crosslinked **PFS** system enabled the shape retention of monolithic shaped objects and formation of micron scale patterned materials (Figure 14).[150] A possible mechanism for ceramic formation from the **PFS** network involved the controlled release of Fe atoms from the matrix, and nucleation and growth of iron nanoparticles.

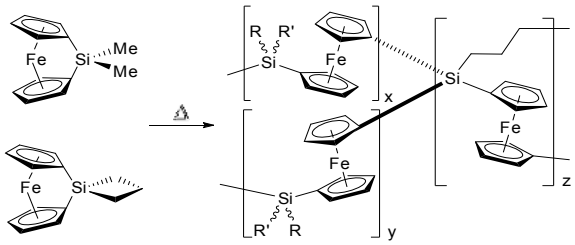

Scheme 10. Thermal ROP of **PFDMS** with a spirocyclic crosslinker to give a crosslinked matrix.

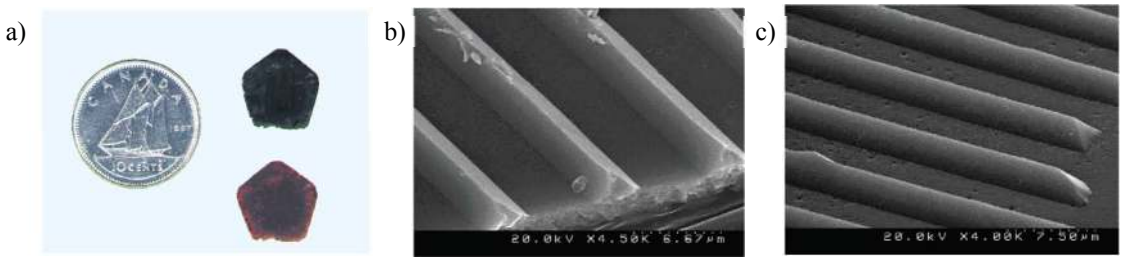

Figure 14. A) Pentagon-shaped polymer (bottom) and the resulting pentagon-shaped ceramic after pyrolysis (top). B) SEM images of a patterned polymer film, it is evident that the polymer film replicated the triangular grooves patterned on the Si wafer. C) SEM image of the resulting ceramic film, illustrating the shape retention of the polymer without the presence of a mould during pyrolysis. Reproduced with permission from reference 150.

The pyrolysis of hyperbranched **PFDMS** has also been studied and this yielded conductive, magnetic ceramics that exhibited a negligibly small hysteresis loss.[155] A 3-D mesoporous network of nanoclusters was generated *via* simultaneous evaporation of volatile organics and agglomeration of inorganic elements during pyrolysis. These hyperbranched polymers were determined to be superior to the linear analogues in terms of ceramic yield and retention of iron in the product (respectively 48 - 62% and 36 - 43%, vs 36% and 11% for the linear polymer).[155] The high ceramic yield for magnetic Fe nanoclusters with high magnetic susceptibilities was corroborated by further work on a hyperbranched **PFS** polymer from ferrocenyl dilithium and silicon tetrachloride ($SiCl_4$).[156] However, the solubility of the resulting polymers was remarkably reduced. Similarly, hyperbranched polymers were produced from dilithioferrocene with trichlorosilanes.[157] It was noted that the polymers with small substituents at silicon were partially soluble, while those with long alkyl chains were completely soluble and readily formed films which were then pyrolysed to give ferromagnetic ceramics. The roles of atmosphere and heating rate on the composition and magnetic properties of Fe/Si/C ceramics formed from hyperbranched **PFS** has also been investigated. The iron present in the ceramics sintered at 900 °C under N_2 and NH_3 atmospheres appeared as α-Fe, while those sintered under air contained γ-Fe_2O_3 and carbon.[158] Ceramics sintered under all three atmospheres were ferromagnetic with low remnant magnetisation and coercivity; however, those sintered under NH_3 displayed the largest saturation magnetisation. This was increased further when ceramics were prepared at a slow heating rate. The pyrolysis of the hyperbranched **PFS** at different temperatures was used to obtain porous ceramic microspheres with porous structures by solvent extraction/evaporation-based microencapsulation methods (Figure 15).[159] Fe nanoparticles were also produced on the internal surface of the pores, giving the ceramic microspheres catalytic properties.

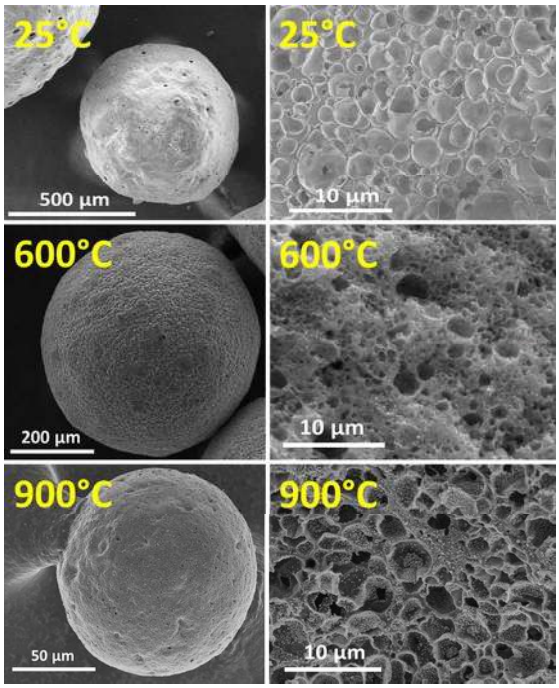

Figure 15. SEM images of hyperbranched **PFS** microspheres (25 °C) and ceramic microspheres after pyrolysis at 600 and 900 °C: the overall appearance (left) and cross-section morphology (right). Reproduced with permission from reference 159.

A bimetallic system was developed to combine the processability of linear high molecular weight polymers, the high ceramic yields achieved by thermally crosslinked systems, and the presence of a high concentration of two different metal atoms. An acetylene-substituted **PFS** was functionalised in a high yield post polymerisation by reaction with $Co_2(CO)_8$.[160] Ceramics prepared from $[Fe(\eta^5\text{-}C_5H_4)_2Si(Me)]_n$ (Co-**PFS**) at 600 °C were superparamagnetic, and those prepared at 900 °C ferromagnetic or superparamagnetic with a $T_b > 355$ K. It was also reported that at 500 °C pyrolysis, smaller NPs were formed in the underlying layer of the ceramic film, while partially embedded uniform and larger CoFe alloy nanoparticles formed on the film surface.[161] Pyrolysis of Co-**PFS** at higher temperatures yielded larger nanoparticles with a broad size distribution at the film surface (800 °C: 36.5 ± 12.5 nm, 900

°C: 40.5 ± 14.8 nm). Moreover, surface nanoparticles were found to be oxidised upon exposure to air.

Fabrication of patterned arrays of magnetic ceramics on the sub-micron scale was achieved by electron-beam lithography and pyrolysis of thin films with Co-**PFS** acting as a negative resist. Co-**PFS** was also found to act as a negative-tone UV-photoresist.[162] Furthermore, reactive ion etching of a thin film of Co-**PFS** with either a hydrogen or an oxygen plasma in a secondary magnetic field, afforded ferromagnetic ceramic films in a viable alternative to pyrolysis. **PFEMS** was doped with palladium(II)acetylacetonate either by sublimation of $Pd(acac)_2$ which formed Pd nanoparticles in the **PFEMS** films, or by mixing $Pd(acac)_2$ with the **PFEMS** polymer precursor prior to film deposition.[163] The magnetic susceptibility of the resultant soft processable paramagnetic polymer films increased with palladium content. Upon pyrolysis of the precursors, ferromagnetic ceramics were formed. Unusually, FePd alloys were observed for ceramics pyrolysed under argon at 1000 °C, which resulted in their enhanced coercivity, remnant magnetisation, and saturation magnetisation.

Composite materials of mesoporous silica and **PFDMS** have been prepared using a vapour-phase impregnation technique, where ROP occurs *in situ* inside the channels of silica. The pyrolysis of the resultant materials gave composites with Fe nanoparticles (20 ± 5 Å) confined to the channels of the mesoporous silica.[164] In a later report, $Fe(\eta^5\text{-}C_5H_4)_2SiMe_2$ and $Fe(\eta^5\text{-}C_5H_4)_2Si(CH_2)_3$ were incorporated into the hexagonal channels of mesoporous silica. However, in the latter case the ferrocenophane ring was completely opened, whilst the silacyclobutane ring remained mostly intact. When pyrolysed, the composites containing **PFDMS** formed Fe nanoparticles in the 30-40 Å channels of mesoporous silica. Characterisation indicated that the nanostructured ceramic was superparamagnetic.[165]

PFS materials have also been investigated as burning rate promotors. The formation of iron oxide nanoparticles has been advanced as an explanation for the observed behaviour.[166] Thermolysis of **PFS** precursors in the presence of Au and acetylene gas has also been explored and is reported to give Au-carbon nanotube composites.[167]

3.7 Redox-Active and Preceramic Microspheres

Solid **PFS**-microspheres with diameter of *ca* 2 μm have been prepared by precipitation polymerisation of dimethyl[1]silaferroceophane with a spirocyclic crosslinker.[168] Chemical oxidation with iodine gave positively charged particles. These then underwent electrostatic self-assembly with negatively charged silica spheres to form composite superstructures in which the larger organometallic core was surrounded by the smaller silica particles (Figure 16).[169] Thermal treatment proceeded with shape retention to give ceramic microspheres containing α-Fe nanoclusters embedded within a silicon carbide-carbon matrix. The magnetic properties of the ceramics could be tuned from the superparamagnetic to the ferromagnetic state by varying the pyrolysis conditions.[168] Moreover, the ceramics formed into organised 2-D arrays at the air-water interface under the influence of an externally applied magnetic field.

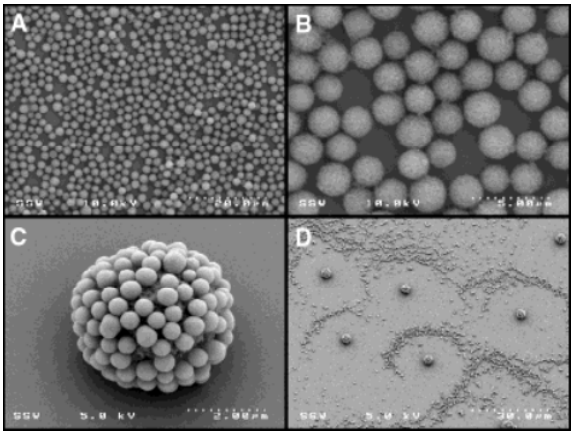

Figure 16. SEM micrographs of: A) **PFS** microsphere monolayer. B) Higher magnification of a close packed region. C) Negatively charged silica microspheres electrostatically bound to the surface of oxidised polyferrocenylsilane microspheres. D) Surface patterns of core-corona oxidised **PFS** microsphere-silica assemblies circumscribed by regions of silica spheres. Reproduced with permission from reference 169.

PFSs with acrylate and vinyl imidazole side groups have been used as microgel precursors.[170] Microfluidic processing enabled a liquid jet of the two immiscible monomers to form monodisperse **PFS** macro-crosslinker droplets. Cross-linked microgel particles were then obtained *via* UV-induced crosslinking of the colloids (Figure 17). The redox active microspheres could act as a reducing agent for the formation of silver nanoparticles from $AgPF_6$, as well as directing the growth of the Ag structures. Moreover, the loading and release of guest molecules such as Rhodamine 6G, a fluorescent dye, was demonstrated.

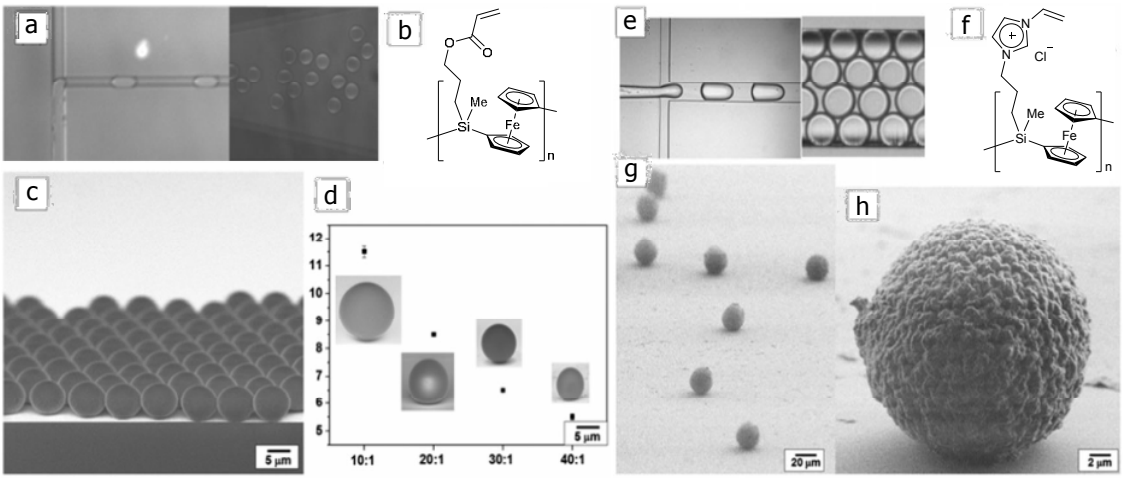

Figure 17. a) Images of head-on forming droplets of **PFS** (b). c) SEM images of the microgels formed from (b). d) The diameter of **PFS** (b) microspheres produced at increasing water-to-oil flow rate ratios, e.g. 10: 1 Q_w = 1 mL min^{-1}, Q_{PFS} = 0.1 mL min^{-1}. e) Hydrogel precursor droplets of **PFS** (f) formed in a flow focusing microfluidic device. (g) SEM images

of **PFS** (f) microgels, and (h) SEM image of a single **PFS** (f) microgel particle. Reproduced with permission from reference 170.

3.8 Layer-by-Layer Assembly of Water-Soluble Polyferrocenylsilane Polyelectroytes

Electrostatic superlattices formed by layer-by-layer (LbL) self-assembly of oppositely charged polymers have been of interest since the technique was first reported in 1991 by Decher.[171, 172] The LbL self-assembly method is based on electrostatic intermolecular forces; it involves the sequential adsorption of polyanions and polycations from aqueous electrolyte solutions onto a substrate surface, forming multilayer films and hollow nanostructures with defined structure and function. The formation of organic-organometallic **PFS**-based superlattices by the layer-by-layer deposition process involved anionic poly(styrenesulfonate) and the a cationic water-soluble **PFS** on primed Au, Si, and quartz substrates. This yielded regularly stacked, homogeneous electrostatic superlattices.[173] In another study, poly(ferrocenyl(3-ammoniumpropyl)methylsilane) was used in conjunction with poly(sodium vinylsulfonate) to form a multilayer film on quartz.[69] It was noted that a linear relationship between optical absorbance and the number of bilayers was indicative of the formation of well-defined multilayers.

Transition metal catalysed ROP and nucleophilic substitution methodologies allowed the production of both water soluble **PFS** polycations and polyanions, compounds with charges on the polymer side groups which made them suitable for fabrication of all-organometallic multilayer thin films using a LbL method.[174, 175] The polyions were deposited electrostatically onto a variety of substrates, such as silicon, gold, and hydrophilic/hydrophobically patterned substrates, the latter of which led to the formation of laterally structured **PFS** multilayers.[176]

It was reported that hydroxyl-terminated monolayer alkanethiol regions prevented deposition of the polyions due to hydrogen-bonding interactions with the solvent.

The syntheses of **PFS** polyelectrolytes *via* photolytic ROP gave well-controlled architectures with desired molecular weight and low polydispersity, which are not accessible by transition metal catalysed ROP.[61] Furthermore, such control was not possible using *n*-BuLi-initiated anionic ROP due to its intolerance towards the necessary functional groups. Preliminary studies on LbL assembly indicated that films made from monodisperse low molecular-weight **PFS**s possessed a considerably thinner bilayer thickness and higher refractive index than those made from **PFS**s with relatively polydisperse high molecular-weight. Subsequent findings determined that the number of deposited bilayers primarily controlled bilayer thickness, though ionic strength had a significant influence.[177, 178] The refractive index of films up to 55 nm were considerably higher than those of other common electrolytes, and values varied over the spectral range from 1.53 (near-infrared) to 1.8 (ultraviolet). Multilayer films have also been fabricated from LbL deposition of **PFS** and a redox-inert polymer, **PEI** (**PEI**: poly(ethylene imine)), onto various substrates (Figure 18).[179] Interconnected by a covalent linker, the **PFS**/**PEI** multilayers were effective for the electrochemical sensing of ascorbic acid and hydrogen peroxide *via* an amperometric response, and showed improved sensing performance at higher bilayer numbers.

In 2014 a new technique was reported to allow the quantitative visualisation of subnanometer height changes occurring in thin films of **PFS**s upon reversible electrochemical oxidation/reduction in situ and in real-time, electrochemistry imaging ellipsometry (EC-IE).[180] For example, a height change of 6 ± 1 Å was deduced from imaging ellipsometry data on the two step oxidation of surface grafted **PFS** on a patterned area of 600 x 400 μm^2. The

layer-by-layer self-assembly of high molar mass, double stranded DNA and **PFS** polycations into thin films and microcapsules with three-dimensional macroporous structures was also demonstrated.[181] It was noted that the formation of the porous architecture was likely due to the persistence length and chain-length mismatch of the two components, as well as the hydrophobicity of the **PFS** backbone.

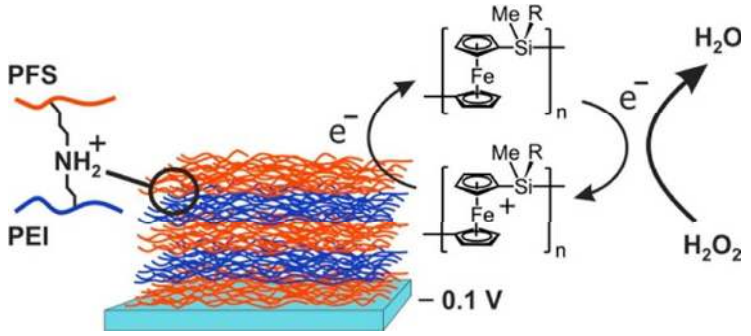

Figure 18. Poly[ferrocenyl(3-bromopropyl)methylsilane] and **PEI** were employed in a layer-by-layer deposition process to form covalently connected, redox-active multilayer thin films. Upon oxidation and reduction, these covalently interconnected layers do not disassemble, in contrast to **PFS** layers featuring similar backbone structures that are held together by electrostatic forces. Reproduced with permission from reference 179.

The disassembly of polyferrocenylsilane LbL assembled thin films has been electrochemically controlled by prolonged exposure to a low potential. The kinetics and profile of the multilayer release were controlled by blocking layers, surface charge, and the type of supporting electrolyte solution.[182] The driving force for this release of **PFS** was proposed to be electrostatic polyion binding and electrostatic repulsion. A high degree of control over the release of a fluorescent dye labelled Dextran positioned within the multilayer structure was achieved by varying the electrode potential.[183] The application potential of the **PFS** system in controlled molecular delivery, such as dosing in microfluidics, was also

demonstrated with nanotubes. A template assisted layer-by-layer technique was used to fabricate redox responsive nanotubes from composite mixtures of **PFS** and **PAA**. Multilayers of the polyions were deposited onto the inner pores of either anodised porous alumina or track-etched polycarbonate membranes, followed by subsequent removal of the template (Figure 19).[184] Electrochemically controlled release of dye labelled dextran molecules and negatively charged quantum dots were achieved upon electrochemical stimulation of the nanotubes.

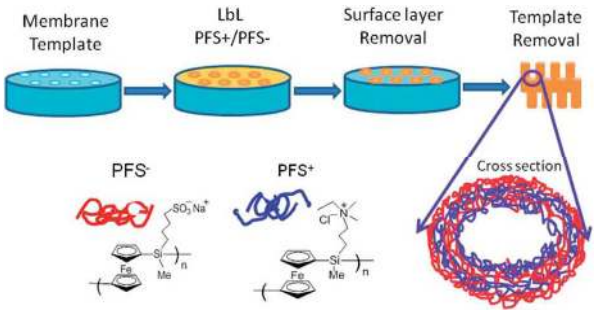

Figure 19. LbL assembly of redox polyelectrolyte nanotubes. Reproduced with permission from reference 184.

Various approaches have been reported for introducing redox-active molecules onto metallic electrodes. One of the first methods involved the insertion of **PFS**s into preformed self-assembled monolayers of hydroxyl-terminated alkane thiols on gold from toluene solution.[185] Very low surface coverages were achieved by inserting from very dilute **PFS** solutions. Alternatively, **PFS** with a thiol end-group was end-grafted onto gold substrates, forming redox-active monolayers.[186] In aqueous $NaClO_4$, two reversible redox peaks were seen, as expected for the stepwise oxidation of **PFS**s. It was determined that the oxidation process in the first step was controlled by the diffusion of counter-ions into the polymer film, while the second displayed greater reversibility. This was attributed to the swelling of the partially

oxidised **PFS** films in the aqueous electrolyte solutions, leading to a higher segmental mobility of the polymer chains and a much increased counter-ion mobility within the film. In a similar manner, sulfur end-functionalised **PFDMS** was grafted onto gold surfaces to form a redox responsive monolayer. The adherence and friction of the films were reversibly controlled from an oxidised state (high adhesion, high friction) to a reduced neutral state (low adhesion, low friction), with the gold substrate an electrode.[187] This electrode rectification behaviour could be useful in applications in thin film devices based on **PFS** films. Gold electrodes have also been modified by cathodic reduction of the Au substrates, immersed in a solution of imidazolium−functionalised **PFS** chains in the poly(ionic liquid), 1-ethyl-3-methylimidazolium ethyl sulfate.[188] The polymer films were employed as an ascorbic acid sensor, exhibiting high sensitivity, stability, and reproducibility. A high sensitivity to ascorbic acid was also exhibited by **PFS** films formed by an alkylation reaction of an amine monolayer on silicon or gold surfaces with **PFS** chains featuring iodopropyl side groups.[189] Also, as the anchored **PFS** chains possessed unreacted iodopropyl side groups they could be derivatised into a range of functionalities including cationic, anionic, hydrophilic, or hydrophobic moieties. This system constituted a highly versatile platform for facile chemical modification of electrodes. In addition to a **PFS** with iodopropyl side groups (**PFS-I**), undecylsulfonate-substituted thin films (**PFS-SO_3^-**) were immobilised on electrode surfaces (Figure 20).[190] The authors reported that the surface characteristics of the two films could be reversibly switched between hydrophobic and hydrophilic states under electrochemical control: the water contact angle for **PFS-I** varied between 80° (reduced state) to 70° (oxidised state) over repeated cycles. However, an opposite change in wettability was observed for **PFS-SO_3^-**, where the values observed varied from 59° (reduced state) to 77° (oxidised state). Unfortunately, the observed switching of the **PFS-SO_3^-** films was not possible with water as

a solvent, which would restrict the potential in situ application of this system in aqueous solutions, for example in microchannels for flow control.[190]

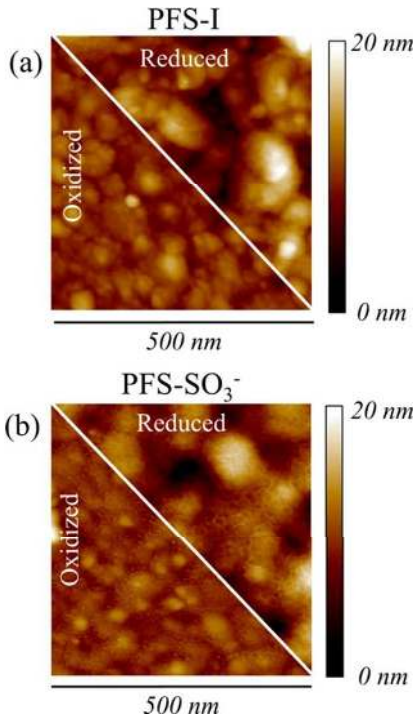

Figure 20. Tapping-mode AFM images in air of (a) **PFS-I** and (b) **PFS-SO$_3^-$** films upon redox at a scan size of 500 nm and a *z* scale of 20 nm. Reproduced with permission from reference 190.

Layer-by-layer assembly has also been used to tune the photonic stop band of colloidal photonic crystals, which were discussed in depth earlier. Silica colloidal photonic crystals with embedded redox active **PFS** polyelectrolyte multilayer planar defects were prepared by growing a **PFS** polyelectrolyte in a LbL fashion onto a polydimethylsiloxane sheet. This multilayer was transfer-printed onto the surface of a colloidal photonic crystal before a second colloidal photonic crystal was grown on top of the defect.[191] The structural defect allowed for reversible tuning of the transmitting state when subjected to redox cycling. Controlled infiltration and LbL assembly of low molecular weight **PFS** electrolytes into the

interstitial voids of colloidal photonic crystals allowed for nanometre-scale fine optical tuning in a cost-effective manner.[192] Low molecular weight and PDI samples were used to ensure uniform coating across the photonic lattice. As this method could be applied to vary the optical response of any porous structure, amorphous photonic media would benefit as multiple or resonant scattering could be accurately modulated by deposition of a dielectric thin coating on the inner pore or cavity walls.

The redox-controllable permeability of **PFS**-based polyelectrolyte microcapsules has also been studied. Polyelectrolyte capsules were prepared *via* layer deposition for polyanion/polycation pairs (in the sequence of $(\mathbf{PSS^-}/\mathbf{PAH^+})_2$ $(\mathbf{PFS^-}/\mathbf{PFS^+})_3$ ($\mathbf{PSS^-}$: poly(styrene sulfonate), $\mathbf{PAH^+}$: poly(allylamine hydrochloride)) on melamine formaldehyde (MF) cores.[193] Once the capsules were assembled, the ferrocene units were chemically oxidised, which triggered capsule swelling, thus increasing shell wall permeability, consistent with the electrostatic repulsion within the polyelectrolyte shell due to the excess positive charge on the chains, which would increase the distance between segments. The substantial swelling could be suppressed by the application of an additional coating bearing common redox-inert species of $\mathbf{PSS^-}$ and $\mathbf{PAH^+}$ on the outer wall of the capsules.[193]

3.9 Plasma and Electron Beam Etch Resists

The constant demand for smaller, faster, and more energy efficient electronic devices has necessitated increased component density, and thus smaller component sizes. The use of lithography has been integral to the progress of integrated circuit technology. PFS homopolymers and also block copolymers (see section 5.2.2) have attracted significant attention for lithographic applications as a result of impressive etch resistance of the

organometallic component which enables pattern transfer to a substrate. Thus, large-area **PFS** patterns have been fabricated by using various soft lithographic techniques, and subsequently transferred into the underlying substrate by reactive ion etching (RIE).

PFMPS has been reported as a high-contrast etch mask material,[194] for example in the fabrication of uniform, nanoporous polyethersulfone membranes.[195, 196] Under RIE **PFS** was remarkably stable compared to organic polymers, due to the presence of iron and silicon in the main chain.[49] For example, when exposed to an oxygen plasma a thin, non-volatile oxide layer was formed at the surface which gave rise to relatively low etching rates.[197] Low etching rates of **PFMPS** were also obtained when fluorocarbon plasmas were applied. With the oxide layer mask possessing such a high etching barrier, access to structures with high aspect ratios was possible, with potential use also in very thin resist layer applications. For further pattern transfer, the residual layer had to be completely removed by Ar sputtering, as otherwise the oxide layer formation prevented this.[49]

PFSs bearing pendant photo-crosslinkable methacrylate groups were used as negative-tone photoresists for photolithographic patterning.[34] Although a low-cost method for the controlled two dimensional patterning of **PFS** networks over large areas, crosslinking of methacrylate side groups by free radicals that propagated beyond the edges of the exposure pattern did not allow for reproducible features below a 3 μm scale. A **PFS** bearing metal carbonyl moieties has also been used as a negative-tone photoresist and an electron-beam resist. $[Fe(\eta^5\text{-}C_5H_4)_2Si(Me)\{Co_2(CO)_6C_2Ph\}]_n$ (Co-**PFS**), $[Fe(\eta^5\text{-}C_5H_4)_2Si(Me)\{Mo_2Cp_2(CO)_4C_2Ph\}]_n$ (Mo-**PFS**), and $[Fe(\eta^5\text{-}C_5H_4)_2Si(Me)(Ni_2Cp_2C_2Ph)]_n$ (Ni-**PFS**) were synthesised by the clusterisation of carbon-carbon triple bonds in an acetylide substituted **PFS**.[75, 76] All three polymers functioned as negative-tone resists in electron-beam

lithography to give well formed microbars and microdots (Figure 21). Co-**PFS** and Mo-**PFS** were also found to function well as a photoresist for UV-photolithography, giving sharp micron-sized features after UV exposure. On the other hand, Ni-**PFS** was not able to act as a photoresist due to the absence of carbonyl ligands, which prevented decarbonylation and cross-linking of the polymer, the proposed cause of the reduced solubility of exposed regions of Co-**PFS** and Mo-**PFS**.[76]

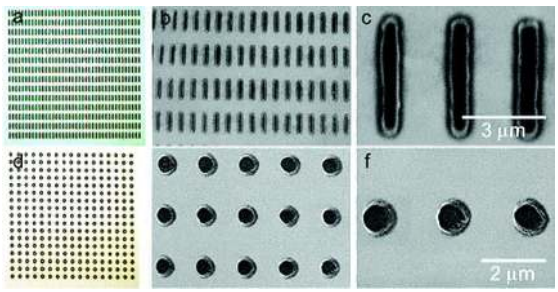

Figure 21. (a) Optical micrograph and (b and c) scanning electron micrographs of Mo-**PFS** microbars (0.5 x 4.0 μm^2), (d) optical micrograph, and (e and f) scanning electron micrographs of Ni-**PFS** microdots (diameter = 1.0 μm). Reproduced with permission from reference 76.

Capillary force lithography (CFL) is a non-photolithographic technique in which a polymer, above its glass transition temperature but initially confined in a thin film, is squeezed out from areas of contact between a **PFDMS** stamp and silicon substrate. It diffuses into the grooves where structures are formed along the vertical walls of the stamp due to capillary rise.[198] The molar mass of a polymer, processing temperature, and initial polymer film thickness all have a direct impact on the quality of the CFL polymer patterns and so must be controlled. Unsymmetrically substituted **PFS**s have been demonstrated to be ideal polymers for CFL as they will not crystallise.[199] Should the polymer resist lines have a uniform thickness, the resulting patterns can then be used as lithographic masks.

Although **PFS**s have seen use and photoresists for photolithographic patterning, conventional lithographic techniques have become increasingly difficult to use for the formation of features with dimensions smaller than 100 nm.[53] Block copolymers have offered an alternative approach for the fabrication of structures on the nanometer scale, as they can self-assemble into a variety of nanoscale morphologies (see Section 5.1).

4. Synthetic Routes to Polyferrocenylsilane Block Copolymers (PFS BCPs)

4.1. ROP Routes to PFS BCPs

Synthetic methods that allow the preparation of well-defined BCPs have been available for all-organic materials since the 1950s. Living anionic polymerisation, and more recently ring-opening metathesis polymerisation and "controlled" radical polymerisation, have played a key role in the development of BCP science.[86, 200-209] Synthetic routes to **PFS**-containing BCPs were first developed in the mid 1990s and, depending on the method, provide either moderate or excellent control over the resulting segmented structures

4.1.1. Metal-Catalysed ROP Routes to PFS BCPs

Transition metal-catalysed ring-opening polymerisation of dimethylsila[1]ferrocenophane, has been shown to proceed in solution at room temperature using Pt, Pd and Rh catalysts.[32, 33, 37, 38, 210] The addition of termination agents bearing a Si-H bond (e.g. Et_3SiH) can be used to control the molecular weight of the polymer by controlling the initial monomer-to-silane ratio.[38, 40, 211] This method can easily be extended to the use of polymers bearing a terminal Si-H group to allow the formation of **PFS**-containing BCPs.[38] For example, the preparation of a **PFDMS-*b*-PEO** (**PFDMS**: polyferrocenyldimethylsilane, **PEO**: polyethylene oxide) amphiphilic BCP was achieved through this method starting from a hydroxyl-terminated **PEO**.[40] Initially, a terminal Si-H functionality was incorporated into the polymer by a condensation reaction between the polymer and methylphenylchlorosilane. Reaction of the hydrosilyl-terminated **PEO** with dimethylsila[1]ferrocenophane in the presence of Karstedt's catalyst under ambient conditions yielded the desired **PFDMS-*b*-PEO** diblock copolymer. A

PFDMS-*b*-PDMS-*b*-PFDMS (**PDMS**: polydimethylsiloxane) triblock copolymer has also been prepared *via* this method by using a difunctional **PDMS** polymer with terminal Si-H bonds at either end of the polymer chain.[212] As transition metal-catalysed ROP of ferrocenophanes is characterised by random chain termination events involving reductive elimination at the metal centre[37] it is not a living process and the **PFS** segment in the resulting BCPs therefore have relatively high polydispersities (PDI > 1.5).

4.1.2. Living Anionic ROP Routes to PFS BCPs

Living polymerisations can allow the synthesis of polymeric materials with excellent control over molecular weights, permit end-group functionalisation and BCP synthesis, and access to materials with low polydispersities (PDI < 1.1) as both chain transfer and chain termination reactions are either absent or minimal.[213-215] These processes are therefore the method of choice for the preparation of tailored, well-defined BCPs. Two mechanistically distinct living anionic polymerisation methods have been developed for the synthesis of **PFS** BCPs using silicon-bridged [1]ferrocenophane monomers and these are discussed in turn.

4.1.2.1. Living Anionic ROP Involving Cp-Si Bond Cleavage

The use aryl- and alkyllithium reagents, such as phenyllithium (PhLi) and *n*-butyllithium (*n*BuLi), as initiators for the synthesis of **PFS** homopolymers and BCPs was reported over the 1994-1996 period.[44, 45] This allowed the preparation of well-defined materials with controlled molecular weights and narrow polydispersities (PDI < 1.2). The proposed mechanism involves nucleophilic attack of the initiator at the bridging silicon centre followed by Cp-Si cleavage to generate an anionic propagating site based on the iron-coordinated Cp

ring.[2] The method has been applied to silicon-bridged [1]ferrocenophanes with a variety of substituents at silicon, allowing access to **PFS** homopolymers and segments in BCPs that are able to crystallise (e.g. **PFDMS**,[45] **PFDES**[216]) or which are amorphous (e.g. **PFEMS**,[47, 48] **PFMPS**,[217] **PFiPMS**[50]). Degrees of polymerisation of 300 and higher have been reported and, although obtaining the high molar masses required to realise PFS-rich BCPs is a challenge, it is achievable.[48, 218] The 'living' nature of this polymerisation allows different monomers to be added sequentially in order of descending propagating site reactivity to form well-defined BCPs. The reactivity of living anionic-chain end groups for a number of common monomers has been found to follow the sequence **PI** ≥ **PS** > **PFDMS** > **P2VP** ≥ **PDMS** ≈ **PMVS** (**PI**: polyisoprene, **PS**: polystyrene, **P2VP**: poly-2-vinylpyridine, **PMVS**: polymethylvinylsiloxane).[45] Following this reactivity series allowed the synthesis of organic-organometallic BCPs such as **PS-*b*-PFDMS** (see Scheme 11A) and organometallic-inorganic BCPs such as **PFDMS-*b*-PDMS** (see Scheme 11B).[45, 219] The use of this method was subsequently extended to other polymerisable monomers, which has allowed the preparation of **PI-*b*-PFDMS**[220] and **PFDMS-*b*-PMVS**.[221] Phosphorus-bridged [1]ferrocenophanes also undergo living anionic ROP in the presence of aryl- and alkyllithium reagents[222] and this has allowed the preparation of **PFPP-*b*-PFDMS-*b*-PDMS** (**PFPP**: poly(ferrocenylphenylphosphine)).[223]

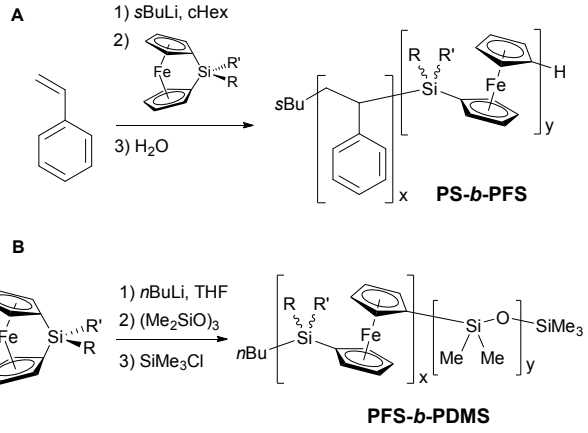

Scheme 11. Sequential living anionic polymerisation of A) styrene in cyclohexane (cHex) and sila[1]ferrocenophane for the formation of **PS-*b*-PFS**, and B) sila[1]ferrocenophane and hexamethylcyclotrisiloxane for the formation of **PFS-*b*-PDMS** (R = R' = Me).

The use of difunctional initiators, such as 1,1'-dilithioferrocene and lithium napthalide, has allowed the formation of symmetrical **PFS**-containing triblock copolymers and pentablock copolymers.[45] The difunctional initiator forms propagating anionic sites at both ends of the resulting polymer chain. This can allow further polymerisation to create a secondary block at both ends of the polymer chain, therefore allowing the formation of symmetric triblock and pentablock copolymers by sequential addition of monomers. A range of **PFS**-containing materials have been prepared by this method, such as **PDMS-*b*-PFDMS-*b*-PDMS**, **PFDMS-*b*-PS-*b*-PFDMS** and **PDMS-*b*-PFDMS-*b*-PS-*b*-PFDMS-*b*-PDMS**.[45]

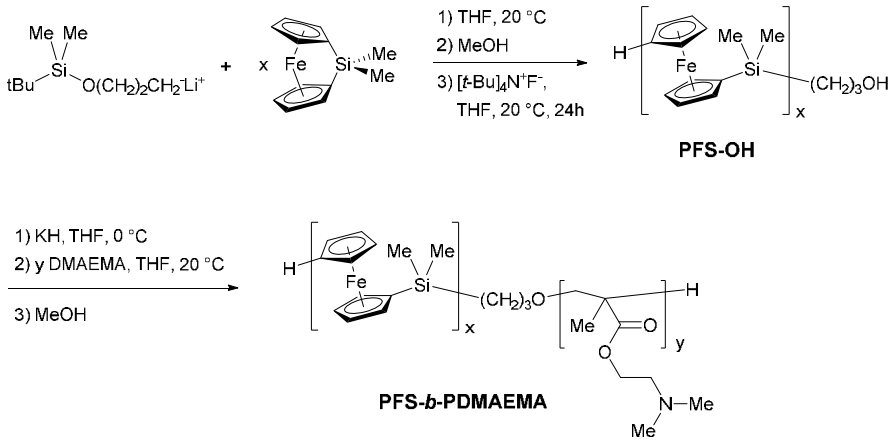

Scheme 12. Synthesis of polyferrocenyldimethylsilane-*block*-polydimethylaminoethylmethacrylate (**PFDMS-*b*-PDMAEMA**).

In principle, this method can be extrapolated to any monomer that can undergo living anionic polymerisation. However, many monomers require modifications to the procedure due to the

presence of side reactions with basic carbanionic initiators and propagating sites. For example, **PFS-*b*-PDMAEMA (PDMAEMA**: poly(dimethylaminoethylmethacrylate)) BCPs have been prepared by a two-step anionic polymerisation (see Scheme 12).[55] **PFDMS** was end-functionalised with a hydroxyl group by using tert-butyldimethylsilyloxy-1-propyllithium as an initiator followed by deprotection of the alcohol functionality under ambient conditions. The deprotected **PFDMS-OH** was then deprotonated using KH to give an alkoxyanion, which can initiate the anionic polymerisation of DMAEMA monomer, giving the **PFDMS-*b*-PDMAEMA** BCP with well-defined block lengths and dispersities (M_n = 11,000, PDI = 1.3).

An alternative method to yield **PFDMS-*b*-PMMA** (**PMMA** : poly(methylmethacrylate) BCPs involved the preparation of a **PFS**-based atom transfer radical polymerisation (ATRP) macroinitiator.[224] Firstly, **PFS** was prepared by anionic polymerisation and capped with a siloxypropylchlorosilane which was followed by deprotection and isolation to give a **PFDMS-OH** polymer. The material was subsequently reacted with 2-bromoisobutyric acid to give the desired **PFDMS** macroinitiator. MMA monomer was then polymerised using the **PFS** macroinitiator and an ATRP-active Ru-based catalyst to give the **PFDMS-*b*-PMMA** BCP. The **PFDMS** content and molecular weights of these materials was easily controlled through varying the macroinitiator-to-monomer ratio, whilst maintaining materials with relatively low molecular weight distributions (PDI < 1.2).

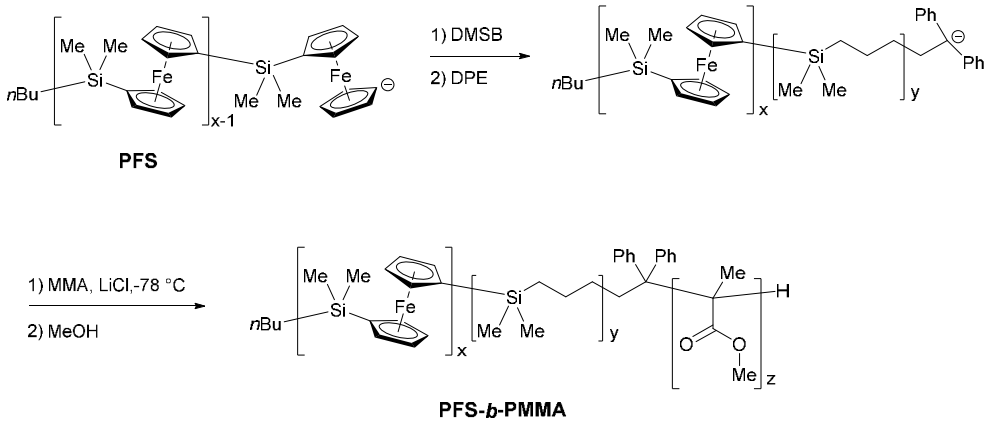

Scheme 13. Synthesis of polyferrocenyldimethylsilane-*block*-polymethylmethacrylate (**PFDMS-*b*-PMMA**) *via* reactivity mediation method using DMSB and DPE.

PFDMS-*b*-PMMA has also been synthesised through moderation of the reactivity of the propagating anion site (see Scheme 13).[52] This is necessary in order to hinder side reactions involving nucleophilic attack at the carbonyl functionality of the MMA. This was achieved using two additional steps that were performed *in situ* and involved the use of dimethylsilacyclobutane (DMSB) and diphenylethylene (DPE). DMSB was used as a "carbanion pump" to ensure efficient coupling of the DPE at the **PFDMS** chain terminus. MALDI-TOF analysis of model systems suggested the level of DMSB incorporation was 1 - 3 repeat units. Significantly, the increased steric bulk associated with the anionic DPE-capped chain end promotes attack at the alkenyl double bond in MMA instead of the carbonyl group. This allowed successful formation of **PFDMS-*b*-PMMA** BCPs of controlled molecular weights (M_n = 27,000 – 84,500) and low polydispersities (PDI < 1.1). This approach for reactivity mediation has allowed the synthesis of a number of other **PFS** BCPs previously unavailable by anionic polymerisation such as, for example, **PFDMS-*b*-P2VP**,[225] **PFDMS-*b*-P*t*BMA** (**PtBMA**: poly-*tert*-butylmethacrylate),[226] **PFDMS-*b*-PEO** diblock copolymers,[227] **PS-*b*-PFDMS-*b*-PMMA**[228] and **PS-*b*-PFEMS-*b*-P2VP** triblock terpolymers,[229] and **PMMA-*b*-PFDMS-*b*-PS-*b*-PFDMS-*b*-PMMA** pentablock terpolymers.[230]

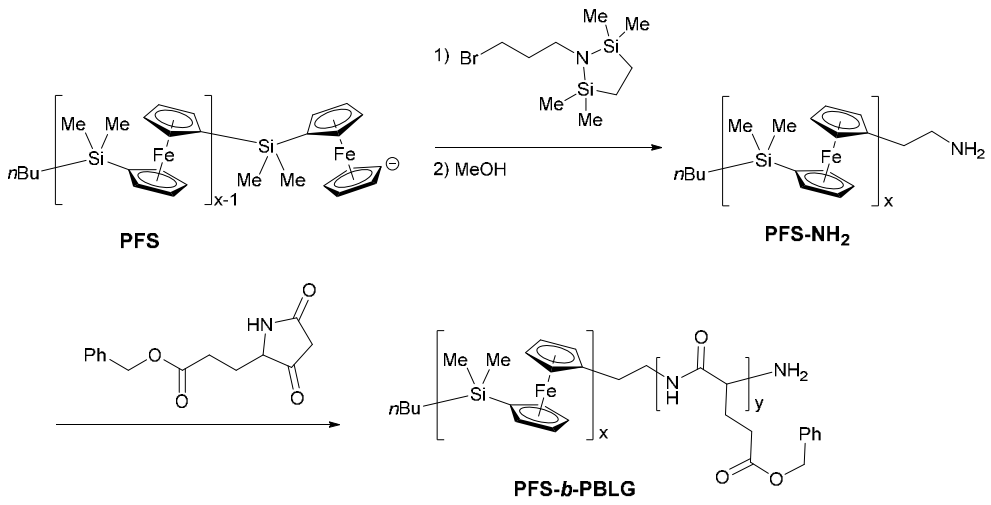

Scheme 14. Synthesis of polyferrocenyldimethylsilane-*block*-poly(*γ*-benzyl-L-glutamate) (**PFDMS-*b*-PBLG**).

A number of **PFS-*b*-polypeptide** BCPs have been prepared by different methods for self-assembly studies and for their potential in biological applications.[231, 232] **PFDMS-*b*-PBLG** (**PBLG**: poly(*γ*-benzyl-L-glutamate)) was prepared by a two-step route.[231] Firstly, the **PFS** segment was synthesised by anionic polymerisation and capped with a protected amine group (see Scheme 14), which was subsequently deprotected upon precipitation into MeOH due to the lability of the protecting group in lower alcohols to give **PFDMS-NH_2**. This telechelic polymer was used to induce the ROP of *γ*-benzyl-L-glutamate to afford **PFDMS-*b*-PBLG** BCPs with controlled molecular weights (M_n = 15,300 – 30,200) and narrow molecular weight distributions (PDI = 1.13 – 1.21). This method has also been used for the formation of **PFDMS-*b*-PZLys** (**PZLys**: poly(ε-benzyloxycarbonyl-L-lysine)[233] and a range of **PFS-*b*-tetrapeptide** materials.[234, 235] Use of hydroxyl-functionalised **PFDMS** as an initiator for the ROP of D/L-lactide has allowed the preparation of **PFDMS-*b*-PLA** (**PLA**: poly-D/L-

lactide).[236] A further strategy to access **PFS-*b*-polypeptide** BCPs involves the conjugation of two independent homopolymers through a Diels-Alder cycloaddition mechanism to form **PFDMS-*b*-PBLG**.[232]

Organometallic-organic heteroarm star polymers have also been prepared.[237] A **PFDMS-*arm*-(PI)$_3$** was synthesised in a two-step method (see Scheme 15); firstly **PFS** was prepared by anionic polymerisation and was quenched by adding dropwise to an excess of tetrachlorosilane to give a **PFDMS-SiCl$_3$**. This was to ensure that only one polymeric chain was grafted onto each silane capping agent. After purification, the **PFDMS-SiCl$_3$** was added to an excess of polyisoprenyllithium as a capping agent, which ensured complete substitution of all 3 Cl groups to afford the desired star polymer. Linear-dendritic **PFS**-containing BCPs have been synthesised by quenching living **PFDMS** chain ends with chlorine-functionalised **PBE** (**PBE**: poly(benzyl ether)) first- or second-generation dendrons.[238, 239]

An **PS-*b*-PFDMS-*b*-PS** triblock copolymer with unsymmetrical **PS** blocks was prepared *via* a similar method in a "universal methodology" for the preparation of BCPs using chemoselective stepwise coupling between living polymer chains and a heterobifunctional linking agent.[240] **PS-*b*-PFDMS** was prepared by living sequential anionic polymerisation and the living chains were quenched with chloro(3-chloropropyl)dimethylsilane to yield a Cl end-functionalised BCP. The **PS-*b*-PFDMS** was subsequently used to quench living **PS** anions to yield the desired triblock copolymer. This system could essentially allow the preparation of BCPs with block sequences that are unobtainable for materials exclusively prepared by sequential living anionic polymerisation methods.

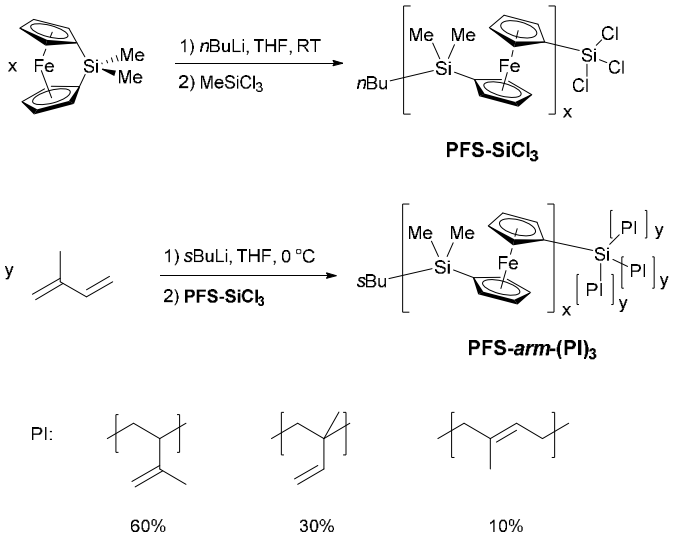

Scheme 15. Synthesis of polyferrocenyldimethylsilane-*arm*-(polyisoprene)$_3$ (**PFDMS-*arm*-(PI)$_3$**) heteroarm star polymer.

The formation of the organometallic-inorganic BCP, **PFDMS-*b*-PP** (**PP**: polyphosphazene) was reported[241] by combining the living anionic ROP route to **PFS** with the living cationic polymerisation of phosphoranimines[242-244] (see Scheme 16). This was achieved by capping living **PFDMS** anions with an excess of chlorodiphenylphosphine to give **PFS-PPh$_2$** after purification. The homopolymer end group was then chlorinated using hexachloroethane to give the dichlorodiphenylphosphino-functionalised **PFS** derivative. The telechelic **PFS-PPh$_2$Cl$_2$** reacted with different amount of phosphoranimine monomer and finally the material was treated with an excess of $NaOCH_2CF_3$ to make the materials air- and moisture-stable. Materials were prepared with a range of molecular weights (M_n = 27,170 – 84,490) and block ratios with narrow molecular weight distributions (PDI = 1.09 – 1.19).

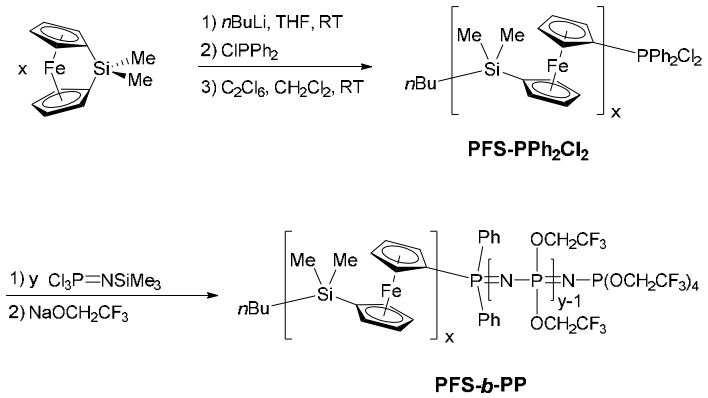

Scheme 16. Synthesis of polyferrocenyldimethylsilane-*block*-polyphosphazene (**PFDMS-*b*-PP**).

The combination of living anionic polymerisation techniques with copper-catalysed azide-alkyne Huisgen cycloaddition (CuAAC) "click" chemistry has facilitated the rapid expansion of accessible functional macromolecular materials.[245] This type of approach has been used for the convenient preparation of a range of **PFS**-containing diblock copolymers (see Scheme 17),[54] of which several have not been previously possible to access through sequential anionic methods. Azide-functionalised **PFDMS** was synthesised by quenching living **PFDMS** chains with the protected alkyne, 4-[(trimethylsily)ethynyl]lbenzaldehyde (TSEBA). The polymer was deprotected, reacted with a small excess of the relevant azide-functionalised polymer with a Cu(I) catalyst and subsequently purified to give the targeted BCP in high yield. This method has been effective in the preparation of **PFS** three-armed miktoarm star materials by sequential click reactions of azide-terminated polymers to a central functional core molecule.[246]

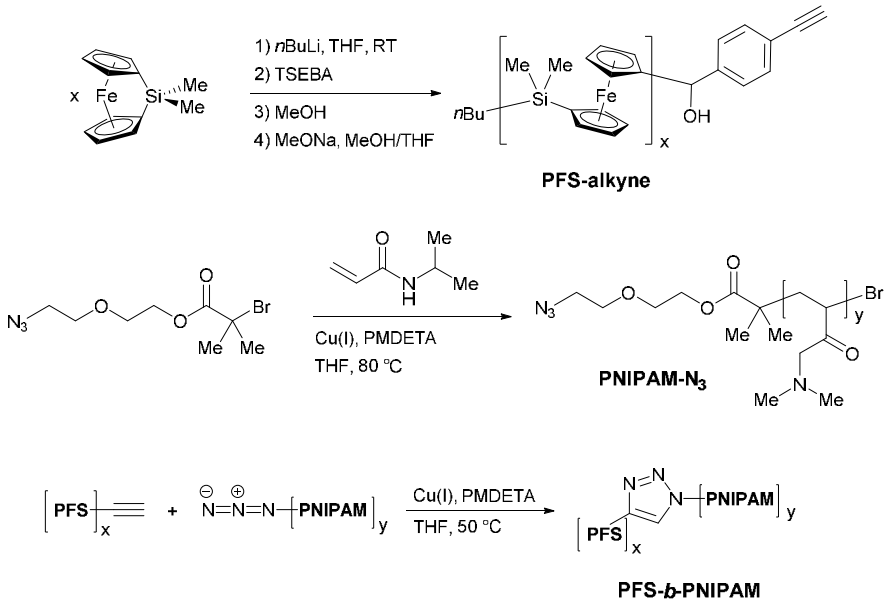

Scheme 17. Synthesis of polyferrocenyldimethylsilane-*block*-poly(N-isopropylacrylamide) (**PFS-*b*-PNIPAM**) *via* an azide-alkyne Huisgen cycloaddition (CuAAC) "click" reaction.

4.1.2.2. "Photocontrolled" Living Anionic ROP Involving Fe-Cp Bond Cleavage

In the presence of light, silicon-bridged [1]ferrocenophanes can also be polymerised by anionic reagents which are insufficiently reactive to attack the bridging silicon atom. The unusual and interesting mechanism has been shown to involve Fe-Cp bond cleavage and therefore differs from the aryl- or alkyllithium-initiated living anionic polymerisation in which Cp-Si bonds are broken.[247] The detailed role of light has not been fully elucidated but it appears to involve enhancement of electrophilicity of the Fe centre *via* the population of excited states with some ligand character, presumably accompanied by solvent co-ordination at iron and a haptotropic shift of the Cp ring.[66] Mildly basic cyclopentadienyl anions $[C_5H_4R]^-$ (R = H/Me), rather than highly basic reagents such as *n*BuLi, have been used as the anionic initiators. This leads to a relatively mild protocol that is functional group tolerant and

a useful method for the synthesis of **PFS** BCPs with substituents that are inaccessible by the aryl- or alkyllithium-initiated route due to side reactions.

An example of such a BCP prepared through the "photocontrolled" living anionic ROP method is **acetylidePFS-*b*-PFDMS** (see Scheme 18) which possesses acetylide groups attached to silicon.[247] Initially, an acetylide-substituted monomer in THF was irradiated with UV light in the presence of $Na[C_5H_5]$ initiator to yield living **PFS** with pendant acetylide groups. After turning off the irradiation source, dimethylsila[1]ferrocenophane was added and the reaction mixture was irradiated again. The **acetylidePFS-*b*-PFDMS** was isolated after addition of methanol to quench the reaction giving BCPs with predictable molecular weights (based on the monomer to $M[C_5H_5]$ ratio) and low polydispersities. This method has also allowed the formation of a range of **PFE-*b*-PFDMS** (**PFE**: polyferrocenylethylene),[248] **PFP-*b*-PFDMS**[249], **PFP-*b*-PFS$_F$**[59] (**PFS$_F$**: **PFS** with fluorinated side groups), **PFEMS-*b*-PFS$_A$**[250] (**PFS$_A$**: **PFS** with aminoalkyl side groups) and **PFS-*b*-PCE**[251] (**PCE**: poly(cobaltoceniumethylene)) materials to be synthesised.

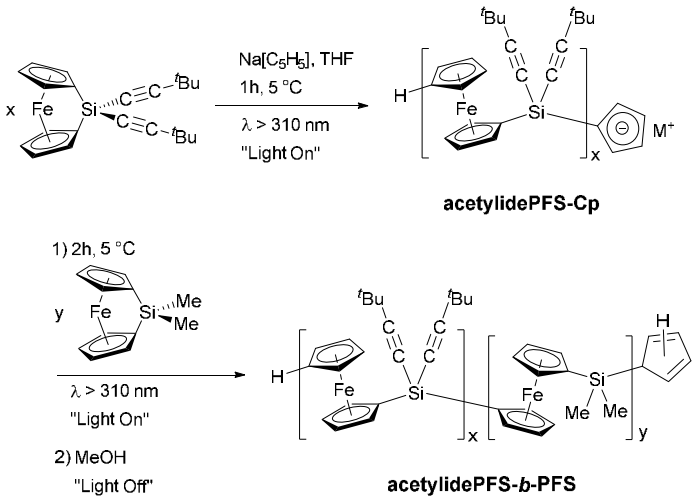

Scheme 18. Synthesis of polyferrocenyldi(*t*-butylacetylidyl)silane-*block*-polyferrocenyldimethylsilane (**acetylidePFS-*b*-PFDMS**) via photolytic living anionic polymerisation.

Organic-organometallic **PS-*b*-PFS** BCPs have been prepared by a combination of conventional and photocontrolled anionic polymerisation.[252] Firstly, **PS** was prepared using an alkyllithium initiator and the living anionic chain ends were capped with dichlorodimethylsilane. The resulting **PS-SiMe$_2$Cl** homopolymer was subsequently reacted with magnesocene and then chlorotrimethylsilane to give a **PS-Cp** macroinitiator. The telechelic polymer was irradiated with UV light in the presence of acetylide-functionalised sila[1]ferrocenophane monomer to give the targeted **PS-*b*-PFS** diblock copolymer. Materials were prepared with excellent molecular weight control and narrow distributions (PDI < 1.2). This synthetic approach has been extended to use with ferrocenophane monomers with pendant ruthenocene units.[62]

4.1.3. Post-Polymerisation Functionalisation of PFS BCPs

A further route to targeted **PFS**-based BCPs involves post-polymerisation functionalisation using side groups introduced during living anionic ROP. For example, **PFDMS-*b*-PBLG** BCPs were prepared by hydrogenative cleavage of the benzyl group in the **PBLG** block with H_2/Pd.[231] This yielded amphiphilic **PFDMS-*b*-PGA** (**PGA**: poly-L-glutamic acid) BCPs which were soluble in 0.1M NaOH.

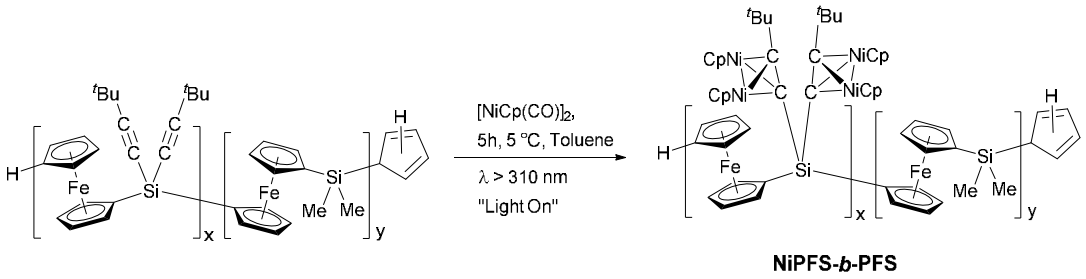

Scheme 19. Synthesis of highly metallised **NiPFS-*b*-PFS** through post-polymerisation functionalisation of **acetylidePFS-*b*-PFDMS** with $[NiCp(CO)]_2$.

A highly metallised **PFS**-based BCP has been prepared by post-functionalisation of **acetylidePFS-*b*-PFDMS**.[247] The pendant acetylide groups were reacted with a nickel-based cluster reagent $[NiCp(CO)]_2$ (Cp = η^5-C_5H_5) (see Scheme 19), forming **NiPFS-*b*-PFDMS** materials which can form novel bulk-state morphologies with Ni/Fe and Fe only domains. Similar methods have been to functionalise organic-organometallic **PS-*b*-PFS** BCPs with cobalt and gold complexes.[252]

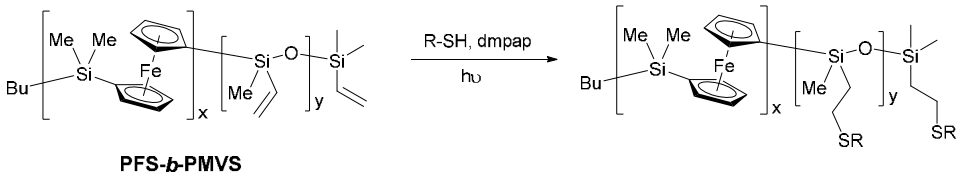

PFS-*b*-PMVS

Scheme 20. Functionalisation of polyferrocenyldimethylsilane-*block*-polymethylvinylsiloxane (**PFDMS-*b*-PMVS**) via a UV initiated thiol-ene "click" reaction.

Recently, a general route for the controlled functionalisation of **PFS-*b*-PMVS** via a thiol-ene "click" reaction has been reported (see Scheme 20).[253] Firstly, **PFDMS-*b*-PMVS** was synthesised by sequential living anionic polymerisation. This was followed by functionalisation of the pendant vinyl groups along the **PMVS** block backbone with a range of thiols using UV irradiation and a photoinitiator. However, due to the localised density of vinyl groups within the block, significant cross-linking occurred along the **PMVS** block. Copolymerisation of the **PMVS** block with **PDMS** to reduce the number of vinyl groups and decrease unintended cross-linking was performed, which increased the efficiency of thiol functionalisation. This approach is particularly effective for tuning the solubility of the resulting material or for incorporation of complex functionality for specific applications.

Linear-hyperbranched **PFS** BCPs have been prepared by post-polymerisation functionalization.[254] First, a linear diblock copolymer was prepared by sequential photocontrolled anionic ROP of dimethyl[1]silaferrocenophane and methylvinyl[1]silaferrocenophane. The second block was then functionalised by the hydrosilylation polyaddition of different silane-based AB_2 monomers.

5. PFS BCPs: Properties and Applications

5.1 PFS BCP Self-Assembly in Bulk and Thin Films

5.1.1. Self-Assembly of PFS Diblock Copolymers to Form Phase-Separated Materials

PFS BCPs phase-separate on the nanoscale due to the immiscibility of the **PFS** block with a wide range of organic or inorganic coblocks. This allows the formation of a variety of interesting nanostructured materials with periodic iron-rich domains and varied morphologies.[255] Following initial reports in the mid 1990s,[45] bulk and thin film self-assembly has been studied in detail for a variety of **PFS**-containing BCPs including **PFDMS-*b*-PMMA**,[52, 256] **PI-*b*-PFDMS**[257], **PS-*b*-PFDMS**[258, 259], **PS-*b*-PFEMS**[48, 218, 260] and **PS-*b*-PFiPMS**[50]. TEM micrographs of different solid state bulk morphologies for **PS-*b*-PFEMS**,[48, 261] **PFDMS-*b*-PMMA** (blended with homopolymer),[256] and **PMMA-*b*-PFDMS-*b*-PS-*b*-PFDMS-*b*-PMMA** BCPs are shown in Figure 22.[230] Phase diagrams for both **PS-*b*-PFDMS**[258] and **PS-*b*-PFEMS**[48, 218] BCPs have been reported previously. In the bulk, microtomed sections of these materials can be observed by TEM without the need of staining due to the increased scattering ability of the electron-rich **PFS** domains compared to those of organic polymers.[45] Complications can arise during the solid-state self-assembly of **PFS** BCPs with symmetrical *n*-alkyl substituents at the silicon centre (e.g. poly(ferrocenyldimethylsilane), **PFDMS**) due to the semi-crystallinity of the **PFS** block; this is because crystal break-out competes with the incompatibility of the blocks as the driving force for self-assembly.[262] Formation of self-assembled structures with a high volume fraction of the organometallic **PFS** block has also proved challenging, however examples of these have now been reported.[50, 218] In the case of lamellae-forming **PS-*b*-PFDMS**,

crystallisation of the **PFDMS** can be confined by the higher T_g organic domains.[263] The effect of crystallisation can be avoided by using unsymmetrically substituted **PFSs** (e.g. poly(ferrocenylethylmethylsilane), **PFEMS**) which do not crystallise.[48] It has been shown that, for the **PS-*b*-PFDMS** and **PI-*b*-PFDMS** systems, oxidation of the **PFDMS** block influences the order-disorder transition temperature of the phase-separated morphologies. [264, 265] Moreover, in depth studies of the thermodynamic interactions in **PS-*b*-PFDMS** by birefringence, SAXS, and SANS allowed the determination of the Flory Huggins interaction parameter χ between **PS** and **PFDMS** to be ca. 0.037 at 25°C, and is similar to that for **PS** and **PI**.[265] The value of $\chi_{PI\text{-}PFEMS}$ has been estimated as 0.17.[266]

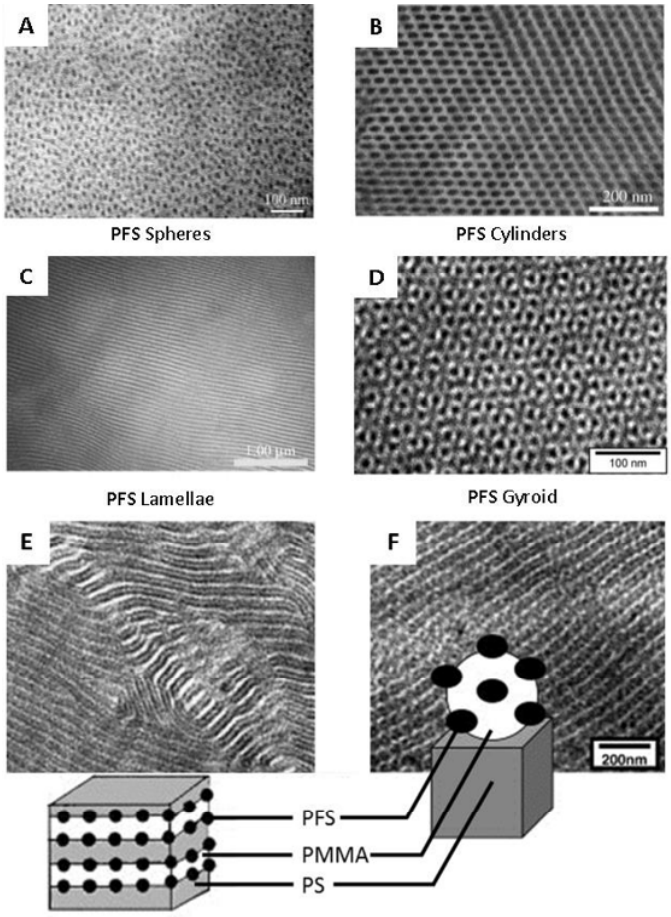

Figure 22. TEM micrographs for morphologies in the bulk state of **PS-*b*-PFEMS** (a-c), **PFDMS-*b*-PMMA** (blended with homopolymer) (d) and **PMMA-*b*-PFDMS-*b*-PS-*b*-PFDMS-*b*-PMMA** (e-f) Reproduced with permission from references [48, 230, 256].

Self-assembled BCP thin films can be prepared by spin coating dilute solutons of the BCP onto surfaces. The orientation of cylinder-forming self-assembled **PFS** BCP thin films can be controlled through manipulation of the film thickness.[267] When the films were thinner than the equilibrium periodicity of the microdomains, cylinders orientated themselves perpendicular to the substrate, whilst films with a thickness close to the equilibrium periodicity exhibited in-plane cylinders. Annealing conditions also affected the orientation of the cylindrical nanostructures.

PFS BCPs can form mesoscale dendritic structures when subjected to hybrid annealing conditions, where thermal and solvent annealing are implemented simultaneously, *via* dewetting phenomena.[268] These hybrid annealing conditions are essential to forming mesoscale morphologies, as using only one of these annealing methods does not forms notable mesostructures. Alteration of film thickness and the solvent annealing time can lead to the formation of different types of mesostructure.

Blending of a **PFS** BCP with a different incompatible BCP has shown to allow the preparation of host-guest-type hybridised thin films that cannot be prepared with an individual **PFS** BCP on its own.[269] For example, blending of **PS-*b*-PDMS** and **PS-*b*-PFDMS** BCPs has afforded hexagonally perforated lamellae thin films with **PFDMS** "guest" spheres, coated in **PS** spheres in a **PDMS** "host" matrix. These kind of hybrid films are unattainable without blending of two BCPs.

The effects of confinement upon the self-assembly of **PS-*b*-PFDMS** diblock copolymer has been studied in order to understand how topographically patterned substrates affect the packing and morphology obtained.[270-273] **PS-*b*-PFDMS** thin films were assembled under confinement in etched nanochannels with differing widths (30 – 80 nm) followed by O_2 RIE.[273, 274] When the row spacing of the diblock copolymer and the channel width were equal, spheres of **PFDMS** were formed. As the width of the nanochannels increased, hence becoming incommensurate to the period of the BCP, elliptical domains were obtained due to distortion of the **PFDMS** spheres, as shown in Figure 23. Once the nanochannel became wide enough to support a second row of spheres the ellipsoidal distortion was removed. Confinement in V-shaped grooves promoted the formation of a well-ordered face-centred cubic (fcc) close packed sphere morphology within the trough; this is in contrast to the body-centred cubic (bcc) packing that is obtained with the equilibrium bulk state. Studies into the topographical ordering of a statistical BCP **PI-*b*-PFDMS-*stat*-PFEMS** has also been reported.[275] These manipulations of the BCP morphologies using different substrates are seen as a useful route for the formation of new geometries and features *via* BCP lithography.

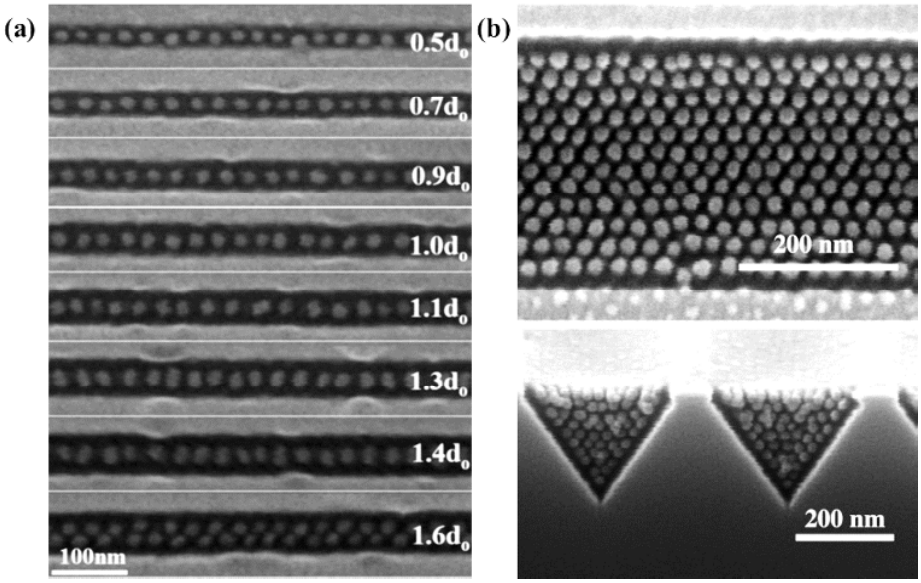

Figure 23. SEM images of **PS-*b*-PFEMS** thin films following O_2 RIE in (a) channels of different confinement widths (b) and in V-shaped grooves Reproduced with permission from references [273, 274].

The effect of periodic 3D confinement on the behaviour of a **PS-*b*-PFEMS** in two different colloidal crystal (CC) templates was examined by TEM and energy-dispersive X-ray spectroscopy (EDX).[276, 277] In the bulk state with no confinement a lamellae structure was observed. In the CC lattice consisting of air spheres in a silica matrix, concentric shells were obtained, whilst in a CC lattice composed of silica spheres in an air matrix, a lamellae structure oriented perpendicular to the silica spheres was observed.

5.1.2. Self-Assembly of Linear PFS Triblock Terpolymers to Form Phase-Separated Materials

Although diblock copolymers are the simplest and most well-studied BCPs for thin film self-assembly, they are mostly limited to simple line and dot pattern geometries which restricts

their potential device applications.[200, 203, 278, 279] By increasing the complexity of the system used, for example by using ABC triblock terpolymers or miktoarm star polymers, a host of previously unattainable morphologies become available with a diverse range of possible geometries and applications. For example, a polystyrene-block-polyferrocenylethylmethylsilane-*block*-poly(2-vinylpyridine) (**PS-*b*-PFEMS-*b*-P2VP**) triblock terpolymer was spin coated and annealed to give bulk and films under different solvent annealing conditions composed of a **PS** core/**PFEMS** shell cylinder morphology in a **P2VP** matrix perpendicular to the film (Figure 24).[229] Thin films of a polyisoprene-block-polysyrene-block-polyferrocenylethylmethylsilane (**PI-*b*-PS-*b*-PFEMS**) and **PI-*b*-PS-*b*-PFEMS/PS** homopolymer blend have been used to prepare nanosquare symmetrical arrays of **PI** and **PFEMS** cylinders in a **PS** matrix.[280] Both of these examples are unobtainable with simple AB diblock copolymers and demonstrate the complexity of the nanostructures that can be achieved with **PFS** BCPs.

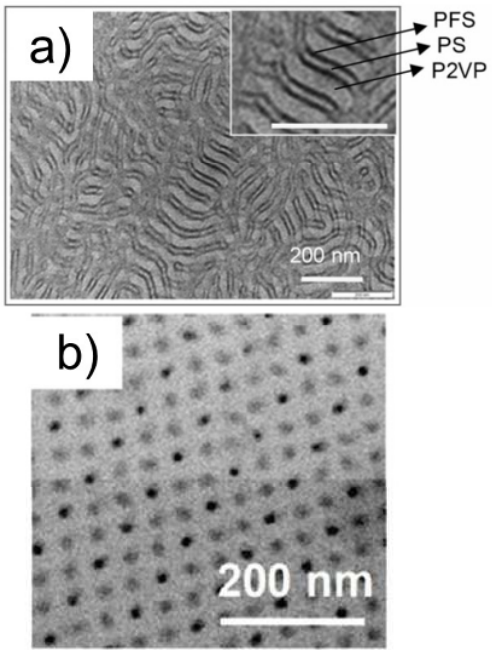

Figure 24. Bright field TEM images of (a) the bulk morphology of **PS-*b*-PFEMS-*b*-P2VP** and b) **PI-*b*-PS-*b*-PFEMS** triblock terpolymers. Reproduced with permission from references [229, 280].

Topographical studies of **PFS** triblock terpolymers have also been performed. The **PI-*b*-PS-*b*-PFEMS/PS** blend were also attempted on silicon substrates with shallow grooves etched into the surface.[280, 281] The orientation of the **PFS** cylindrical domains could be manipulated by treatment of the substrate with a **PS** brush whilst the periodicity of the square array templates could be controlled upon varying trench width. Increasing the thickness of the film allowed the formation of in-plane cylinders where the influence over their orientation once again could be controlled using a **PS** brush. Preferential wetting of the central **PS** block to the trench wall alters the lattice vector of the **PFEMS** square array from 90° to 45° with respect to the trench edge. In addition, the grain size of the square pattern could be greatly increased to several microns.[281] This was achieved through a combination of using brush layers, specific solvent annealing conditions and using templates composed of topographical sidewalls and posts.

5.1.3. Self-Assembly of PFS Star Triblock Terpolymers to Form Phase-Separated Materials

A miktoarm star polymer is a star polymer consisting of arms with different chemical composition coming off a central core. The simplest miktoarm star material with each arm with different composition is a μ-ABC miktoarm star, with one arm each composed of polymers A, B and C respectively. These materials have shown interesting bulk self-assembly with complex and novel morphologies,[282] such as Archimedean tiling patterns. However, until recently thin film behaviour of miktoarm star polymers or the possible extension to their

use in nanolithography had not been investigated. Examples of these types of morphologies are shown in Figure 25 for a range of polyisoprene-*arm*-polystyrene-*arm*-polyferrocenylethylmethylsilane (***μ*-ISF**) miktoarm star terpolymers where different polymer block lengths afforded cylinders, lamellae and two different Archimedean tiling patterns.[246]

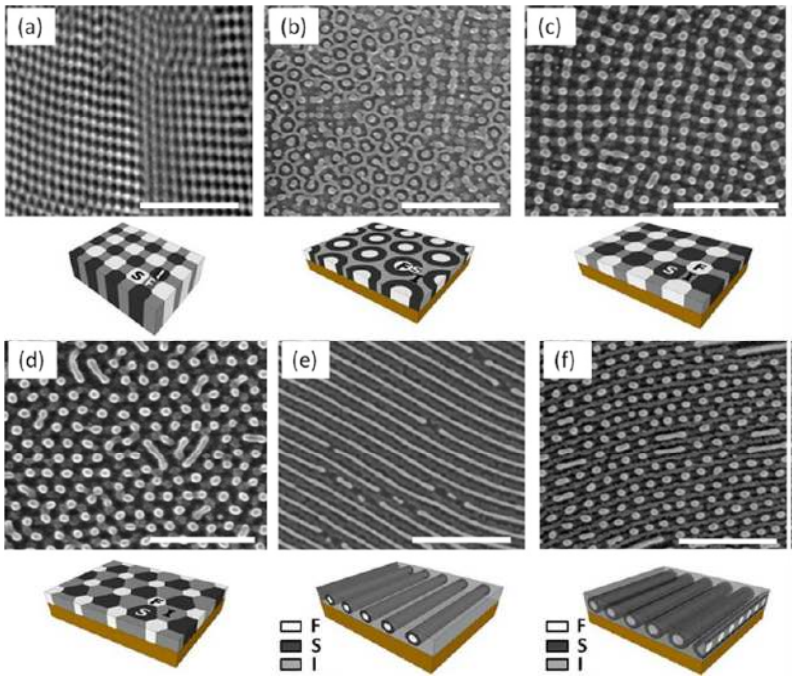

Figure 25. Images and microscopy images of some of the obtained morphologies of ***μ*-ISF**; (a) TEM image of unblended bulk film; (b-d) SEM images of thin films blended with varying amounts of **PS** homopolymer on Si wafer; (e, f) SEM images of thin films blended with varying amounts of **PS** homopolymer on **P2VP**-coated surface. Scale bars are 200 nm. Reproduced with permission from reference 266.

5.2 Applications of PFS BCP Thin Films

The incorporation of blocks containing inorganic elements together with complementary organic segments into BCPs is desirable as such materials typically have high χ values and

greater etch selectivity when compared to all-organic materials.[283-287] The presence of iron and silicon atoms into the backbone of **PFS** means that it has a high resistance to reactive ion etching (RIE) when compared to organic polymers.[257] For example, PMMA has an O_2 RIE etching rate of 200 nm min^{-1}, whilst **PFS** has an etching rate of 4 nm min^{-1}.[197, 288] Films containing **PFS** have shown the formation of an iron/silicon oxide layer at the film surface, in contrast to many organic polymers which are volatised and are removed from the surface. This allows the formation of nanopatterned surfaces of **PFS** after the removal of organic coblocks with a variety of uses and applications.[5, 6, 287, 289, 290]

5.2.1. PFS BCP Thin Films for Carbon Nanotube Formation

Periodic **PFS** nanodomains have been shown to be converted into iron-containing nanostructured ceramics that can be utilised as catalysts in the formation of single-walled carbon nanotubes (SWCNTs).[291-294] **PS-*b*-PFEMS** thin films were self-assembled and treated with UV-ozone to remove volatile organics and convert non-volatile inorganics into SiO_2 and Fe_2O_3. After pyrolysis, the films were used for chemical vapour deposition (CVD) growth of SWCNTs, which were subsequently characterised by scanning electron microscopy (SEM), atomic force microscopy (AFM), X-ray photoelectron spectroscopy (XPS) and Raman spectroscopy. Films with uniformly distributed SWCNTs were prepared where the growth density was easily and reproducibly controlled. Figure 26a shows a SEM image of a SWCNT array prepared by CVD onto a **PS-*b*-PFEMS** film.[293] The ability of PFS BCP to generate catalytically-active Fe nanoparticles for the formation of SWCNTs is significantly greater than that shown by PFS homopolymers. This appears to be a consequence of the formation of smaller, higher surface area particles from confined PFS nanodomains.[295] Multi-walled

carbon nanotubes (MWCNTs) have been grown off of **PS-*b*-PFEMS** films by an analogous method using a plasma treatment approach.[291]

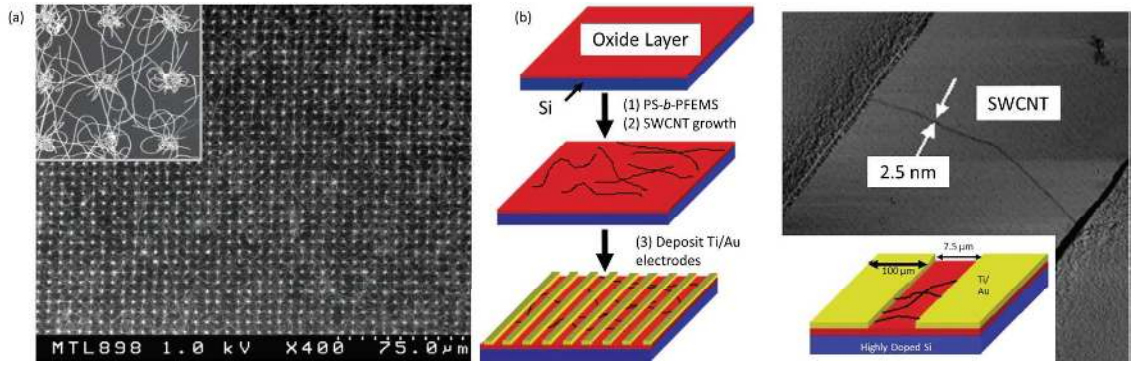

Figure 26. (a) SEM images for single-walled carbon nanotubes (SWCNT) synthesised by chemical vapour deposition (CVD) with **PS-*b*-PFEMS** derived catalytic ceramic particles; (b) schematic and AFM height images of high throughput field effect transistors (FET) prepared from SWCNTs via **PS-*b*-PFEMS** derived catalytic ceramic particles. Reproduced with permission from references [293, 296].

The SWCNTs grown from **PS-*b*-PFEMS** films could then be used in high throughput individually addressable field-effect transistors (FETs) with high device yield (96%).[296] The schematic in Figure 26b shows the method for the preparation of high throughput FETs from SWCNTs. Facile preparation of over 160 devices on a 15 x 15 mm^2 chip were achieved which are ideally suited to a variety of nanoscale sensing applications due to the excellent uniformity and dispersity of the SWCNT films. In a similar vein, self-assembled **PS-*b*-PFEMS** films containing a Co catalyst has been used as a template for the generation of suspended SWCNTs across a large surface area.[297]

5.2.2. PFS BCP Thin Films for Nanolithography and Nanotemplating

The ability for BCPs to phase separate into a number of different morphologies has meant they have generated significant interest in nanolithographic applications.[203, 287, 298-304] BCPs with a metalloblock have garnered significant attention with respect to the formation of nanotemplates. One of the earliest examples involves the formation of arrays of tungsten-capped cobalt nanodots using a **PS-*b*-PFEMS** diblock copolymer thin film, which is outlined in the schematic in Figure 27.[305] First, the diblock copolymer was spin-coated followed by O_2 and a subsequent CF_3H RIE, removing the PS matrix and underlying silica layer respectively. Further CF_4 + O_2 RIE and successive ashing allowed direct pattern transfer to the underlying tungsten layer. Finally an ion beam etch was used to form the desired tungsten-capped cobalt dots which has dimensions and whose pattern is inherent of that of the original **PS-*b*-PFEMS** film. These methodologies are promising for the preparation of high density materials for data storage.

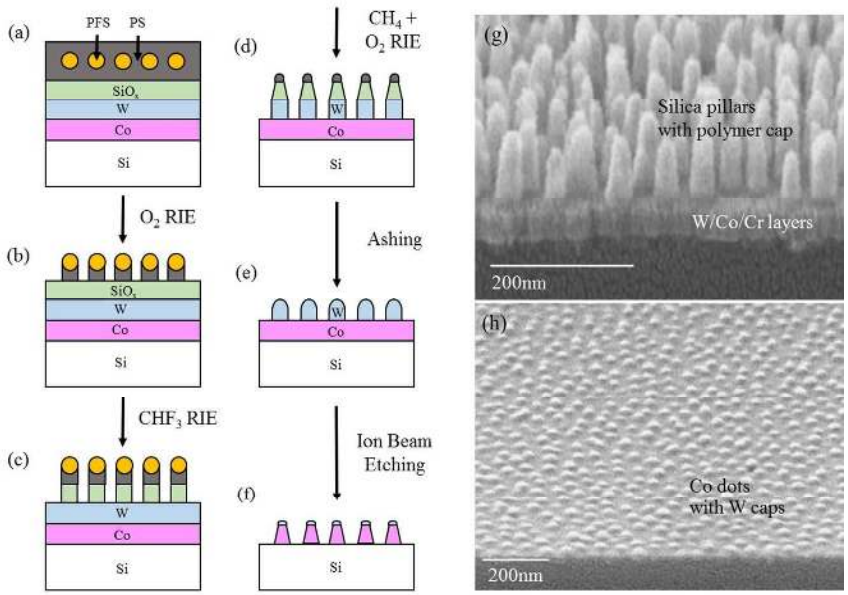

Figure 27. Schematic (a-f) for the fabrication of W-capped Co nanodot arrays using **PS-*b*-PFEMS** thin film BCP lithography and TEM images for (g) the preparation of silica pillars with polymer cap and (h) Co nanodots with W caps. Reproduced with permission from reference 305.

Densely packed arrays of high aspect ratio (> 200) single crystalline Si nanowires have been prepared using a similar combined approach of metal-assisted etching and BCP lithography.[306] Gratings were also used to show effective preparation of high aspect-ratio Si nanowires on topographical substrates which facilitate the application of these arrays as photonic and sensing devices.

Similar methods have been used for the preparation of a nanotextured Ag surface from a **PS-*b*-PFEMS** diblock copolymer.[307] Initially a thin film of the diblock copolymer was self-assembled into hexagonally close-packed standing cylinders of **PFS** in a **PS** matrix, followed by UV-ozonation to remove the matrix and convert the **PFS** into iron/silicon oxide nanocylinders. A thin layer of Ag was then sputtered over the cylinders to afford the nanotextured silver surface (Figure 28). Such materials have great promise as Surface Enhanced Raman Spectroscopy (SERS) substrates. In this case, Raman spectroscopic analysis of adsorbed benzenethiol showed uniform enhancement factors of up to 10^6. Significantly, this system can be tailored effectively to change the size and spacing of the cylinders merely by changing BCP segment lengths, as well as allowing facile reproduction and fabrication of uniformly enhancing SERS-active substrates.

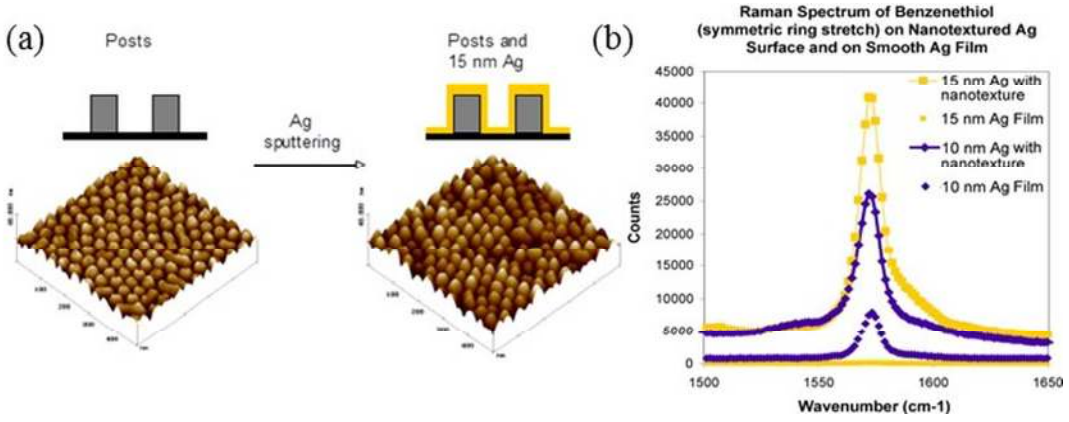

Figure 28. (a) Schematic and corresponding AFM height images for the preparation of a silver nanotextured surface for SERS using a **PS-*b*-PFEMS** diblock copolymer thin film; (b) corresponding SERS of benzenethiol on nanotextured Ag films. Reproduced with permission from reference 307.

A sample of **PS-*b*-PFEMS** BCP that forms cylindrical domains of the metalloblock has been pyrolysed following self-assembly into a thin film with an orientation of the **PFEMS** cylinders perpendicular to the substrate. Crosslinking of the **PS** using UV-light followed by pyrolysis at 600 °C afforded arrays of magnetic ceramic cylinders that were characterised by magnetic force microscopy.[308]

A **PS-*b*-PFiPMS** BCP has been used to prepare wire grid polarisers with extremely high aspect ratios over cm^2 areas.[309] Firstly, an amorphous layer of silicon (α-Si) was deposited onto a fused silica substrate by plasma-enhanced chemical vapour deposition (PECVD). This was followed by spin coating a thin film of **PS-*b*-PFiPMS** which was shear aligned and the resulting **PS** domains were removed by O_2 RIE. Finally, the α-Si layer is deeply and anisotropically etched through the BCP mask layer by SF_6 using the Bosch process. The substrates were characterised by SEM, AFM and UV/visible spectroscopy, showing the formation of α-Si nanowire grids with widths of 15 nm and heights of 80 nm (see Figure 29). These grids can be used as wire grid polarisers on UV-transparent substrates, with polarisation efficiencies as high as 90% for deep UV light (193 nm), significantly greater than for other reported compact transmission polarisers.

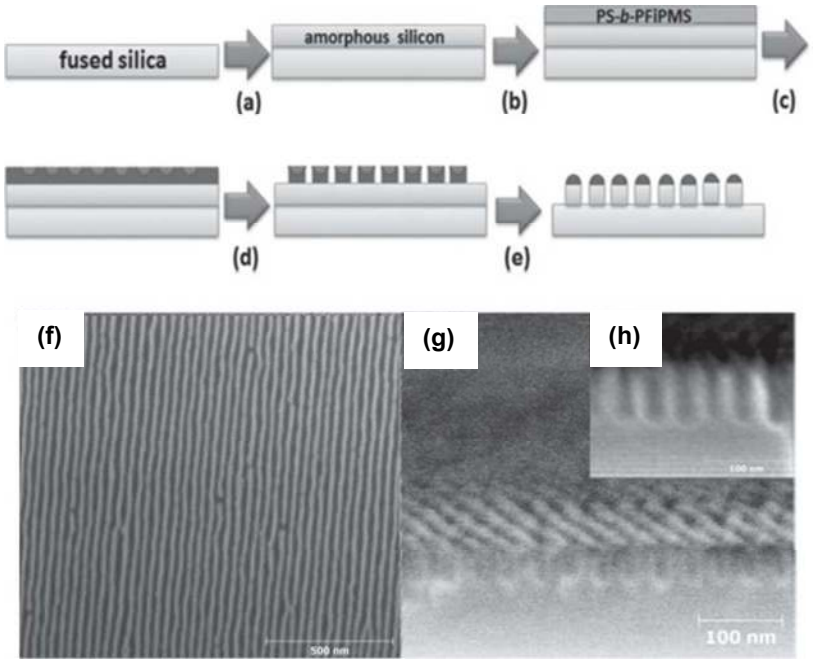

Figure 29. (a-e) Schematic for fabrication of high aspect ratio wire grid polarisers formed from **PS-*b*-PFiPMS** diblock copolymer thin films; (f) SEM images of wire grid polarisers after Bosch etching and (g, h) of cross-sections formed by etching of α-Si layers. Reproduced with permission from reference 309.

Using the same **PS-*b*-PFiPMS** diblock copolymer, large-area nanoscopic square arrays of distinct layers of the BCP were prepared that had been shear-aligned perpendicular to each other.[310] This in turn allowed the fabrication of dense, substrate-supported arrays of different nanostructures depending on the final step, as shown in Figure 30. Initially the diblock copolymer was spin coated onto the substrate and film ordering was induced by shear alignment. The film was exposed to UV irradiation to cross-link the **PS** block. A second layer was subsequently spin-coated on top of the first layer and aligned with the same shearing conditions perpendicular to the directionality of the first shear, followed by removal of the **PS** matrix by O_2 RIE to give a nanosquare grid composed of **PFiPMS** residues (Figure 30e). These domains' resistance to SF_6 RIE allowed the preparation of nanowells by deep Si

etching *via* the Bosch process (Figure 30f), giving wells up to 80 nm deep, which could potentially be used to contain individual biomolecules or as a master mould nanoimprint lithography. Treatment by controlled wet etching with 5% HCl yields a square array of nanoposts (Figure 30g), which could be used to permit further pattern into the substrate. If the nanosquare grids are treated by metal evaporation and subsequent lift-off by sonication in 5% HCl, metal nanodot arrays are formed (Figure 30h) which are of particular interest for high density magnetic storage and plasmonics. The pattern symmetry of these structures can easily be manipulated by changing the molecular weights of the BCPs and through controlling shear directions, allowing square, rectangular and rhombic structures to be formed.

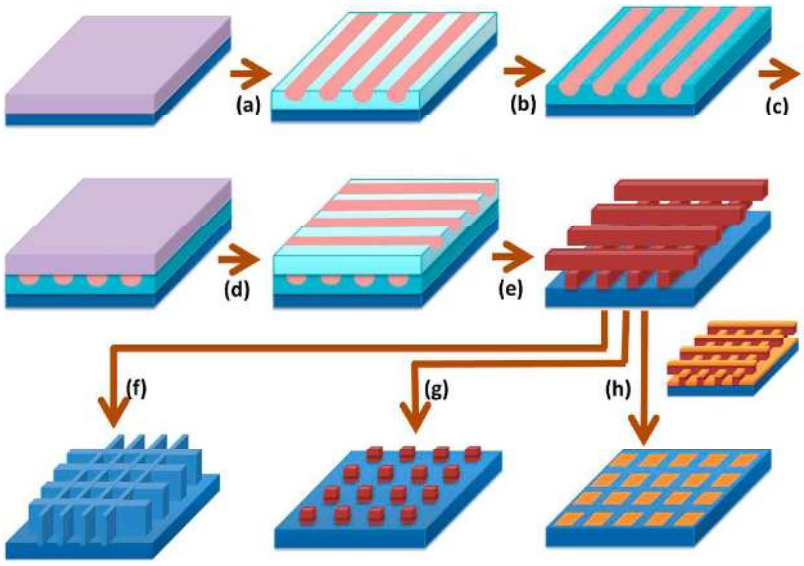

Figure 30. (a-e) Schematic towards the preparation of a cross-pattern by sequential perpendicular shear alignment of **PS-*b*-PFiPMS** diblock copolymer thin films for the subsequent formation of (f) square nanowells, (g) square arrays of nanoposts and (h) metal nanodot arrays Reproduced with permission from reference 310.

Blending of a **PFS** BCP with a different incompatible BCP to form hybridised host-guest-type thin films as previously outlined has allowed the preparation of hollow phase change

memory devices.[311] A **PS-*b*-PFDMS** BCP, when blended with a **PS-*b*-PDMS** BCP, forms hexagonally perforated lamellae thin films with **PS** coated **PFDMS** spheres in a **PDMS** matrix, as outlined previously. These systems were optimised to form dot-in-hole structures on $Ge_2Sb_2Te_5$/TiN/(Ti)W/SiO_2/Si phase-change memory substrates to allow formation of ring-shaped nanostructures through a combination of Pt evaporation and a pattern-reversal process. The high-density nanoring patterns exhibited a low switching current and could be effectively extended to other non-volatile memory device applications.

Nanoscale arrays of rings have been prepared from a **PS-*b*-PFEMS-*b*-P2VP** triblock terpolymer.[229] These are of particular interest in the fabrication of memories or sensors and in quantum devices. Spin-coating and annealing of the material gave a **PS** core/**PFEMS** shell cylinder morphology in a **P2VP** matrix perpendicular to the film substrate with a period of 50 nm, as shown in Figure 31. The **PS** and **P2VP** domains were removed by O_2 RIE, leaving partially oxidised **PFS** nanorings with a diameter and width of 33 nm and 11 nm respectively. The remaining **PFS** pattern could be used as a mold for pattern transfer and was imprinted into a **PS** layer, showing this is a useful system for self-assembled nanolithography.

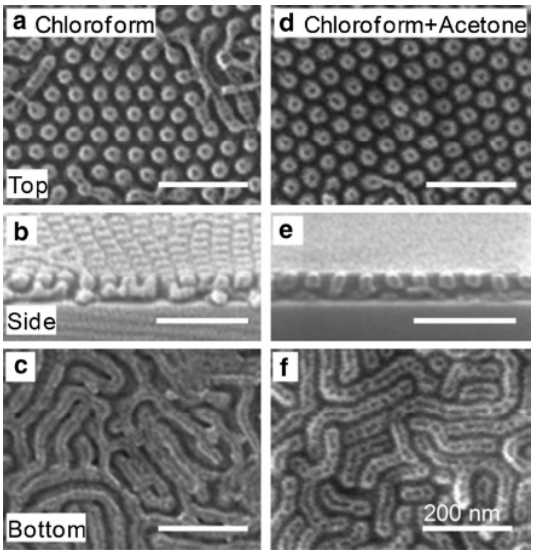

Figure 31. SEM images of **PS-*b*-PFS-*b*-P2VP** diblock copolymer thin films after annealing in (a-c) chloroform and (d-f) a chloroform/acetone mixture for 4 h followed by O_2 RIE; (a, d) plane view, (b, e) side view, (c, f) bottom view. Scale bars are 200 nm. Reproduced with permission from reference [229].

Thin films of **PI-*b*-PS-*b*-PFEMS** and **PI-*b*-PS-*b*-PFEMS/PS** homopolymer blend have been used to prepare square symmetrical arrays.[280] Such a geometry is essential for furthering BCP lithography in areas such as developing array structures in integrated circuits. Square-packed cylinders of **PI** and **PFEMS** in a **PS** matrix were formed in thin films of both materials, however addition of **PS** homopolymer improved the long-range ordering of the morphology by allowing relaxation of the highly stretched triblock terpolymer chains by occupying volume between the **PI** and **PFEMS** cylinders. **PI** and **PS** domains were removed by O_2 RIE to give square-packed **PFEMS** cylinders with a 40.5 nm period. This pattern was transferred into a 30 nm thick silica film by successive CF_4 RIE and O_2 RIE (see Figure 32), affording silica posts 30 nm in height and 20 nm in diameter with a greater aspect ratio than that of the original **PFEMS** posts.

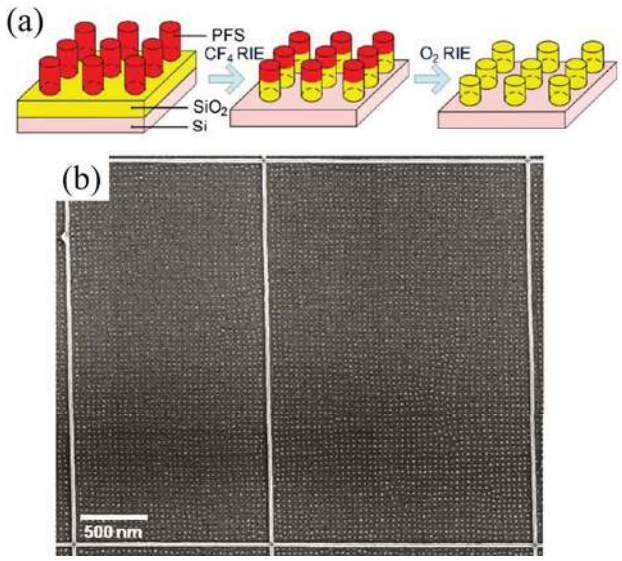

Figure 32. (a) Schematic for formation of pattern transfer to prepare square arrays of silica posts from **PI-*b*-PS-*b*-PFS** diblock copolymer thin films; (b) corresponding SEM image showing highly-ordered square arrays of **PFS** microdomains within topographical HSQ sidewalls. Reproduced with permission from references [280, 281].

Surface reconstruction of thin films of a **PI-*b*-PS-*b*-PFEMS/PS** blend resulted in either a positive pattern of **PFEMS** posts by O_2 RIE or a negative pattern of holes using a selective solvent for the **PI** block. Square arrays of posts, pits and inverted pyramids were fabricated in silicon substrates by dry and wet etching processes.[312] Coexisting post and hole patterns could also be formed.

The negative hole pattern described above has been exploited in the hierarchical templating of $BiFeO_3$-$CoFe_2O_4$ multiferroic vertical nanocomposites, which is outlined in the schematic in Figure 33.[313] A thin film of **PI-*b*-PS-*b*-PFEMS/PS** blend with the negative hole pattern was prepared on a Nb-doped $SrTiO_3$ substrate by surface reconstruction in hexane (a **PI** selective solvent). The residual polymer layer of **PI** on the bottom of the holes was removed by a short O_2 RIE. The pattern was used as a mask to etch pits into the substrate by wet etching with aqua regia, followed by calcination to remove the polymer template. $CoFe_2O_4$ nuclei were selectively grown into the pattered pits and a thin layer of $BiFeO_3$ was deposited to cover the unetched area of the substrate. The $BiFeO_3$-$CoFe_2O_4$ thin film was then used as a guide to grow a thick layer of the nanocomposite, composed of $CoFe_2O_4$ pillars in a $BiFeO_3$ matrix. This hierarchical process whereby one self-assembling system templates the epitaxial growth of oxide nanocomposite films could allow the incorporation of multiferroic nanocomposite structures into magnetic memory or logic devices.

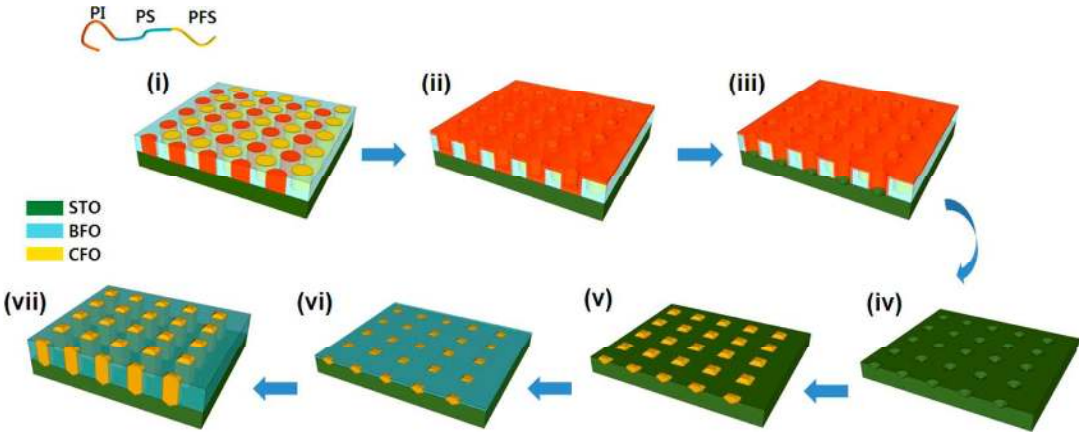

Figure 33. (i-vii) Schematic for the fabrication of a templated $BiFeO_3$-$CoFe_2O_4$ nanocomposite thin film by thin film self-assembly of **PI-*b*-PS-*b*-PFS/PS** blend. Reproduced with permission from reference 313.

Thin film self-assembly of a ***μ*-ISF** miktoarm star polymer blended with PS homopolymer was then studied towards the preparation of 2D Archimedean tiling patterns to be utilised in nanolithography.[266, 314] Self-assembly was achieved by solvent vapour annealing in chloroform, and samples were characterised by SEM, TEM and AFM. A range of Archimedean tiling patterns were obtained, as shown in Figure 25, and the morphology could be controlled by altering solvent annealing conditions, amount of blended homopolymer used and the substrate used. Pattern transfer from the tiling arrays was demonstrated following CF_4 and O_2 RIE to remove the **PI** and **PS** domains, leaving only oxidised **PFEMS** domains and the resulting pattern was effectively transferred into a silicon substrate. These kind of geometries are not obtainable through linear BCPs and can provide a toolset for the preparation of novel patterns for nanolithographic applications, as well as the potential to form a range of surfaces with chemical heterogeneity that can be used in a host of nanoscale devices.

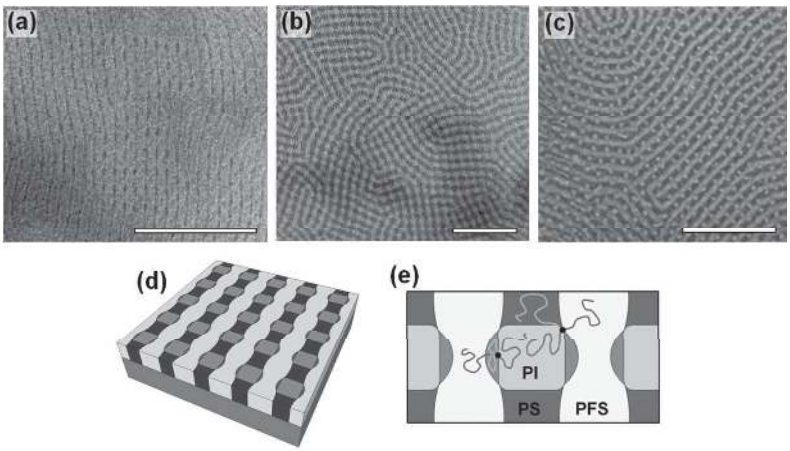

Figure 34. TEM images of ***μ*-ISF** (a) before staining and (b) after staining with OsO_4; (c) SEM image of bottom interface of ***μ*-ISF**; schematics showing (d) thin film patter and (e) its chain conformation within the microdomain. Scale bars are 300 nm. Reproduced with permission from reference 315.

The self-assembly behaviour of the neat ***μ*-ISF** miktoarm start polymer was studied, which yielded a novel morphology described as a "knitting pattern", a morphology that had been previously predicted from simulations (see Figure 34).[315] Films were prepared by spin-coating onto silicon wafers followed by solvent vapour annealing in chloroform, giving films that showed extraordinary periodicity composed of undulating **PFEMS** lamellae and alternating **PI** and **PS** cylinders. The morphology of the knitting pattern could be controlled by altering the film thickness and the etching process. Interestingly some films showed sharp 90° bends and T-junction configurations which had only previously been seen with diblock copolymers by using topographical or chemical templates. Transfer of various patterns into silicon substrates was also possible by RIE of the films.

5.2.3. Redox-Properties: Fabrication of Surface Relief Gratings and Protein Arrays

Stable surface-relief gratings (SRGs) can be written into complexes of phase-separated **PFS** block polyelectrolytes assembled with azobenzene-based surfactants.[316] The presence of the redox-active and etch-resistant **PFS** polymer allows the SRGs to be post-modified. For example, on oxidation, enhancement of the modulation depth occurs, allowing feature sizes to be tuned. In addition, as a result of their excellent etch resistance, the organic components can be removed leaving behind ceramic SRGs.

The controlled adsorption of the iron-containing cage protein ferritin to stimuli-responsive self-assembled **PS-*b*-PFEMS** BCP thin films has also been studied.[317] A thin film with an orientation of the **PFEMS** cylinders perpendicular to the substrate was prepared. To prevent any spontaneous protein adsorption on either block, the electrolyte pH was selected to leave the ferritin negatively charged, and the protein concentration and solution ionic strength were carefully tuned. Selective adsorption of ferritin on the **PFS** domains of the self-assembled thin films was triggered in situ by applying a positive potential, simultaneously oxidising the **PFS** and attracting the ferritin electrostatically.

5.3 Self-Assembly of PFS BCP in Solution

5.3.1 General Considerations for PFS BCP Solution Phase Self-Assembly

The solution self-assembly of organic coil-coil BCPs has been very well studied. These materials self-assemble in block-selective solvents to form core-shell or corona nanoparticles

referred to as micelles.[207, 208, 318, 319] It is well established that the increase in volume of the solvent-swollen corona relative to the dry state favours curvature of the core-corona interface. Generally, the effect causes phase diagrams of BCPs in selective solvents to be shifted so as to generate an expanded region of phase space corresponding to the spherical morphology relative to the analogous phase diagram in the bulk state. For BCPs with relatively short coronal chain lengths relative to those for the core-forming block an extraordinarily broad range of morphologies have been characterised. These are often difficult to predict in advance. The lack of predictability and increased complexity compared to self-assembly in the bulk state arises from two main factors. First, additional competing interactions between the different blocks and the solvent exist. Second, the low or negligible rates of unimer exchange for micelles formed by high molar mass amphiphiles leads to a high propensity to form kinetically-trapped rather than equilibrium structures.[320]

As anticipated based on the well-established behaviour of all-organic analogues, **PFS** BCPs also form micelles in selective solvents. The presence of **PFS** in the core or corona is attractive for a variety of applications based on the properties of the material established through the studies of the homopolymer (see Section 3). To date, the vast majority of the reported investigations have focused on micelles in which the **PFS** constitutes the solvophobic block that forms the micelle core to minimise enthalpically or entropically unfavourable interactions with solvent molecules. Colloidal stabilisation is provided by the swollen solvophilic corona formed by the complementary organic or inorganic solvophilic block.

As for the studies in bulk and thin films, many of the investigations of **PFS** BCPs in solution have aimed to exploit the inherent functionality provided by the **PFS** block. In addition,

studies of the solution self-assembly of **PFS** BCPs have made an unexpected contribution to the broad field of polymer and colloidal science through the emergent discovery of a process termed "Living Crystallisation-Driven Self-Assembly (CDSA)". Living CDSA provides a route to nanomaterials with tailored complexity and dimensions that is of potentially broad significance and this method is discussed within the following sections below.

5.3.2. Crystallisation-Driven Self-Assembly of PFS BCP in Solution

The overwhelming majority of the literature reports on BCP self-assembly in solution involve materials in which the core-forming block does not crystallise. Studies of the self-assembly of BCPs with an amorphous **PFS** core-forming block reveal behaviour that is broadly similar to that observed for the well-studied all-organic analogues. Nevertheless, the redox-activity of the **PFS** block has been utilised to create stimuli-responsive self-assembling systems that reversibly form micelles on oxidation and disassemble on reduction.[321] Redox-active vesicles with a cationic **PFS** polyelectrolyte as the corona have also been prepared.[322]

Investigations of BCPs with a short crystallisable **PFDMS** core-forming block in the late 1990s revealed highly unexpected results with a preference for the formation of micelles with lower mean curvature of the core-corona interface such as cylinders rather than spheres.[47] This subsequently led to the discovery that the crystalline cores at the micelle termini were able to elongate by the addition of further BCP.[323] The use of small seed micelles (generated by sonication of longer cylinders) as "initiators" led to a process that is analogous to a living covalent polymerisation of molecular monomers.[324] This process, termed "Living Crystallisation-Driven Self-Assembly (CDSA)", permits control of micelle dimensions, the

formation of low polydispersity samples, and the formation of segmented or "block comicelles" (see the next section, 5.3.3).

BCPs with a **PFS** core-forming block that is symmetrically substituted at silicon (e.g. R = R' = Me, **PFDMS**; R = R' = Et, **PFDES**) and is able to crystallise can self-assemble in various solvents to produce a number of different micellar morphologies including cylinders,[254, 255, 325] tubes,[326-328] fibres,[329] platelets[220] and, if the core-forming block does not crystallise, usually spheres.[47, 225, 330] As an example, when a sample of **PFDMS$_{50}$-*b*-PDMS$_{300}$**, with a block ratio of 1:6, was heated and cooled in a selective solvent for the **PDMS** block such as *n*-hexane, cylindrical micelles were obtained composed of a **PFDMS** core and a **PDMS** corona. These nanostructures are easily visualised by TEM because the **PFDMS** core is electron-rich, allowing effective contrast for imaging without the need for staining.[255] The crystallisation of the core-forming **PFDMS** was believed to be the driving force for the formation of a cylindrical rather than spherical morphology, and the ordered nature of the core and the chain packing has been explored by wide angle X-ray scattering (WAXS).[7, 331]

Spherical micelles are obtainable in certain cases such as when cylindrical micelles are heated above the T_m of the **PFS** core-forming block and the solution is then rapidly cooled to prevent core-crystallisation or when an unsymmetrical **PFS** block, such as poly(ferrocenylethylmethylsilane) (**PFEMS**), is the core-forming block.[47, 332, 333] Unsymmetrically substituted **PFS** blocks generally cannot crystallise and, to date, have only been observed to form spherical micelles in solution. This implies that the crystallinity of the core-forming block is a key factor to the formation of one-dimensional micellar structures. BCPs with an amorphous core-forming **PFS** block can undergo redox-controlled micellisation due to an induced polarity change resulting from partial oxidation of the **PFS**

block.[334] Spherical micelles that have been formed with a crystallisable **PFS** block in an amorphous state due to rapid precipitation[225] have been shown to transform into cylinders with a crystalline core after a maturation period in a corona-selective solvent over a period of weeks or months.[335]

The block ratio plays a key role in determining which morphology is obtained.[220] For example, **PI_{320}-*b*-$PFDMS_{53}$** has a block ratio of 6 : 1 (**PI** : **PFS**) and self-assembles into cylindrical micelles in **PI**-selective hexanes, however **PI_{30}-*b*-$PFDMS_{60}$**, which has a block ratio of 1 : 2, forms tape-like platelet micelles (see Figure 14). Although both materials have similar **PFS** block lengths, the significant difference in coronal block lengths has an obvious effect on the morphology formed. As the **PI** coronal block length increases, there are increased coronal repulsions which favours greater curvature at the core-corona interface, and cylindrical micelles are preferred.[47]

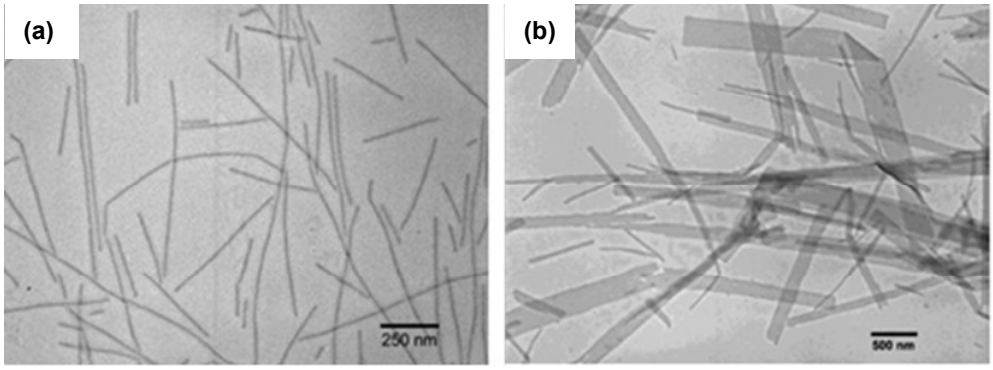

Figure 35. TEM images for the micelles formed from (a) **PI_{320}-*b*-$PFDMS_{53}$** (6 : 1) and (b) **PI_{30}-*b*-$PFDMS_{60}$** (1 : 2) in hexane/THF (9:1) and (7:3) respectively. Reproduced with permission from reference [220].

The effect of molar mass and solvent selectivity upon micellar morphologies and the transitions between these architectures has been investigated.[336] Three **PFDMS-*b*-P2VP**

BCPs were prepared with the same block ratio (1 : 6) but different molar masses and it was shown that sphere-to-cylinder transitions in isopropanol was greatly slowed by increasing the molar mass. Furthermore, increasing the content of THF (a common solvent for both blocks) improved the solvation of the **PFS** core-forming block, which allowed core crystallisation via a plasticisation effect. The morphologies obtained also changed from spheres to cylinders and then to narrow lenticular platelets as the THF content increased.[336]

Shape anisotropic nanoparticles with intrinsic nanostructures within the particles have been reported by self-assembly of an amphiphilic **PFS** BCP in an aqueous mixed surfactant system.[337] Nanosheets with a hexagonal array of **PFS** cylinders in a **P2VP** matrix were formed when a **PFDMS-*b*-P2VP** BCP was self-assembled under neutral wetting conditions (Figure 36a). Self-assembly of the **PFS** BCP with additional **PFS** homopolymer under the same conditions formed ellipsoidal particles with an axially stacked lamellar structure (Figure 36b). These type of structures are in contrast to traditional **PFS** micelle systems as outlined previously. Spatial control over the distinct domains within the nanoparticles was exploited to demonstrate morphological transitions between the two structures.

Several amphiphilic **PFS**-containing BCPs have been shown to be able to self-assemble in water when hydrophilic blocks create the micelle corona.[338, 339] **PFDMS$_9$-*b*-PDMAEMA$_{50}$** was prepared as outlined earlier (see Section 4.1.2.1), and the **PDMAEMA** block quaternised with methyl iodide. Whilst a range of morphologies were obtained for the unquaternised **PFDMS$_9$-*b*-PDMAEMA$_{50}$**, including polydisperse spherical aggregates upon direct dissolution into water, the quaternised analogue was self-assembled into cylindrical micelles upon dissolution in alcoholic solvents. Dialysis of these micelle solutions against water was effective in the preparation of cylinders dispersed in water. The **PFS** core within the micelles

was shown to be amorphous by wide-angle X-ray scattering (WAXS). This was similar for **PFDMS-*b*-PMMA** BCPs[330] upon self-assembly in acetone where variable temperature ^{1}H NMR studies showed an amorphous core in a mobile state and solvent molecules could easily penetrate into the micelle core. It was deduced that the polar solvents used in both these cases were the driving forces for micellisation, with high interfacial energy caused by the exposure of hydrophobic **PFS** core to polar solvents, instead of the crystallisation of the core driving the formation of aggregates.

The introduction of functional groups into the micelle corona allows for the possibility of shell-crosslinking reactions which give rise to a marked increase in the stability for the self-assembled structures.[340-342] BCPs that have corona-forming blocks such as **PI** and **PMVS** with pendant vinyl groups within the polymer backbone have been shown to undergo Pt-catalysed hydrosilylation crosslinking with tetramethyldisiloxane and Karstedt's catalyst,[221, 343-346] or by UV-initiated crosslinking.[34, 347] As a result of this shell-crosslinking, the micellar structures are essentially locked in and are preserved even if they are transferred from a corona-selective solvent into a common solvent for both blocks.[221, 343] For example, cylindrical micelles composed from **PI_{320}-*b*-$PFDMS_{53}$** were self-assembled and the coronal chains were subsequently crosslinked. The micellar solution was dialysed against THF, which is a good solvent for both the **PFS** and **PI** blocks, but there was no discernible difference in structure after transferring into THF (see Figure 36a).[343] Reversible cross-linking of **PI-*b*-PFDMS** BCPs has also been reported.[348] By using only Karstedt's catalyst in the absence of any silanes, crosslinking of the **PI** corona occurs through Pt(0)-olefin coordination which can be reversed through the addition of 2-bis(diphenylphosphine)-ethane (dppe) (see Figure 36b).

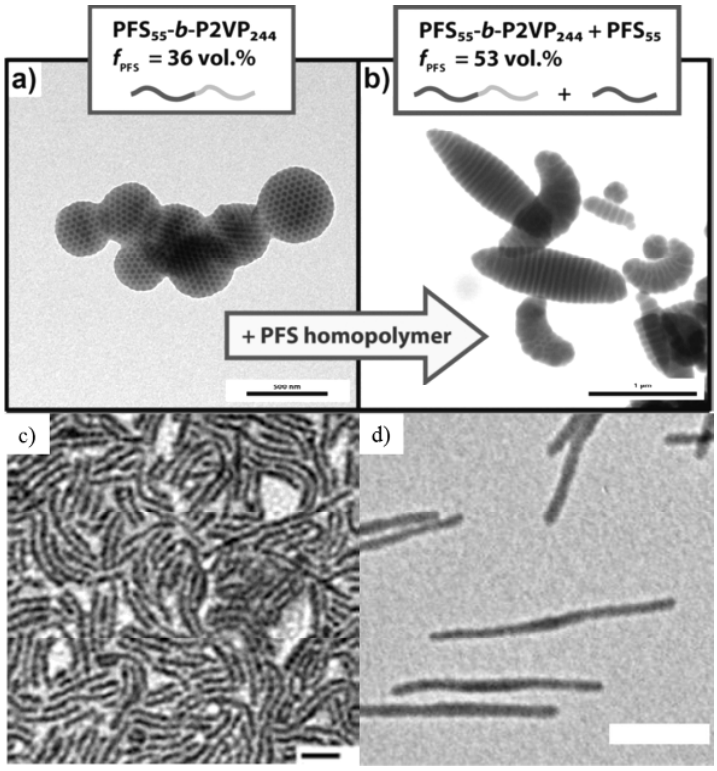

Figure 36. (Top) TEM images showing (a) nanosheets with a hexagonal packed cylinder structure and (b) ellipsoidal particles with an axially stacked lamellar structure formed from blending of **PFS-*b*-P2VP** and **PFS** homopolymer. (Bottom) TEM images showing (c) irreversibly and (d) reversibly crosslinked **PI-*b*-PFDMS** micelles. Scale bars are 250 nm. Reproduced with permission from references [343, 348], and [337].

5.3.3. Living CDSA of PFS BCPs

Control over the growth of **PFS**-containing cylindrical micelles has been demonstrated by using living CDSA approaches.

Initial studies into this area focused on the stability of **PFDMS-*b*-PDMS** cylindrical micelles. Upon ultrasonication of the preformed fiber-like structures, the formation of shorter cylinders through fragmentation of the micelles was observed without any apparent change in the

micelle width.[325] This was also detected for **PI-*b*-PFDMS** cylindrical micelles. Significantly, it was found that addition of further unimer to these short micelles resulted in longer cylinders, with the preformed micelles essentially acting as "seeds" for further unimer nucleation.[323] The length of the micelles depended linearly on the unimer-to-seed ratio and was also found to be of low polydispersity. This demonstrated an analogy with a living covalent polymerisation of molecular monomers.[324] The micelles grown by this method were also shown to be stable with respect to a change in dimensions in the selective solvent at ambient temperature over a period of many months with no change in their average length or the length distribution. This implied that the micelles were kinetically-trapped in that the constituent BCP chains were resistant to significant dynamic exchange between micelles under these conditions. The micelles were stable to fusion in solution over long periods of time; the addition of BCP unimer in solution was found to be required for this process to occur.[349] In addition, when a corresponding diblock copolymer unimer with an amorphous **PFS** block (**PFEMS-*b*-PMVS**) was added, no growth was detected. This seeded growth method exploits the crystallisation of the **PFDMS** block and has been termed as "living" CDSA.[324] Cylindrical micelles with length dispersities of 1.01 and overall length greater than 2 μm have been prepared by this protocol (see Figure 37).[323, 324]

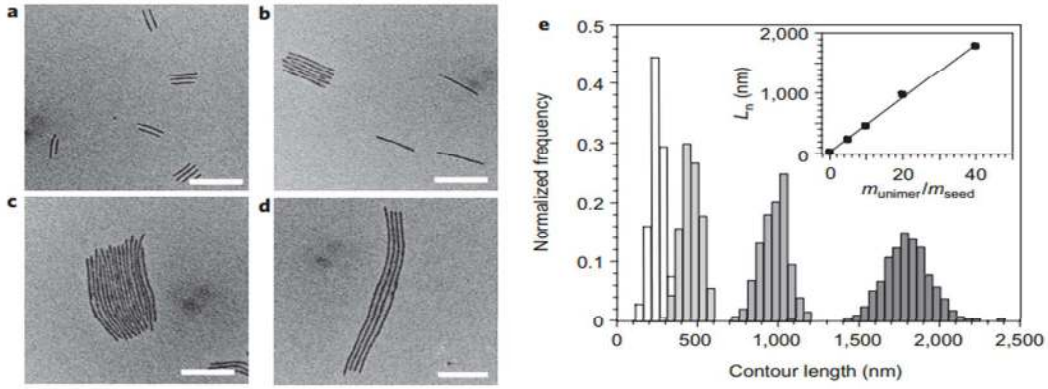

Figure 37. (a-d) TEM images of monodisperse **PFDMS-*b*-PDMS** cylindrical micelles grown from uniform stub-like seed micelles with increasing amounts of unimer solution added; (e) histogram of the contour length distribution of the samples; scale bars are 500 nm. Reproduced with permission from reference 324.

An alternative approach to length control of **PFS** BCP micelles, termed a "self-seeding" process, has also been reported for the preparation of monodisperse cylindrical architectures.[350-353] To facilitate the process, relatively short cylindrical micelles were prepared through ultrasonication of long, polydisperse **PI-*b*-PFDMS** cylinders. Within the **PFDMS** micelle core, regions of different crystallinity and therefore different melting points exist. When heated, the least crystalline domains dissolve first to give unimers. This leaves very short, more highly crystalline seeds. Upon cooling, the dissolved unimer will grow from the remaining seed micelle termini via epitaxial growth to a length that will depend inversely on temperature.

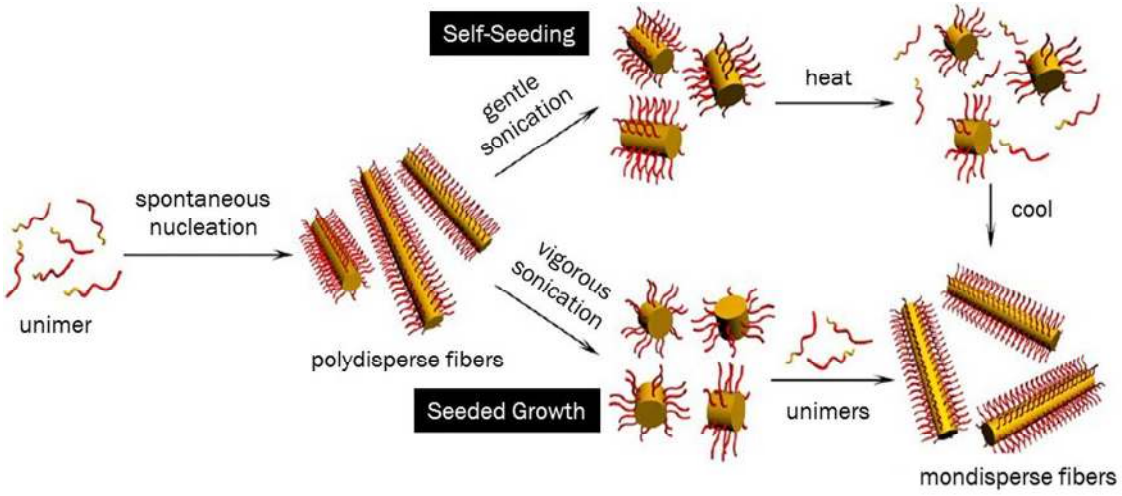

Figure 38. Schematic for the preparation of monodisperse cylindrical micelles by (top) self-seeding and (bottom) seeded growth methods. Reproduced with permission from reference 354.

Block comicelles with spatially segregated regions of different chemistry in the corona can be readily prepared by the sequential addition of different **PFS**-containing diblock copolymer unimers to seeds.[323, 348] For example, addition of **PFDMS-*b*-PMVS** to cylinders of **PI-*b*-PFDMS** created block comicelles with a central compartment with **PI** corona and end compartments with **PMVS** corona whilst having a continuous crystalline **PFS** core. Similar block comicelles were prepared using a **PFDMS-*b*-P2VP** BCPs, where seeds were quaternised, and this was followed by the addition of neutral **PFDMS-*b*-P2VP** unimer to the seed termini. Composite nanostructures have been prepared from this kind of block comicelle through the aggregation of nanoparticles or quantum dots at the quaternised block of the comicelle.[355]

It has been shown that epitaxial growth of cylinder-forming **PFS** BCPs can also occur off of the edges of platelet micelles.[356] When the block ratio for a **PI-*b*-PFDMS** BCP is 1 : 1 (**PI** : **PFS**), platelet micelles are formed selectively over cylinders when self-assembled in a solvent selective for the corona-forming block. These platelet micelles can also be fragmented using ultrasound to form small platelets in the same manner as that for cylindrical micelles, although with much less control over size and polydispersity. Addition of cylinder-forming unimer to the platelet seed micelles resulted in epitaxial growth from only two of the available six faces, forming hybrid "scarf-like" micelles with tassels of uniform length (see Figure 39a). Hollow "scarf-like" micelles have been prepared in an analogous manner by dissolving out a **PFDMS-*b*-PDMS** platelet inside a surrounding layer of crosslinked **PI-*b*-PFS** diblock copolymer.[348]

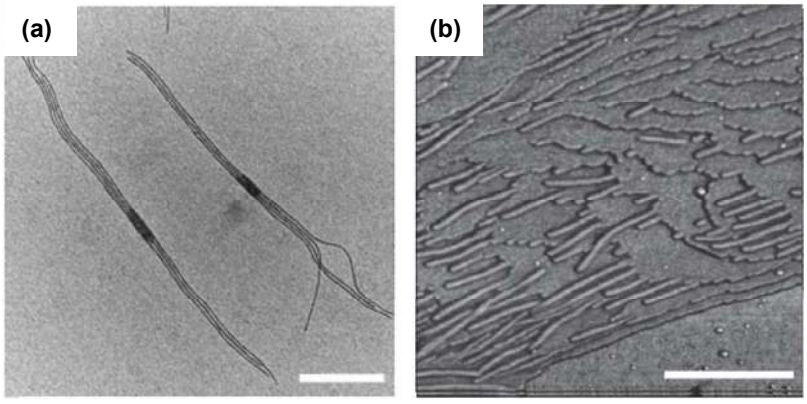

Figure 39. (a) TEM images of "scarf"-like micelles and (b) AFM phase image of cylindrical micelles grown from a PFDMS thin film. Scale bars are 500 nm. Reproduced with permission from reference [356].

Annealed **PFS** homopolymer films have been used to seed the growth of cylindrical micelles.[356] Unimer growth occurred at steps and ridges at the surface of the crystalline substrate corresponding to stacked layers of crystalline lamellae. The cylinders formed off the surface grew parallel to the surface giving a cylindrical micelle mat (see Figure 39b). In addition, epitaxial growth from **PFS** nanocrystals was also demonstrated forming multi-armed micelles that possessed hierarchical "multipod" structures with monodisperse and controllable arm lengths.[357]

Heteroepitaxial growth, where unimer containing one core-forming block can grow off a seed micelle composed of a different core-forming block, has also been reported.[356] In principle, for this to occur, crystal lattice parameters with a mismatch of less than 15% in lattice spacing is required.[358, 359] Poly(ferrocenyldimethylgermane) (**PFDMG**) BCPs, isostructural analogues to **PFS** BCPs, were studied because they had a layer spacing 6% larger than of **PFS**.[360] **PFDMG** BCP unimers were added to both **PFS**-containing monodisperse cylindrical micelles and platelets, resulting in the formation of composite nanostructures via

heteroepitaxial growth. **PFS** BCP unimer was also effectively added to cylindrical micelles with ends composed of a **PFDMG** core.

Addition of BCPs with different composition and functionality can allow the preparation of a variety of discrete, well-defined micelle and block comicelle structures.[355, 361-365] Branched micelles have been prepared by adding BCP unimer with a short **PFS** block to a preformed cylindrical micelle with a core composed of a longer **PFS** block.[366] Monodisperse cylindrical micelles were prepared by seeded growth of **PFDMS$_{48}$-*b*-P2VP$_{414}$**. A unimer solution of **PFDMS$_{20}$-*b*-P2VP$_{140}$** was then added to the micelle solution, resulting in epitaxial growth usually of two branches from either end of the seed micelle, as shown in Figure 40A-C. Due to the redox-activity of the core-forming block, one-dimensional arrays of Ag nanoparticles were prepared through in-situ redox chemistry after shell-crosslinking of the **P2VP** corona. Branched micelles of various **PFS**-containing BCPs have been shown to undergo living CDSA under kinetic control.[354] These branched-type micelles offer a promising scaffold for the preparation of more complex branched nanomaterials.

Living CDSA has been effective in the preparation of light-responsive micellar structures with a photocleavable junction at the core-corona interface.[363, 367] **PFDMS-ONB-P2VP** BCPs (**ONB**: *o*-nitrobenzyl junction) were synthesised through a combination of living anionic polymerisation, reversible addition-fragmentation transfer (RAFT) polymerisation and "click" chemistry. The BCPs were self-assembled into monodisperse cylindrical micelles and the coronal chains removed by UV irradiation (see Figure 40D). These materials could then be used effectively to form well-defined branched micelles, as well as **P2VP** nanotubes through crosslinking of the coronal chains.

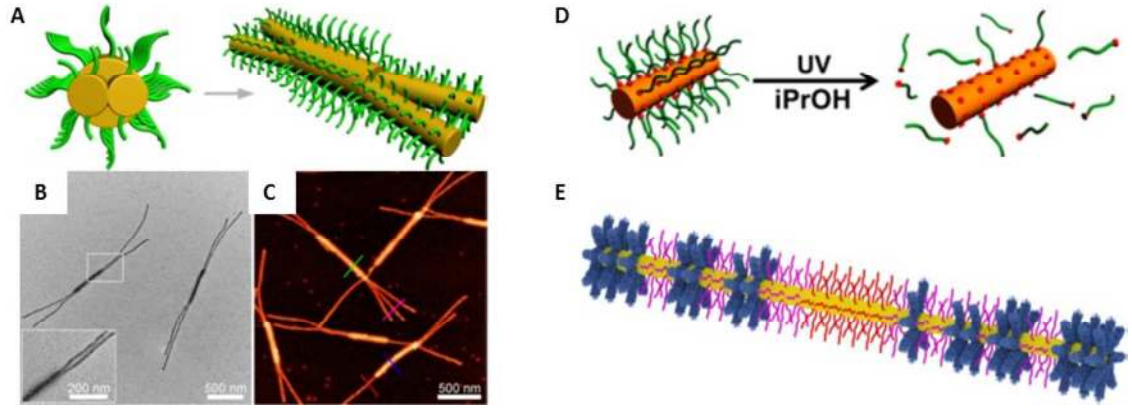

Figure 40. (A) Schematic representation, (B) TEM image and (C) AFM height image of branched comicelles of **PFDMS-*b*-P2VP**; (D schematic representation for coronal photocleavage of **PFDMS-ONB-P2VP**; (E) schematic representation of "patchy" cylindrical block comicelles from gradient CDSA. Reproduced with permission from references [363, 364, 366].

Cylindrical micelles with "patchy" coronal structures have been prepared through the co-assembly of linear **PFDMS-*b*-PMVS** and brush **PFDMS-*b*-PMVS** diblock copolymers that had been functionalised with *n*-alkyl branches off of a **PFDMS-*b*-PDMS** cylindrical micelle (see Figure 40E).[364] Previous attempts at preparing "patchy" architectures by co-assembly of non-brush BCPs had apparently been unsuccessful.[368] Co-assembly of brush BCPs was necessary because the increased steric bulk hindered micelle growth. Tapping-mode AFM showed that co-assembly afforded a gradient type structure with an initial bias for the assembly of the linear **PFDMS-*b*-PMVS** over the brush **PFDMS-*b*-PMVS**, which was reversed slowly as the linear BCP was consumed. A miktoarm-star **PFS**-containing polymer has also been shown to form phase-segregated "patchy"-type cylindrical micelles and comicelles.[369]

5.3.4. Non-Centrosymmetric PFS Block Comicelles

As previously discussed, cylindrical micelles that have corona with pendant vinyl groups are able to undergo shell-crosslinking reactions (see Section 5.3.2). Through a combination of selective micelle corona shell-crosslinking and living CDSA of **PFS**-containing block comicelles, non-centrosymmetric unidirectional micelles have been prepared (see schematic (a, b) in Figure 41).[370] For example, symmetric ABA triblock comicelles with a central **PFDMS-*b*-PDMS** block and outer **PI-*b*-PFDMS** blocks can undergo selective shell-crosslinking of the **PI** corona (Figure 41c, d). If the **PI** corona is sufficiently long, crosslinking can effectively cover the ends of the cylindrical micelle which inhibits the addition of further unimer. The central block can be removed through the addition of common solvent such as toluene to the micelle solution, leaving shell-crosslinked **PI-*b*-PFDMS** micelles with only one open face for unimer addition and solvated **PFDMS-*b*-PDMS** unimer in solution (Figure 41e). Subsequent evaporation of toluene promoted **PFDMS-*b*-PDMS** unimer addition to the **PI-*b*-PFDMS** seeds, forming asymmetric AB diblock comicelles that grow selectively in one direction from the singular open crystalline face of the micelle (Figure 41f-h). Asymmetric diblock comicelles have also been prepared *via* self-assembly of BCP off **PFDMS** homopolymer nanocrystals.[357] A **PI-*b*-PFDMS** BCP unimer solution was added to **PFDMS** nanocrystals, which acted as a nucleation point for the BCP, to give cylindrical micelle arms off the central nanoparticle. The **PI** coronal chains were crosslinked, and a second **PFDMS-*b*-PMVS** unimer solution was added to afford asymmetric AB block comicelles, followed by a second crosslinking reaction for the **PMVS** coronal chains. Dissolution of the **PFS** homopolymer led to the release of non-centrosymmetric AB cylindrical diblock comicelles.

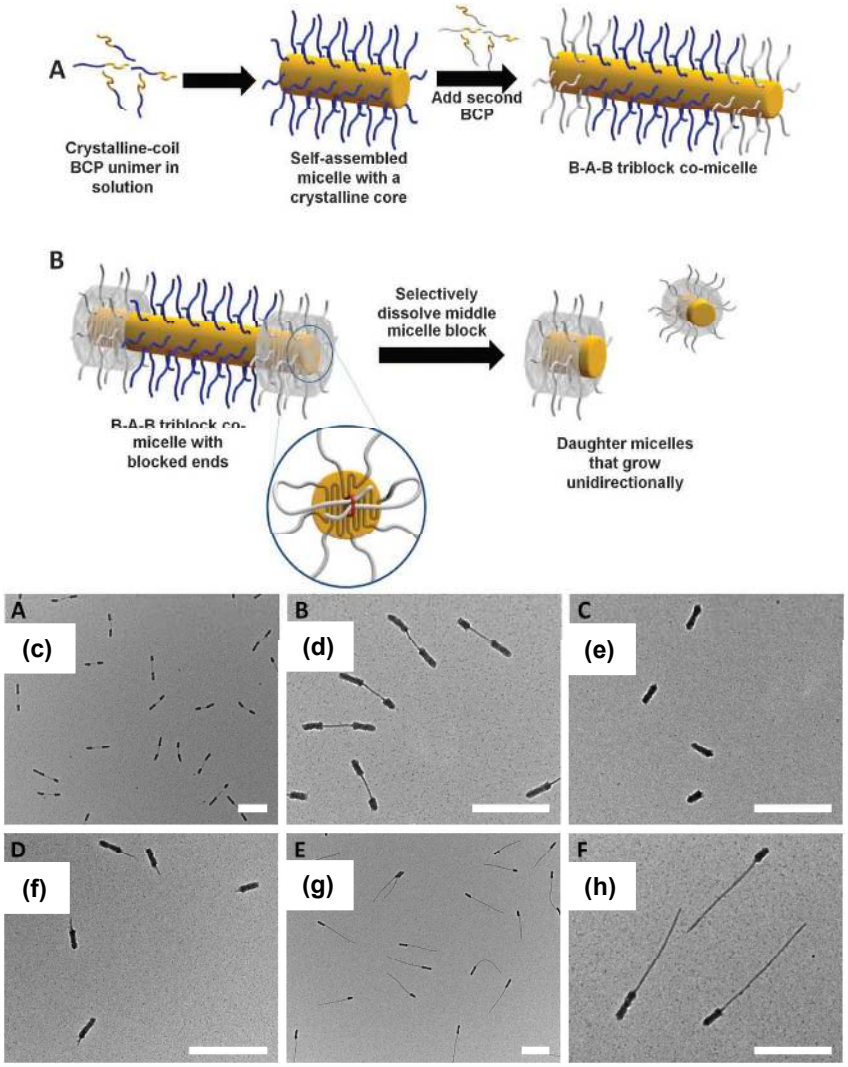

Figure 41. Schematic (a, b) showing the preparation of unidirectional seed micelles; TEM images of (c, d) ABA triblock comicelles with crosslinked end blocks; (e) crosslinked unidirectional A block seed micelles after dissolution of the central block; (f) unidirectional AB diblock comicelles after removal of toluene; (g, h) unidirectional AB diblock comicelles after the addition of further unimer. Scale bars are 500 nm. Reproduced with permission from reference [370].

As an extension of this work, fluorescent non-centrosymmetric multi-compartment block comicelles have been prepared that can act as nanoscale pixels with fully tunable colour

emissions.[347] A **PFS**-containing BCP with a random copolymer corona-forming block (**PFDMS$_{62}$-*b*-[(PDMS$_{605}$)/(PMVS$_{21}$)]$_{626}$**) was prepared through sequential living anionic polymerisation. The pendant vinyl groups on the **PMVS** components within the second block were then functionalised through a thiol-ene "click" reaction with a number of different fluorescent dye molecules to form red, blue and green fluorescent BCPs. Co-assembly of various amounts of these unimers enabled the preparation of cylindrical micelles that emitted different colours depending on the amounts of each fluorescent unimer used. Individual imaging of each coloured micelle could be tracked with laser scanning confocal microscopy (LSCM), revealing that the luminescence distribution was uniform throughout the micelle. Fluorescent BCP unimer was then added to a pre-formed **PFDMS-*b*-PDMS** cylindrical seed micelle, followed by a non-fluorescent **PFDMS-*b*-PDMS** BCP to act as a spacer between each fluorescent block in order to increase optical resolution. This allowed the formation of centrosymmetric 11-block comicelles where each colour represented along the micelle can be individually addressable due to the narrow absorption bands of each dye. Furthermore, by using unidirectional cylindrical seed micelles, non-centrosymmetric 7-block comicelles could be prepared through the sequential addition of each florescent BCP followed by small segments of non-fluorescent BCP (see Figure 42). The regions of colour are stable over long periods with no detected rearrangement of the fluorescent unimers along the length of the cylinders, which indicated that they exist as static, kinetically trapped structures.

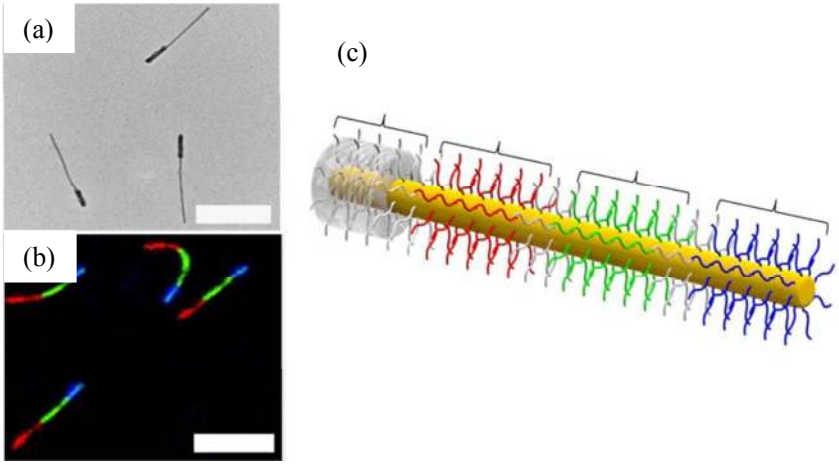

Figure 42. (a) TEM image, (b) LSCM image and (c) schematic representation of non-centrosymmetric RGB "nanopixel" block comicelles. Scale bars are (a) 500 nm and (b) 2 μm. Reproduced with permission from reference [347].

5.3.5. Formation of PFS Supermicelles by Hierarchical Self-Assembly

It has been demonstrated that the level of control over the formation of individual micelles by living CDSA can allow the preparation of a variety of micron-sized superstructures with intrinsic nanodomains of different composition and functionality. For example, the ability to be able to tailor **PFS**-containing block comicelles through the assembly of a variety of BCPs can allow the introduction of amphiphilicity. The resulting building blocks can be used for the preparation of complex hierarchical structures.[371-376]

For example, **PFS** homopolymer can be used to aggregate short BCP cylindrical micelles into networks.[349] End-to end coupling of two or more micelles gave linear, linked or branched structures depending on the composition of the BCP micelle and the **PFS** polymer added.

Cylindrical non-centrosymmetric ABC triblock comicelles composed of two hydrophobic blocks (A and B) and a long hydrophilic block (C) have been shown to undergo hierarchical self-assembly in a selective solvent for the hydrophilic block.[370] The block comicelles self-assembled into star-shaped supermicelles with a "core" composed of the hydrophobic blocks and a "corona" of the hydrophilic blocks.

The use of amphiphilic ABA triblock comicelles as building blocks for hierarchical self-assembly can allow the formation of a range of different supermicellar morphologies (see Figure 43).[377] Block comicelles with a central hydrophobic **PFDMS-*b*-PDMS** block and terminal hydrophilic **PFDMS-*b*-P2VP** blocks can self-assemble upon dialysing the micellar solutions against isopropanol, a selective solvent for the end hydrophilic blocks. Depending on the length of the central B block within the pre-formed micelles, the aggregation number, morphology, packing and symmetry of the resulting supermicelles can be tuned to achieve crossed and elongated network structures.

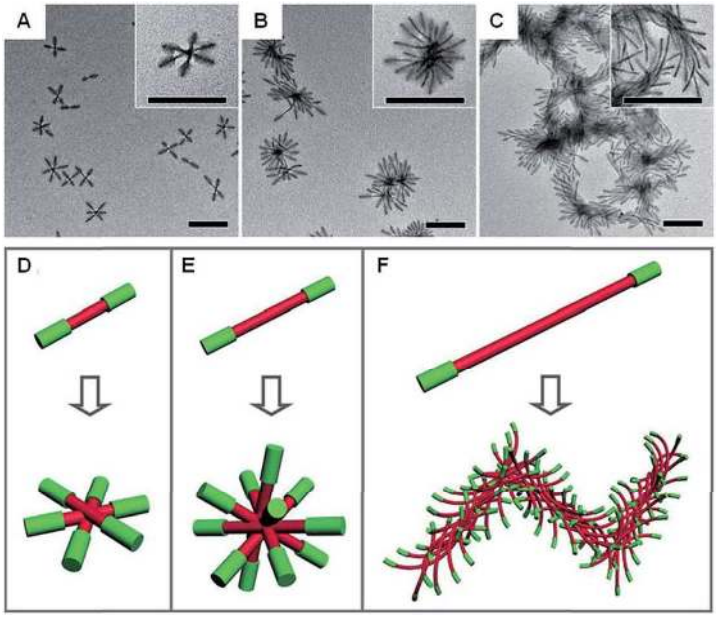

Figure 43. (a-c) TEM images and (d-f) corresponding schematic representations of hierarchical self-assembly of ABA amphiphilic triblock comicelles with different B block lengths after dialysis against isopropanol. Scale bars are 500 nm. Reproduced with permission from reference [377].

As a continuation of this work on amphiphilic block comicelles, it was reported that the resulting micron-scale assemblies can be easily controlled through altering the dimensionality, functionality and ordering of the starting block comicelles.[378] Monodisperse BAB amphiphilic triblock comicelles with either hydrophilic or hydrophobic central or terminal blocks were prepared. These structures were found to stack either side by side in non-solvents for the central block, or end to end in non-solvents for the terminal block, which allows the formation of a variety of 1D and 3D superlattice structures (see Figure 44).[378] These aggregates possess multiple levels of structural hierarchy on length-scales that are normally only apparent in nature. In addition, as the functionality of the micelle coronas is unchanged throughout the self-assembly process from the initial stages to the formation of superstructures. Therefore it is an effective way of incorporating function to these

supermicelles, which is demonstrated by using BCPs tagged with fluorescent dyes, allowing fluorescent superstructures to be prepared.

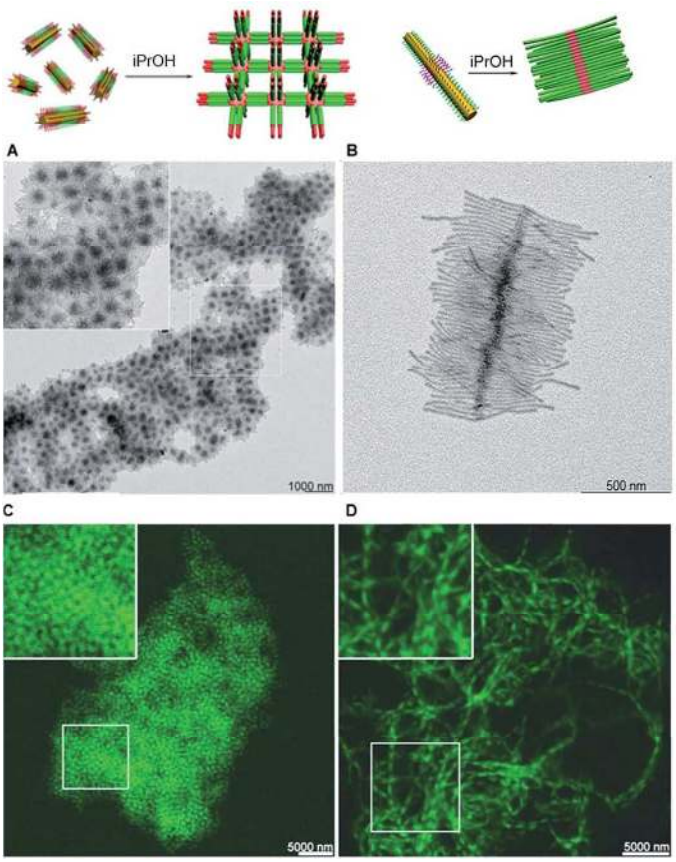

Figure 44. (top) Schematic representations for the formation of 1D and 3D supermicelles and superlattices through stacking of ABA and BAB triblock comicelles; (a, b) corresponding TEM images and (c, d) LSCM images of 1D and 3D supermicelle aggregates. Reproduced with permission from reference [378].

Due to the size of many of these superstructures, they can be observed using optical microscopy techniques and can be efficiently manipulated in three dimensions using optical tweezers. This can allow the fabrication of hierarchical chain-like superstructures *via* crosslinking of "arms" of multiple supermicelles and patterning of supermicelles into arrays

by dynamic holographic assembly, which is outlined in Figure 45.[379] These supermicelles are able to undergo further living CDSA processes and "grow" under flow conditions with a unimer-containing solution. This technique exposes a new method towards creating even more complex superstructures and assemblies through controlled in situ chemistry with diverse functionality and a variety of potential applications.

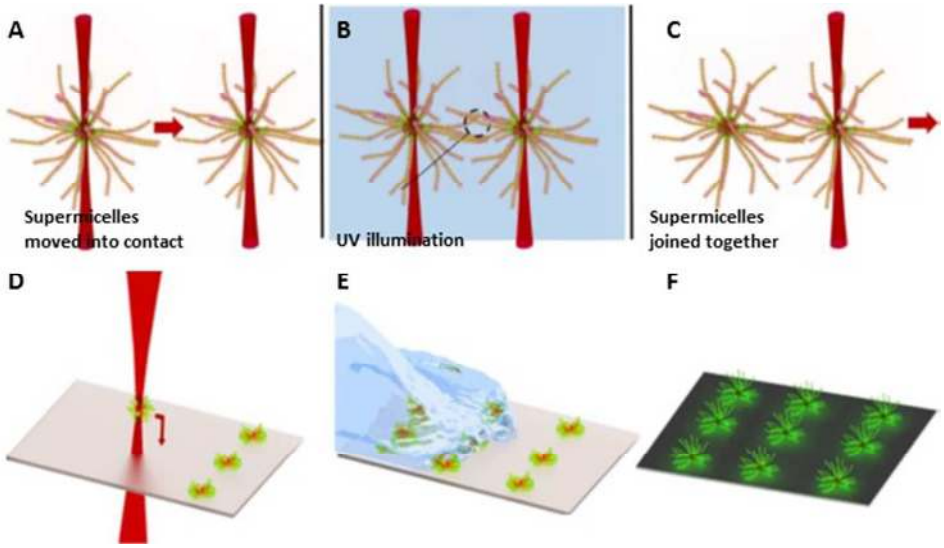

Figure 45. (a-c) schematic representation showing the assembly process of crosslinking multiple supermicelles together; (d-f) schematic representation of patterned deposition and growth of supermicelle arrays. Reproduced with permission from reference [379].

Supermicelles with complex architectures have been prepared through a combination of solvophobic interactions and hydrogen bonding.[380] Amphiphilic block comicelles with a very short hydrophobic **PFDMS-*b*-PMVS** central block and long hydrophilic **PFDMS-*b*-P2VP** end blocks could self-assemble into cross-type structures after dialysing into a selective solvent for the terminal blocks. Following crosslinking of the central **PFDMS-*b*-PMVS** blocks, **PFDMS-*b*-PtBA** (**PtBA**: poly-*tert*-butylacrylate) unimer was added to the cross arms, and the preceding **PFDMS-*b*-P2VP** blocks were crosslinked using Karstedt's catalyst.

Secondly, **PFDMS-*b*-P2VP** blocks were grown off the cross arms and short stub-like seeds of **PFDMS-*b*-PMVSOH** (**PMVSOH**: hydroxyl-functionalised **PMVS**) were then added to the micellar solution. The seeds selectively hydrogen bonded with the un-crosslinked **PFDMS-*b*-P2VP** blocks of the cross superstructures and following addition of further **PFDMS-*b*-PtBA** unimer, intricate "windmill"-type supermicelles were formed (see Figure 46). This approach shows an efficient methodology towards the fabrication of highly complex and potentially functional architectures through the use of a range of different non-covalent interactions.

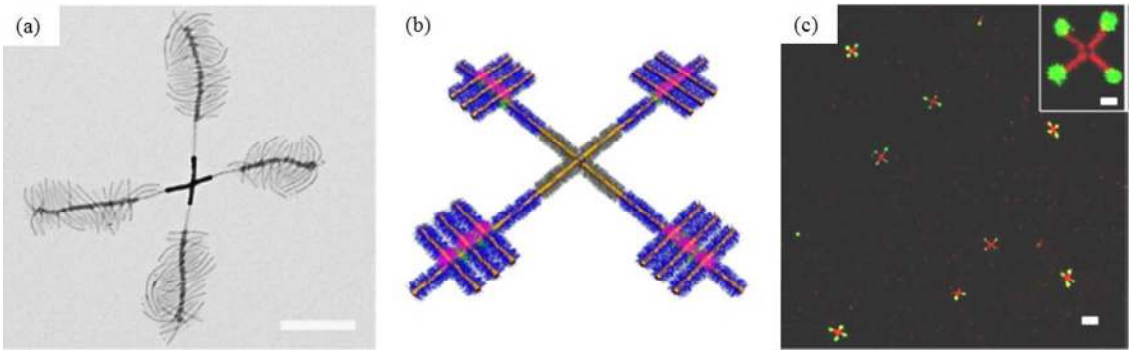

Figure 46. (a) TEM image, (b) schematic representation and (c) LSCM image of "windmill"-like supermicelles. Scale bars are (a) 500 nm, (c) 5 μm and 1 μm (inset). Reproduced with permission from reference [380].

5.3.6. Living CDSA of PFS BCPs in Two Dimensions

Despite the significant work on the formation of one-dimensional micellar aggregates from **PFS**-containing BCPs and the excellent control exhibited, the ability to be able to form two-dimensional assemblies has proven more difficult. Early investigations into the influence of the BCP block ratio upon self-assembly yielded two-dimensional platelet micelles composed

of **PFS**-containing BCPs when the block ratio between the two blocks is 1 : 1.[220] However, recently more systems forming 2D structures have been reported.

Lenticular platelets have been reported in recent years as a result of solvent composition, however little to no control over their size was demonstrated.[336, 381] Pointed oval platelets have been prepared through a living CDSA type method by the addition of **PFDMS-*b*-PP** BCP unimer to **PFDMS-*b*-P2VP** seed micelles.[382] It was shown that the use of monodisperse rather than polydisperse seed micelles led to ovals with a uniform shape and size by living CDSA. AFM analysis revealed 3D growth around the **PFDMS-*b*-P2VP** seed which occurs due to interplay of the relative growth rates in all three orthogonal directions around the seed. Additionally, these pointed oval micelles could be used as initiators for the growth of cylindrical micelles to yield hierarchical assemblies.

The formation lenticular platelets and multicompartment 2D structures of controlled area has been reported.[383] A range of platelet-forming **PFS** BCPs were prepared and unimer solutions of these were added to short cylindrical seed micelles. The resulting 2D lenticular platelets were shown to be uniform in size and grew linearly with unimer-to-seed ratio and with narrow area polydispersity (< 1.1). Block comicelle platelet structures were also formed through the sequential addition of different **PFS**-containing platelet-forming BCP unimer. These concentric multicompartment aggregates were easily visualise by LSCM through the use of BCPs functionalised with red, green and blue fluorescent dyes (see Figure 47). Single- and double-headed arrow- and spear-type architectures were also formed through using both unidirectional non-centrosymmetric and longer cylindrical seed micelles, respectively.[383]

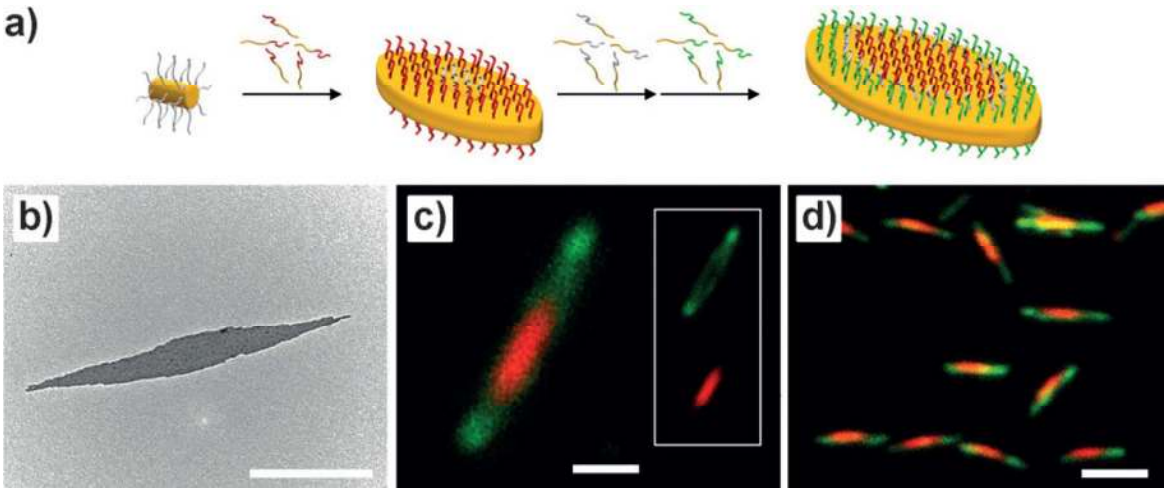

Figure 47. (a) schematic representation for the formation of uniform concentric 2D lenticular platelets; (b) TEM image and (c, d) LSCM images of lenticular platelet micelles showing their concentric structure. Scale bars are (b, c) 500 nm and (d) 2 μm. Reproduced with permission from reference [383].

Polydisperse two-dimensional structures have been prepared by the simple blending of cylinder-forming **PFS**-containing BCP with lamellae-forming **PFS** homopolymer, where co-crystallisation of the polymer blends play a vital role in the structure obtained during micellisation. Self-assembly of the homopolymer and block copolymer blends leads to the formation of assemblies with elongated 2D cores and fibre-like protrusions from the core ends. The morphology obtained could be varied by changing the ratio of homopolymer to block copolymer, as well as the molecular weight of the homopolymer.[384] The use of a seeded growth approach allows the preparation of well-defined platelet micelles, including segmented structures. Perforated and hollow rectangular micelles can be prepared by spatially selective crosslinking and dissolution procedures.[385]

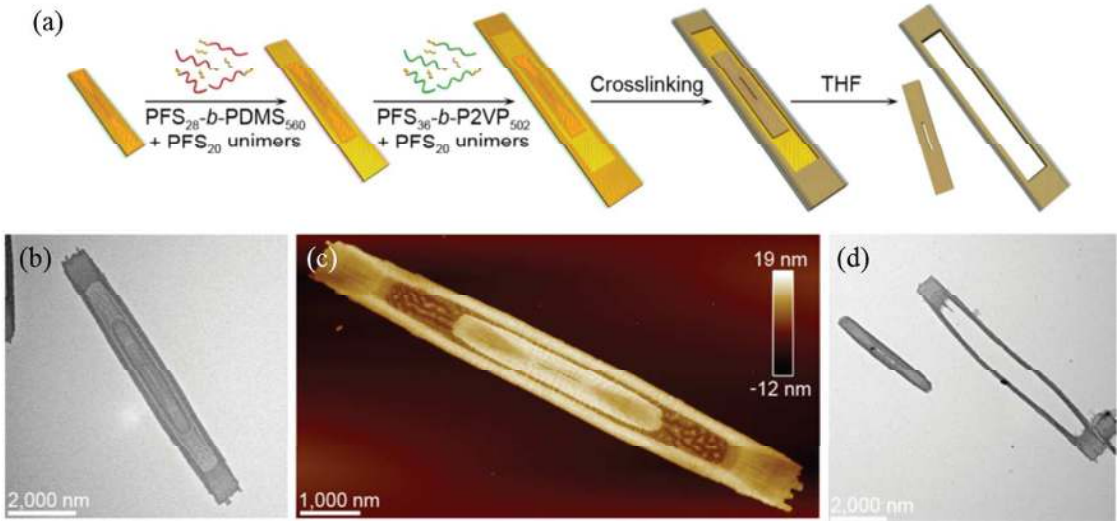

Figure 48. (a) Schematic representation for the formation of uniform concentric and hollow rectangular platelet micelles; (b) TEM and (c) AFM images of a concentric rectangular micelle micelle and (d) TEM image of a perforated rectangular platelet micelle and the corresponding rectangular ring platelet micelle after crosslinking and subsequent dissolution of the non-crosslinked segment. Reproduced with permission from reference [385].

5.3.7. Hybrid Mesostructures with Polyferrocenylsilane-Containing Materials

Synthetic approaches towards hierarchical materials have posed significant challenges.[386-388] As a result of recent developments, a number of hybrid mesostructures through the collaborative self-assembly of a range of scaffolds with **PFS**-based BCPs and micelles.

Controlled hybrid architectures have been reported by anchoring **PFDMS-*b*-P2VP** seed micelles onto the surfaces of silica nanoparticles (see Figure 49a). The adsorbed seed micelles were active towards living CDSA and addition of further **PFDMS-*b*-P2VP** unimer afforded "sunflower"-type assemblies.[389] Following the same rationale, when using silica-coated Ni-nanorods, "butterfly"-type architectures were formed. Furthermore, when

quaternised unimer was added to the seed micelles, the structures could be functionalised with Au nanoparticles, showing that the hybrid mesostructures are robust enough to undergo post-modifications.

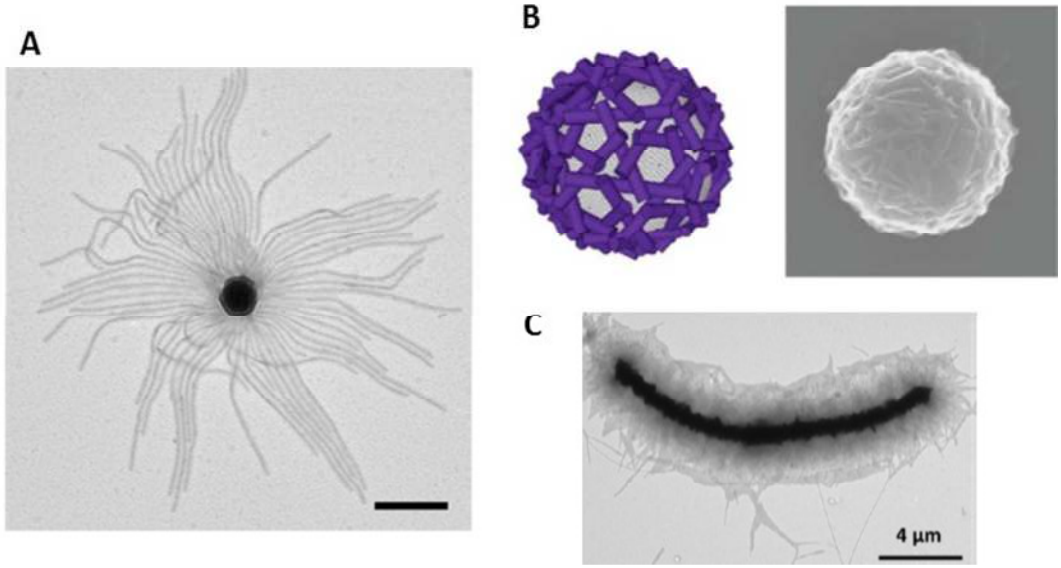

Figure 49. Images showing hybrid mesostructures possible with **PFS**-containing materials; (a) TEM image of "sunflower"-type assembly *via* seeded growth off a silica nanoparticle; (b) schematic representation and SEM image of fibre-basket polymersome by crosslinking of **PFDMS-*b*-P2VP** seed micelles on the surface of a **PS** bead; (c) TEM image of **PFS**-carbon nanotube hybrid structure. Scale bar is (a) 500 nm. Reproduced with permission from references [389-391].

In a similar procedure, **PFDMS-*b*-P2VP** seeds have been shown to adsorb onto the surface of **PS** nanobeads which can allow the formation of fibre-basket polymersomes via corona-crosslinking of the micelles (see Figure 49b).[390] The **PS** scaffold acted as a sacrificial template, affording hollow vesicular assemblies which can be efficiently post-functionalised both at the micelle cores and corona.

Hybrid "shish kebab"-type mesostructures have also been prepared through the functionalisation of carbon nanotubes with **PFS**-containing materials.[391] **PFS** homopolymer crystals were attached to multi-walled carbon nanotubes which could subsequently act as nucleation sites for **PFS**-containing BCPs, yielding the aforementioned hybrid assemblies (see Figure 49c). After crosslinking of the surrounding micelles, these architectures could then be used as scaffolds for the growth of Ag nanoparticles within the micelle cores.

5.4 Applications of PFS BCP Micelles

Crosslinking of **PFS**-containing micelles has been shown to be necessary for certain applications of cylindrical and nanotube morphologies. Crosslinking is essential for accessing one-dimensional **PFS** nanoceramics in high yield.[221, 343] Pyrolysis of the shell-crosslinked micelles occurs upon heating to 600 °C which results in ceramics with excellent shape retention. Uncrosslinked micelles were also pyrolysed however this lead to the destruction of the micellar core. Shell-crosslinked micelles have also been aligned and patterned on silicon substrates by microfluidic techniques, which may have interesting applications as magnetic memory materials or catalysts after pyrolysis.[291-293]

PFS shell-crosslinked nanotubes have been shown allowing potential for encapsulation of guest particles or compounds within the hollow of the nanotube via in-situ redox reaction using **PFS** as a reductant.[344, 346, 366] Silver nanoparticles were prepared within the nanotubes through reaction with $Ag[PF_6]$. Partial pre-oxidation of the **PFS** domains with an organic oxidant is needed for efficient formation of one-dimensional arrays of nanoparticles within

the nanotube (see Figure 50). Redox-controlled self-assembling PFS BCP systems and redox-active vesicles have also been studied.[321, 322]

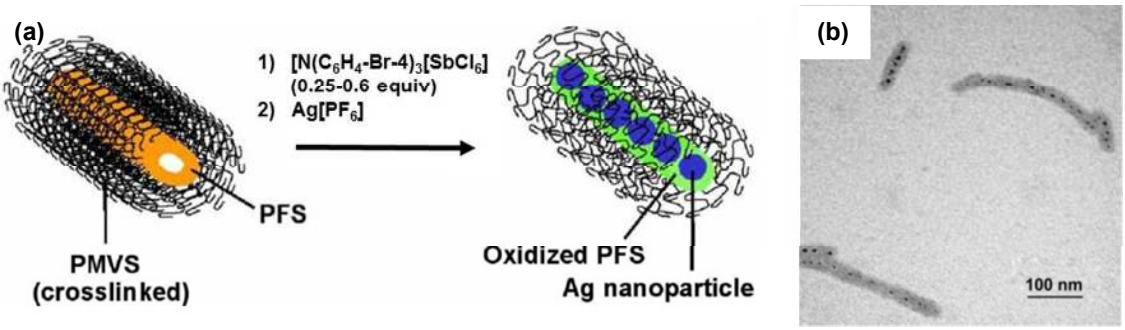

Figure 50. (a) Scheme for the generation of Ag nanoparticles within self-assembled **PFDMS-*b*-PMVS** tube micelles and (b) TEM images with Ag nanoparticles within micelle cores. Reproduced with permission from reference [344].

Cylindrical PFS BCP micelles have potential applications as nanolithographic etch resists for semiconducting substrates like GaAs or Si with potential for the fabrication of magnetic or semiconducting nanoscopic patterns.[53, 392] Cylindrical micelles have been deposited onto a GaAs surface by capillary forces into grooves etched out by electron beam patterning and following plasma etching generated connected ceramic lines with reduced size.

PFS BCPs with a polypeptide corona-forming block has been found to form thermally reversible gels.[393] **PFDMS-*b*-PBLG** materials are soluble in hot toluene but upon cooling to room temperature they form amber, optically transparent gels. The critical concentration for gelation was dependant on the **PBLG** block length and the block ratio. However when the block ratio became greater than 1 : 3 (**PFS** : **PBLG**), incomplete gelation was observed.

Functional electrodes composed of glucose oxidase and crosslinkable **PI-*b*-PFDMS** nanostructures including nanoparticles and cylinders have been shown to be effective as biosensors.[394] The morphology of the **PFS** BCP was shown to have a key role in affecting the electrochemical properties and the catalytic activities of the enzyme integrated electrodes. The biosensing ability of optimised electrodes showed good sensitivity at the physiological concentration of glucose in blood, and could be applicable to other types of nanostructured enzymatic biofuel cells.

Shape anisotropic **PFS** BCP nanoparticles have been shown to exhibit both morphological transitions and shape changes upon either exposure to selective solvents or redox agents such as $FeCl_3$, respectively.[337] This opens up these materials for applications as stimuli-responsive materials. Fluorescent multiblock comicelles present a novel approach towards the preparation of encoded nanomaterials with potential applications in high density data storage materials and biological diagnostics.[347]

6. Summary and Future Work

Since the first syntheses of high molar mass materials were reported in the early 1990s, PFS materials have developed into a large class of metal-containing organosilicon hybrid polymers. Living anionic ROP methods have allowed the preparation of well-defined main chain polymers with controlled architectures such as end functionalised homopolymers and PFS block copolymers. As is clear from this detailed review, PFS homopolymers and block copolymers have attracted much interest as a result of their interesting properties and functions.

Although many further advances in the area of functional PFS materials that exploit their unique combination of easy processing and unusual physical and chemical properties are anticipated, the development of these materials has clearly led to an even broader scientific impact. For example, the phenomenon "living crystallisation-driven self-assembly" discovered for PFS BCPs has also now been transposed to other organic BCP systems.[395-397] In addition, PFS materials represent a key new class of readily accessible metallopolymer[398] and their development has provided an excellent illustration of the potential of this very broad and vibrant field.[1] Thus, analogues of PFS with other elements in the bridge or containing different metals to iron (in some cases in combination with alternative π-hydrocarbon ligands) have been prepared and their ROP has been successfully demonstrated in a growing number of cases. This provides a route to new and fascinating metallopolymers with modified properties,[222, 399-405] and studies of these materials are likely to constitute a broad new area of future research.

The development of PFS materials has also helped stimulate further development of other polymer systems with metallocene side groups, such as poly(vinylferrocene),

poly(ferrocenylmethacrylates), and related materials,[406, 407] and also side chain polycobaltocenes.[408] Importance advances in these areas with respect to living polymerisation, self-assembly, and applications have been recently reported. Overall, these considerations all suggest that the prospects for various polymer classes containing metallocene units appears to be very bright.

References

1. G. R. Whittell, M. D. Hager, U. S. Schubert and I. Manners, *Nature Mater.*, 2011, **10**, 176-188.
2. I. Manners, *Polyhedron*, 1996, **15**, 4311-4329.
3. E. W. Neuse and H. Rosenberg, *J. Macromol. Sci. Polym.Rev.*, 1970, **4**, 1-145.
4. I. Manners, *Chem. Commun.*, 1999, 857-865.
5. V. Bellas and M. Rehahn, *Angew. Chem., Int. Ed.*, 2007, **46**, 5082-5104.
6. D. A. Rider and I. Manners, *Polym. Rev.*, 2007, **47**, 165-195.
7. K. Kulbaba and I. Manners, *Macromol. Rapid Commun.*, 2001, **22**, 711-724.
8. A. Osborne and R. Whiteley, *J. Organomet. Chem.*, 1975, **101**, C27-C28.
9. I. R. Butler and W. R. Cullen, *Organometallics*, 1986, **5**, 2537-2542.
10. I. R. Butler, W. R. Cullen, J. Ni and S. J. Rettig, *Organometallics*, 1985, **4**, 2196-2201.
11. J. J. Bishop, A. Davison, M. L. Katcher, D. W. Lichtenberg, R. E. Merrill and J. C. Smart, *J. Organomet. Chem.*, 1971, **27**, 241-249.
12. R. A. Musgrave, A. D. Russell and I. Manners, *Organometallics*, 2013, **32**, 5654-5667.
13. A. B. Fischer, J. B. Kinney, R. H. Staley and M. S. Wrighton, *J. Am. Chem. Soc.*, 1979, **101**, 6501-6506.
14. R. A. Musgrave, A. D. Russell, G. R. Whittell, M. F. Haddow and I. Manners, *Organometallics*, 2015, **34**, 897-907.
15. P. Nguyen, G. Stojcevic, K. Kulbaba, M. J. MacLachlan, X.-H. Liu, A. J. Lough and I. Manners, *Macromolecules*, 1998, **31**, 5977-5983.
16. F. Jäkle, E. Vejzovic, K. N. Power-Billard, M. J. MacLachlan, A. J. Lough and I. Manners, *Organometallics*, 2000, **19**, 2826-2828.
17. Y. Hatanaka, S. Okada, T. Minami, M. Goto and K. Shimada, *Organometallics*, 2005, **24**, 1053-1055.
18. S. C. Bourke, F. Jäkle, E. Vejzovic, K.-C. Lam, A. L. Rheingold, A. J. Lough and I. Manners, *Chem. Eur. J.*, 2003, **9**, 3042-3054.
19. M. J. MacLachlan, A. J. Lough, W. E. Geiger and I. Manners, *Organometallics*, 1998, **17**, 1873-1883.
20. A. Berenbaum, F. Jäkle, A. J. Lough and I. Manners, *Organometallics*, 2001, **20**, 834-843.
21. D. A. Foucher, B. Z. Tang and I. Manners, *J. Am. Chem. Soc.*, 1992, **114**, 6246-6248.
22. J. K. Pudelski, D. A. Foucher, C. H. Honeyman, A. J. Lough, I. Manners, S. Barlow and D. O'Hare, *Organometallics*, 1995, **14**, 2470-2479.
23. J. C. Green, *Chem. Soc. Rev.*, 1998, **27**, 263-272.
24. J.-J. Wang, L. Wang, T. Chen, X.-J. Wang, C.-L. Wang, X.-C. Dong and J.-H. Yang, *Eur. Polym. J.*, 2006, **42**, 843-848.
25. J.-J. Wang, L. Wang, X.-J. Wang, T. Chen, H.-J. Yu, W. Wang and C.-L. Wang, *Mater. Lett.*, 2006, **60**, 1416-1419.
26. G. Calleja, F. Carré, G. Cerveau, P. Labbé and L. Coche-Guérente, *Organometallics*, 2001, **20**, 4211-4215.
27. D. L. Zechel, K. C. Hultzsch, R. Rulkens, D. Balaishis, Y. Ni, J. K. Pudelski, A. J. Lough, I. Manners and D. A. Foucher, *Organometallics*, 1996, **15**, 1972-1978.
28. J. K. Pudelski and I. Manners, *J. Am. Chem. Soc.*, 1995, **117**, 7265-7266.
29. J. K. Pudelski, D. A. Foucher, C. H. Honeyman, P. M. Macdonald, I. Manners, S. Barlow and D. O'Hare, *Macromolecules*, 1996, **29**, 1894-1903.

30. F. Jäkle, R. Rulkens, G. Zech, J. A. Massey and I. Manners, *J. Am. Chem. Soc.*, 2000, **122**, 4231-4232.
31. T. Baumgartner, F. Jäkle, R. Rulkens, G. Zech, A. J. Lough and I. Manners, *J. Am. Chem. Soc.*, 2002, **124**, 10062-10070.
32. Y. Ni, R. Rulkens, J. K. Pudelski and I. Manners, *Macromol. Rapid Commun.*, 1995, **16**, 637-641.
33. N. P. Reddy, H. Yamashita and M. Tanaka, *J. Chem. Soc., Chem. Commun.*, 1995, 2263-2264.
34. P. W. Cyr, D. A. Rider, K. Kulbaba and I. Manners, *Macromolecules*, 2004, **37**, 3959-3961.
35. K. N. Power-Billard and I. Manners, *Macromolecules*, 2000, **33**, 26-31.
36. K. Temple, S. Dziadek and I. Manners, *Organometallics*, 2002, **21**, 4377-4384.
37. K. Temple, F. Jäkle, J. B. Sheridan and I. Manners, *J. Am. Chem. Soc.*, 2001, **123**, 1355-1364.
38. P. Gómez-Elipe, R. Resendes, P. M. Macdonald and I. Manners, *J. Am. Chem. Soc.*, 1998, **120**, 8348-8356.
39. C. A. Jaska, A. Bartole-Scott and I. Manners, *J. Chem. Soc., Dalton Trans.*, 2003, 4015-4021.
40. A. Bartole-Scott, R. Resendes and I. Manners, *Macromol. Chem. Phys.*, 2003, **204**, 1259-1268.
41. H. Tang, Y. Liu, X. Chen, J. Qin, M. Inokuchi, M. Kinoshita, X. Jin, Z. Wang and B. Xu, *Macromolecules*, 2004, **37**, 9785-9792.
42. J. Rasburn, R. Petersen, R. Jahr, R. Rulkens, I. Manners and G. J. Vancso, *Chem. Mater.*, 1995, **7**, 871-877.
43. J. Rasburn, D. A. Foucher, W. F. Reynolds and G. J. Vancso, *Chem. Commun.*, 1998, 843-844.
44. R. Rulkens, Y. Ni and I. Manners, *J. Am. Chem. Soc.*, 1994, **116**, 12121-12122.
45. Y. Ni, R. Rulkens and I. Manners, *J. Am. Chem. Soc.*, 1996, **118**, 4102-4114.
46. R. G. H. Lammertink, M. A. Hempenius, I. Manners and G. J. Vancso, *Macromolecules*, 1998, **31**, 795-800.
47. J. A. Massey, K. Temple, L. Cao, Y. Rharbi, J. Raez, M. A. Winnik and I. Manners, *J. Am. Chem. Soc.*, 2000, **122**, 11577-11584.
48. D. A. Rider, K. A. Cavicchi, K. N. Power-Billard, T. P. Russell and I. Manners, *Macromolecules*, 2005, **38**, 6931-6938.
49. A. Canet, A. H. Mark, G. J. Vancso and H. Jurriaan, *Nanotechnology*, 2009, **20**, 135304.
50. J. Gwyther and I. Manners, *Polymer*, 2009, **50**, 5384-5389.
51. K. N. Power-Billard, P. Wieland, M. Schäfer, O. Nuyken and I. Manners, *Macromolecules*, 2004, **37**, 2090-2095.
52. C. Kloninger and M. Rehahn, *Macromolecules*, 2004, **37**, 1720-1727.
53. J. A. Massey, M. A. Winnik, I. Manners, V. Z. H. Chan, J. M. Ostermann, R. Enchelmaier, J. P. Spatz and M. Möller, *J. Am. Chem. Soc.*, 2001, **123**, 3147-3148.
54. M. Zhang, P. A. Rupar, C. Feng, K. Lin, D. J. Lunn, A. Oliver, A. Nunns, G. R. Whittell, I. Manners and M. A. Winnik, *Macromolecules*, 2013, **46**, 1296-1304.
55. X.-S. Wang, M. A. Winnik and I. Manners, *Macromol. Rapid Commun.*, 2002, **23**, 210-213.
56. M. Tanabe and I. Manners, *J. Am. Chem. Soc.*, 2004, **126**, 11434-11435.
57. M. Tanabe, G. W. M. Vandermeulen, W. Y. Chan, P. W. Cyr, L. Vanderark, D. A. Rider and I. Manners, *Nature Mater.*, 2006, **5**, 467-470.
58. W. Y. Chan, A. J. Lough and I. Manners, *Chem. Eur. J.*, 2007, **13**, 8867-8876.

59. G. S. Smith, S. K. Patra, L. Vanderark, S. Saithong, J. P. H. Charmant and I. Manners, *Macromol. Chem. Phys.*, 2010, **211**, 303-312.
60. W. Y. Chan, A. J. Lough and I. Manners, *Organometallics*, 2007, **26**, 1217-1225.
61. Z. Wang, G. Masson, F. C. Peiris, G. A. Ozin and I. Manners, *Chem. Eur. J.*, 2007, **13**, 9372-9383.
62. M. Erhard, K. Lam, M. Haddow, G. R. Whittell, W. E. Geiger and I. Manners, *Polym. Chem.*, 2014, **5**, 1264-1274.
63. L. Chabanne, I. Matas, S. K. Patra and I. Manners, *Polym. Chem.*, 2011, **2**, 2651-2660.
64. W. Y. Chan, A. J. Lough and I. Manners, *Angew. Chem., Int. Ed.*, 2007, **119**, 9227-9230.
65. D. E. Herbert, J. B. Gilroy, W. Y. Chan, L. Chabanne, A. Staubitz, A. J. Lough and I. Manners, *J. Am. Chem. Soc.*, 2009, **131**, 14958-14968.
66. D. E. Herbert, M. Tanabe, S. C. Bourke, A. J. Lough and I. Manners, *J. Am. Chem. Soc.*, 2008, **130**, 4166-4176.
67. Z. Cheng, B. Ren, D. Zhao, X. Liu and Z. Tong, *Macromolecules*, 2009, **42**, 2762-2766.
68. Z. Wang, A. Lough and I. Manners, *Macromolecules*, 2002, **35**, 7669-7677.
69. M. A. Hempenius, N. S. Robins, R. G. H. Lammertink and G. J. Vancso, *Macromol. Rapid Commun.*, 2001, **22**, 30-33.
70. M. A. Hempenius, F. F. Brito and G. J. Vancso, *Macromolecules*, 2003, **36**, 6683-6688.
71. F. Jäkle, Z. Wang and I. Manners, *Macromol. Rapid Commun.*, 2000, **21**, 1291-1296.
72. S. Hilf, P. W. Cyr, D. A. Rider, I. Manners, T. Ishida and Y. Chujo, *Macromol. Rapid Commun.*, 2005, **26**, 950-954.
73. X.-H. Liu, D. W. Bruce and I. Manners, *J. Organomet. Chem.*, 1997, **548**, 49-56.
74. L. Chabanne, S. Pfirrmann, D. J. Lunn and I. Manners, *Polym. Chem.*, 2013, **4**, 2353-2360.
75. S. B. Clendenning and I. Manners, *Macromol. Symp.*, 2003, **196**, 71-76.
76. W. Y. Chan, S. B. Clendenning, A. Berenbaum, A. J. Lough, S. Aouba, H. E. Ruda and I. Manners, *J. Am. Chem. Soc.*, 2005, **127**, 1765-1772.
77. G. Masson, P. Beyer, P. W. Cyr, A. J. Lough and I. Manners, *Macromolecules*, 2006, **39**, 3720-3730.
78. A. Presa Soto, L. Chabanne, J. Zhou, J. B. Gilroy and I. Manners, *Macromol. Rapid Commun.*, 2012, **33**, 592-596.
79. J. A. Massey, K. Kulbaba, M. A. Winnik and I. Manners, *J. Polym. Sci., Part B: Polym. Phys.*, 2000, **38**, 3032-3041.
80. D. A. Foucher, R. Ziembinski, B. Z. Tang, P. M. Macdonald, J. Massey, C. R. Jaeger, G. J. Vancso and I. Manners, *Macromolecules*, 1993, **26**, 2878-2884.
81. D. Foucher, R. Ziembinski, R. Petersen, J. Pudelski, M. Edwards, Y. Ni, J. Massey, C. R. Jaeger, G. J. Vancso and I. Manners, *Macromolecules*, 1994, **27**, 3992-3999.
82. K. Kulbaba, M. J. MacLachlan, C. E. Evans and I. Manners, *Macromol. Chem. Phys.*, 2001, **202**, 1768-1775.
83. G. R. Whittell, J. B. Gilroy, I. Grillo, I. Manners and R. M. Richardson, *J. Polym. Sci., Part A: Polym. Chem*, 2013, **51**, 4011-4020.
84. Y. Xiong, G. Wang, J. Qin and H. Tang, *J. Inorg. Organomet. Polym.*, 2015, **25**, 91-97.
85. V. A. Du and I. Manners, *Macromolecules*, 2013, **46**, 4742-4753.
86. P. Nguyen, P. Gómez-Elipe and I. Manners, *Chem. Rev.*, 1999, **99**, 1515-1548.

87. M. A. Hempenius, R. G. H. Lammertink and G. J. Vancso, *Macromol. Symp.*, 1998, **127**, 161-163.
88. K. O'Driscoll and R. A. Sanayei, *Macromolecules*, 1991, **24**, 4479-4480.
89. J. Xu, V. Bellas, B. Jungnickel, B. Stühn and M. Rehahn, *Macromol. Chem. Phys.*, 2010, **211**, 1261-1271.
90. S. Barlow, A. L. Rohl, S. Shi, C. M. Freeman and D. O'Hare, *J. Am. Chem. Soc.*, 1996, **118**, 7578-7592.
91. K. H. Pannell, V. V. Dementiev, H. Li, F. Cervantes-Lee, M. T. Nguyen and A. F. Diaz, *Organometallics*, 1994, **13**, 3644-3650.
92. R. Rulkens, A. J. Lough, I. Manners, S. R. Lovelace, C. Grant and W. E. Geiger, *J. Am. Chem. Soc.*, 1996, **118**, 12683-12695.
93. V. S. Papkov, M. V. Gerasimov, I. I. Dubovik, S. Sharma, V. V. Dementiev and K. H. Pannell, *Macromolecules*, 2000, **33**, 7107-7115.
94. Z. Chen, M. D. Foster, W. Zhou, H. Fong, D. H. Reneker, R. Resendes and I. Manners, *Macromolecules*, 2001, **34**, 6156-6158.
95. J.-J. Wang, L.-X. Dai, Q. Gao, P.-F. Wu and X.-B. Wang, *Eur. Polym. J.*, 2008, **44**, 602-607.
96. K. Kulbaba, P. M. Macdonald and I. Manners, *Macromolecules*, 1999, **32**, 1321-1324.
97. W. D. Luke and A. Streitwieser, *J. Am. Chem. Soc.*, 1981, **103**, 3241-3243.
98. K. Kulbaba, I. Manners and P. M. Macdonald, *Macromolecules*, 2002, **35**, 10014-10025.
99. J. Rasburn, F. Seker, K. Kulbaba, P. G. Klein, I. Manners, G. J. Vancso and P. M. Macdonald, *Macromolecules*, 2001, **34**, 2884-2891.
100. H. Dislich, *Angew. Chem., Int. Ed.*, 1979, **18**, 49-59.
101. D. W. Mosley, K. Auld, D. Conner, J. Gregory, X.-Q. Liu, A. Pedicini, D. Thorsen, M. Wills, G. Khanarian and E. S. Simon, *Proc. SPIE*, 2008, **6910**, 691017-691018.
102. R. A. Gaudiana and R. A. Minns, *J. Macromol. Sci., Pure Appl. Chem*, 1991, **28**, 831-842.
103. C.-J. Yang and S. A. Jenekhe, *Chem. Mater.*, 1995, **7**, 1276-1285.
104. C. Lu and B. Yang, *J. Mater. Chem.*, 2009, **19**, 2884-2901.
105. W. Caseri, *Macromol. Rapid Commun.*, 2000, **21**, 705-722.
106. S. D. Bhagat, J. Chatterjee, B. Chen and A. Stiegman, *Macromolecules*, 2012, **45**, 1174-1181.
107. J.-G. Liu and M. Ueda, *J. Mater. Chem.*, 2009, **19**, 8907-8919.
108. C. Paquet, P. W. Cyr, E. Kumacheva and I. Manners, *Chem. Commun.*, 2004, 234-235.
109. C. Paquet, P. W. Cyr, E. Kumacheva and I. Manners, *Chem. Mater.*, 2004, **16**, 5205-5211.
110. L. Espada, M. Shadaram, J. Robillard and K. Pannell, *J. Inorg. Organomet. Polym.*, 2000, **10**, 169-176.
111. D. A. Foucher, C. H. Honeyman, J. M. Nelson, B. Z. Tang and I. Manners, *Angew. Chem., Int. Ed. Eng.*, 1993, **32**, 1709-1711.
112. M. T. Nguyen, A. F. Diaz, V. V. Dement'ev and K. H. Pannell, *Chem. Mater.*, 1994, **6**, 952-954.
113. X. J. Wang, L. Wang and J. J. Wang, *J. Polym. Sci., Part B: Polym. Phys.*, 2004, **42**, 2245-2253.
114. F. Barrière, N. Camire, W. E. Geiger, U. T. Mueller-Westerhoff and R. Sanders, *J. Am. Chem. Soc.*, 2002, **124**, 7262-7263.
115. M. Péter, M. A. Hempenius, E. S. Kooij, T. A. Jenkins, S. J. Roser, W. Knoll and G. J. Vancso, *Langmuir*, 2004, **20**, 891-897.

116. W. Shi, S. Cui, C. Wang, L. Wang, X. Zhang, X. Wang and L. Wang, *Macromolecules*, 2004, **37**, 1839-1842.
117. S. Zou, I. Korczagin, M. A. Hempenius, H. Schönherr and G. J. Vancso, *Polymer*, 2006, **47**, 2483-2492.
118. W. Shi, M. I. Giannotti, X. Zhang, M. A. Hempenius, H. Schönherr and G. J. Vancso, *Angew. Chem., Int. Ed.*, 2007, **46**, 8400-8404.
119. H. J. Chung, J. Song and G. J. Vancso, *Appl. Surf. Sci.*, 2009, **255**, 6995-6998.
120. R. Rulkens, R. Resendes, A. Verma, I. Manners, K. Murti, E. Fossum, P. Miller and K. Matyjaszewski, *Macromolecules*, 1997, **30**, 8165-8171.
121. K. H. Pannell, V. I. Imshennik, Y. V. Maksimov, M. N. Il'ina, H. K. Sharma, V. S. Papkov and I. P. Suzdalev, *Chem. Mater.*, 2005, **17**, 1844-1850.
122. L. Bakueva, E. H. Sargent, R. Resendes, A. Bartole and I. Manners, *J. Mater. Sci., Mater. Electron.*, 2001, **12**, 21-25.
123. L. Espada, K. H. Pannell, V. Papkov, L. Leites, S. Bukalov, I. Suzdalev, M. Tanaka and T. Hayashi, *Organometallics*, 2002, **21**, 3758-3761.
124. M. T. Nguyen, A. F. Diaz, V. V. Dement'ev and K. H. Pannell, *Chem. Mater.*, 1993, **5**, 1389-1394.
125. M. I. Giannotti, H. Lv, Y. Ma, M. P. Steenvoorden, A. R. Overweg, M. Roerdink, M. A. Hempenius and G. J. Vancso, *J. Inorg. Organomet. Polym.*, 2005, **15**, 527-540.
126. F. Ciminale, L. Lopez, G. M. Farinola and S. Sportelli, *Tetrahedron Lett.*, 2001, **42**, 5685-5687.
127. A. C. Arsenault, H. Míguez, V. Kitaev, G. A. Ozin and I. Manners, *Adv. Mater.*, 2003, **15**, 503-507.
128. P. W. Cyr, M. Tzolov, I. Manners and E. H. Sargent, *Macromol. Chem. Phys.*, 2003, **204**, 915-921.
129. P. W. Cyr, M. Tzolov, M. A. Hines, I. Manners, E. H. Sargent and G. D. Scholes, *J. Mater. Chem.*, 2003, **13**, 2213-2219.
130. R. Resendes, A. Berenbaum, G. Stojevic, F. Jäkle, A. Bartole, F. Zamanian, G. Dubois, C. Hersom, K. Balmain and I. Manners, *Adv. Mater.*, 2000, **12**, 327-330.
131. L. Thomi, P. Schaefer, K. Landfester and F. R. Wurm, *Macromolecules*, 2015, **49**, 105–109.
132. M. A. C. Stuart, W. T. S. Huck, J. Genzer, M. Muller, C. Ober, M. Stamm, G. B. Sukhorukov, I. Szleifer, V. V. Tsukruk, M. Urban, F. Winnik, S. Zauscher, I. Luzinov and S. Minko, *Nature Mater.*, 2010, **9**, 101-113.
133. X. Sui, X. Feng, M. A. Hempenius and G. J. Vancso, *J. Mater. Chem. B*, 2013, **1**, 1658-1672.
134. M. J. MacLachlan, A. J. Lough and I. Manners, *Macromolecules*, 1996, **29**, 8562-8564.
135. J. J. McDowell, N. S. Zacharia, D. Puzzo, I. Manners and G. A. Ozin, *J. Am. Chem. Soc.*, 2010, **132**, 3236-3237.
136. D. P. Puzzo, A. C. Arsenault, I. Manners and G. A. Ozin, *Angew. Chem., Int. Ed.*, 2009, **121**, 961-965.
137. A. C. Arsenault, V. Kitaev, I. Manners, G. A. Ozin, A. Mihi and H. Miguez, *J. Mater. Chem.*, 2005, **15**, 133-138.
138. A. C. Arsenault, D. P. Puzzo, I. Manners and G. A. Ozin, *Nature Photon.*, 2007, **1**, 468-472.
139. M. A. Hempenius, C. Cirmi, F. L. Savio, J. Song and G. J. Vancso, *Macromol. Rapid Commun.*, 2010, **31**, 772-783.
140. B. Zoetebier, M. A. Hempenius and G. J. Vancso, *Chem. Commun.*, 2015, **51**, 636-639.

141. M. A. Hempenius, C. Cirmi, J. Song and G. J. Vancso, *Macromolecules*, 2009, **42**, 2324-2326.
142. X. Sui, L. van Ingen, M. A. Hempenius and G. J. Vancso, *Macromol. Rapid Commun.*, 2010, **31**, 2059-2063.
143. X. Sui, X. Feng, A. Di Luca, C. A. van Blitterswijk, L. Moroni, M. A. Hempenius and G. J. Vancso, *Polym. Chem.*, 2013, **4**, 337-342.
144. E. Kutnyanszky, M. A. Hempenius and G. J. Vancso, *Polym. Chem.*, 2014, **5**, 771-783.
145. X. Sui, M. A. Hempenius and G. J. Vancso, *J. Am. Chem. Soc.*, 2012, **134**, 4023-4025.
146. K. Zhang, X. Feng, X. Sui, M. A. Hempenius and G. J. Vancso, *Angew. Chem., Int. Ed.*, 2014, **53**, 13789-13793.
147. D. Janczewski, J. Song, E. Csanyi, L. Kiss, P. Blazso, R. L. Katona, M. A. Deli, G. Gros, J. Xu and G. J. Vancso, *J. Mater. Chem.*, 2012, **22**, 6429-6435.
148. I. Corni, M. P. Ryan and A. R. Boccaccini, *J. Eur. Ceram. Soc.*, 2008, **28**, 1353-1367.
149. P. Colombo, G. Mera, R. Riedel and G. D. Sorarù, *J. Am. Ceram. Soc.*, 2010, **93**, 1805-1837.
150. M. Ginzburg, M. J. MacLachlan, S. M. Yang, N. Coombs, T. W. Coyle, N. P. Raju, J. E. Greedan, R. H. Herber, G. A. Ozin and I. Manners, *J. Am. Chem. Soc.*, 2002, **124**, 2625-2639.
151. B.-Z. Tang, R. Petersen, D. A. Foucher, A. Lough, N. Coombs, R. Sodhi and I. Manners, *J. Chem. Soc., Chem. Commun.*, 1993, 523-525.
152. R. Petersen, D. A. Foucher, B.-Z. Tang, A. Lough, N. P. Raju, J. E. Greedan and I. Manners, *Chem. Mater.*, 1995, **7**, 2045-2053.
153. S. W. Hong, J. Xu, J. Xia, Z. Lin, F. Qiu and Y. Yang, *Chem. Mater.*, 2005, **17**, 6223-6226.
154. M. J. MacLachlan, M. Ginzburg, N. Coombs, T. W. Coyle, N. P. Raju, J. E. Greedan, G. A. Ozin and I. Manners, *Science*, 2000, **287**, 1460-1463.
155. Q. Sun, J. W. Y. Lam, K. Xu, H. Xu, J. A. K. Cha, P. C. L. Wong, G. Wen, X. Zhang, X. Jing, F. Wang and B. Z. Tang, *Chem. Mater.*, 2000, **12**, 2617-2624.
156. M. Häußler, Q. Sun, K. Xu, J. Y. Lam, H. Dong and B. Tang, *J. Inorg. Organomet. Polym.*, 2005, **15**, 67-81.
157. Q. Sun, K. Xu, H. Peng, R. Zheng, M. Häussler and B. Z. Tang, *Macromolecules*, 2003, **36**, 2309-2320.
158. Y. Gou, X. Tong, Q. Zhang, B. Wang, Q. Shi, H. Wang, Z. Xie and Y. Wang, *Ceram. Int.*, 2016, **42**, 681-689.
159. Y. Gou, X. Tong, Q. Zhang, H. Wang, B. Wang, S. Xie and Y. Wang, *J. Mater. Sci.*, 2015, **50**, 7975-7984.
160. A. Berenbaum, M. Ginzburg‐Margau, N. Coombs, A. J. Lough, A. Safa‐Sefat, J. E. Greedan, G. A. Ozin and I. Manners, *Adv. Mater.*, 2003, **15**, 51-55.
161. K. Liu, S. B. Clendenning, L. Friebe, W. Y. Chan, Zhu, M. R. Freeman, G. C. Yang, C. M. Yip, D. Grozea, Z.-H. Lu and I. Manners, *Chem. Mater.*, 2006, **18**, 2591-2601.
162. W. Y. Chan, A. Y. Cheng, S. B. Clendenning and I. Manners, *Macromol. Symp.*, 2004, **209**, 163-176.
163. K. R. Thomas, A. Ionescu, J. Gwyther, I. Manners, C. H. W. Barnes, U. Steiner and E. Sivaniah, *J. Appl. Phys.*, 2011, **109**, 073904.
164. M. J. MacLachlan, P. Aroca, N. Coombs, I. Manners and G. A. Ozin, *Adv. Mater.*, 1998, **10**, 144-149.
165. M. J. MacLachlan, M. Ginzburg, N. Coombs, N. P. Raju, J. E. Greedan, G. A. Ozin and I. Manners, *J. Am. Chem. Soc.*, 2000, **122**, 3878-3891.

166. R. Tong, Y. Zhao, L. Wang, H. Yu, F. Ren, M. Saleem and W. A. Amer, *J. Organomet. Chem.*, 2014, **755**, 16-32.
167. L. Wang, J. Huo, H. Yu, T. Chen and L. Deng, *J. Inorg. Organomet. Polym.*, 2007, **17**, 121-125.
168. K. Kulbaba, A. Cheng, A. Bartole, S. Greenberg, R. Resendes, N. Coombs, A. Safa-Sefat, J. E. Greedan, H. D. H. Stöver, G. A. Ozin and I. Manners, *J. Am. Chem. Soc.*, 2002, **124**, 12522-12534.
169. K. Kulbaba, R. Resendes, A. Cheng, A. Bartole, A. Safa‐Sefat, N. Coombs, H. Stöver, J. Greedan, G. Ozin and I. Manners, *Adv. Mater.*, 2001, **13**, 732-736.
170. X. Sui, L. Shui, J. Cui, Y. Xie, J. Song, A. van den Berg, M. A. Hempenius and G. Julius Vancso, *Chem. Commun.*, 2014, **50**, 3058-3060.
171. G. Decher and J. D. Hong, *Ber. Bunsenges. Phys. Chem*, 1991, **95**, 1430-1434.
172. G. Decher and J.-D. Hong, *Makromol. Chem., Macromol. Symp.*, 1991, **46**, 321-327.
173. M. Ginzburg, J. Galloro, F. Jäkle, K. N. Power-Billard, S. Yang, I. Sokolov, C. N. C. Lam, A. W. Neumann, I. Manners and G. A. Ozin, *Langmuir*, 2000, **16**, 9609-9614.
174. J. Halfyard, J. Galloro, M. Ginzburg, Z. Wang, N. Coombs, I. Manners and G. A. Ozin, *Chem. Commun.*, 2002, 1746-1747.
175. M. A. Hempenius and G. J. Vancso, *Macromolecules*, 2002, **35**, 2445-2447.
176. M. A. Hempenius, M. Péter, N. S. Robins, E. S. Kooij and G. J. Vancso, *Langmuir*, 2002, **18**, 7629-7634.
177. E. S. Kooij, Y. Ma, M. A. Hempenius, G. J. Vancso and B. Poelsema, *Langmuir*, 2010, **26**, 14177-14181.
178. Y. Ma, W.-F. Dong, E. S. Kooij, M. A. Hempenius, H. Mohwald and G. J. Vancso, *Soft Matter*, 2007, **3**, 889-895.
179. X. Feng, A. Cumurcu, X. Sui, J. Song, M. A. Hempenius and G. J. Vancso, *Langmuir*, 2013, **29**, 7257-7265.
180. A. Cumurcu, X. Feng, L. D. Ramos, M. A. Hempenius, P. Schon and G. J. Vancso, *Nanoscale*, 2014, **6**, 12089-12095.
181. Y. Ma, W.-F. Dong, M. A. Hempenius, H. Möhwald and G. J. Vancso, *Angew. Chem., Int. Ed.*, 2007, **46**, 1702-1705.
182. J. Song, D. Jańczewski, Y. Ma, M. Hempenius, J. Xu and G. J. Vancso, *J. Colloid Interface Sci.*, 2013, **405**, 256-261.
183. J. Song, D. Janczewski, Y. Ma, M. Hempenius, J. Xu and G. J. Vancso, *J. Mater. Chem. B*, 2013, **1**, 828-834.
184. J. Song, D. Janczewski, Y. Guo, J. Xu and G. J. Vancso, *Nanoscale*, 2013, **5**, 11692-11698.
185. S. Zou, Y. Ma, M. A. Hempenius, H. Schönherr and G. J. Vancso, *Langmuir*, 2004, **20**, 6278-6287.
186. M. Péter, R. G. H. Lammertink, M. A. Hempenius and G. J. Vancso, *Langmuir*, 2005, **21**, 5115-5123.
187. J. Song and G. J. Vancso, *Langmuir*, 2011, **27**, 6822-6829.
188. X. Feng, X. Sui, M. A. Hempenius and G. J. Vancso, *J. Am. Chem. Soc.*, 2014, **136**, 7865-7868.
189. X. Sui, X. Feng, J. Song, M. A. Hempenius and G. J. Vancso, *J. Mater. Chem.*, 2012, **22**, 11261-11267.
190. L. Dos Ramos, S. de Beer, M. A. Hempenius and G. J. Vancso, *Langmuir*, 2015, **31**, 6343-6350.
191. F. Fleischhaker, A. C. Arsenault, Z. Wang, V. Kitaev, F. C. Peiris, G. von Freymann, I. Manners, R. Zentel and G. A. Ozin, *Adv. Mater.*, 2005, **17**, 2455-2458.

192. Z. Wang, M. E. Calvo, G. Masson, A. C. Arsenault, F. Peiris, M. Mamak, H. Míguez, I. Manners and G. A. Ozin, *Adv. Mater. Interfaces*, 2014, **1**, 1-5.
193. Y. Ma, W.-F. Dong, M. A. Hempenius, H. Mohwald and G. Julius Vancso, *Nature Mater.*, 2006, **5**, 724-729.
194. C. Acikgoz, B. Vratzov, M. A. Hempenius, G. J. Vancso and J. Huskens, *ACS Appl. Mater. Interfaces*, 2009, **1**, 2645-2650.
195. C. Acikgoz, X. Y. Ling, I. Y. Phang, M. A. Hempenius, D. N. Reinhoudt, J. Huskens and G. J. Vancso, *Adv. Mater.*, 2009, **21**, 2064-2067.
196. X. Y. Ling, C. Acikgoz, I. Y. Phang, M. A. Hempenius, D. N. Reinhoudt, G. J. Vancso and J. Huskens, *Nanoscale*, 2010, **2**, 1455-1460.
197. R. G. H. Lammertink, M. A. Hempenius, V. Z. H. Chan, E. L. Thomas and G. J. Vancso, *Chem. Mater.*, 2001, **13**, 429-434.
198. K. Y. Suh, Y. S. Kim and H. H. Lee, *Adv. Mater.*, 2001, **13**, 1386-1389.
199. I. Korczagin, H. Xu, M. A. Hempenius and G. J. Vancso, *Eur. Polym. J.*, 2008, **44**, 2523-2528.
200. F. S. Bates and G. H. Fredrickson, *Phys. Today*, 1999, **52**, 32-38.
201. I. Manners, *J. Opt. A, Pure Appl. Op.*, 2002, **4**, S221-S223.
202. A.-V. Ruzette and L. Leibler, *Nature Mater.*, 2005, **4**, 19-31.
203. R. A. Segalman, *Mat. Sci. Eng. R*, 2005, **48**, 191-226.
204. C. J. Hawker and K. L. Wooley, *Science*, 2005, **309**, 1200-1205.
205. I. Manners, *Angew. Chem., Int. Ed.*, 2007, **46**, 1565-1568.
206. T. Smart, H. Lomas, M. Massignani, M. V. Flores-Merino, L. R. Perez and G. Battaglia, *Nano Today*, 2008, **3**, 38-46.
207. Y. Mai and A. Eisenberg, *Chem. Soc. Rev.*, 2012, **41**, 5969-5985.
208. F. H. Schacher, P. A. Rupar and I. Manners, *Angew. Chem., Int. Ed.*, 2012, **51**, 7898-7921.
209. J. Zhou, G. R. Whittell and I. Manners, *Macromolecules*, 2014, **47**, 3529-3543.
210. Y. Ni, R. Rulkens, J. K. Pudelski and I. Manners, *Macromol. Rapid Commun.*, 1995, **16**, 637-641.
211. P. Gómez-Elipe, P. M. Macdonald and I. Manners, *Angew. Chem., Int. Ed.*, 1997, **36**, 762-764.
212. R. Resendes, J. A. Massey, H. Dorn, K. N. Power, M. A. Winnik and I. Manners, *Angew. Chem., Int. Ed.*, 1999, **38**, 2570-2573.
213. M. Szwarc, *Nature*, 1956, **178**, 1168-1169.
214. O. W. Webster, *Science*, 1991, **251**, 887-893.
215. M. Szwarc, *J. Polym. Sci., Part A: Polym. Chem*, 1998, **36**, IX-XV.
216. T. Gädt, F. H. Schacher, N. McGrath, M. A. Winnik and I. Manners, *Macromolecules*, 2011, **44**, 3777-3786.
217. K. Temple, J. Massey, Z. Chen, N. Vaidya, A. Berenbaum, M. Foster and I. Manners, *J. Inorg. Organomet. Polym.*, 1999, **9**, 189-198.
218. J.-C. Eloi, D. A. Rider, J.-Y. Wang, T. P. Russell and I. Manners, *Macromolecules*, 2008, **41**, 9474-9479.
219. I. Manners, *J. Polym. Sci., Part A: Polym. Chem*, 2002, **40**, 179-191.
220. L. Cao, I. Manners and M. A. Winnik, *Macromolecules*, 2002, **35**, 8258-8260.
221. X. S. Wang, M. A. Winnik and I. Manners, *Angew. Chem., Int. Ed.*, 2004, **43**, 3703-3707.
222. T. J. Peckham, J. A. Massey, C. H. Honeyman and I. Manners, *Macromolecules*, 1999, **32**, 2830-2837.
223. X. S. Wang, M. A. Winnik and I. Manners, *Macromolecules*, 2002, **35**, 9146-9150.

224. I. Korczagin, M. A. Hempenius and G. J. Vancso, *Macromolecules*, 2004, **37**, 1686-1690.
225. H. Wang, M. A. Winnik and I. Manners, *Macromolecules*, 2007, **40**, 3784-3789.
226. N. McGrath, F. H. Schacher, H. Qiu, S. Mann, M. A. Winnik and I. Manners, *Polym. Chem.*, 2014, **5**, 1923-1929.
227. A. Natalello, A. Alkan, A. Friedel, I. Lieberwirth, H. Frey and F. R. Wurm, *ACS Macro Lett.*, 2013, **2**, 313-316.
228. C. Kloninger and M. Rehahn, *Macromol. Chem. Phys.*, 2007, **208**, 833-840.
229. V. P. Chuang, C. A. Ross, J. Gwyther and I. Manners, *Adv. Mater.*, 2009, **21**, 3789-3793.
230. U. Datta and M. Rehahn, *Macromol. Rapid Commun.*, 2004, **25**, 1615-1622.
231. K. T. Kim, G. W. M. Vandermeulen, M. A. Winnik and I. Manners, *Macromolecules*, 2005, **38**, 4958-4961.
232. G. Molev, Y. Lu, K. S. Kim, I. C. Majdalani, G. Guerin, S. Petrov, G. Walker, I. Manners and M. A. Winnik, *Macromolecules*, 2014, **47**, 2604-2615.
233. Y. Wang, S. Zou, K. T. Kim, I. Manners and M. A. Winnik, *Chem. Eur. J.*, 2008, **14**, 8624-8631.
234. G. W. M. Vandermeulen, K. T. Kim, Z. Wang and I. Manners, *Biomacromolecules*, 2006, **7**, 1005-1010.
235. S. Tangbunsuk, G. R. Whittell, M. G. Ryadnov, G. W. Vandermeulen, D. N. Woolfson and I. Manners, *Chem. Eur. J.*, 2012, **18**, 2524-2535.
236. M. Roerdink, T. S. van Zanten, M. A. Hempenius, Z. Zhong, J. Feijen and G. J. Vancso, *Macromol. Rapid Commun.*, 2007, **28**, 2125-2130.
237. X. S. Wang, M. A. Winnik and I. Manners, *Macromol. Rapid Commun.*, 2003, **24**, 403-407.
238. T. Chen, L. Wang, G. Jiang, J. Wang, X. Wang, J. Zhou and W. Wang, *Eur. Polym. J.*, 2006, **42**, 687-693.
239. Jian-Hua Li, Li Wang, Hao-Jie Yu, Qiao-Hua Tan, Li-Bo Deng and J. Huo, *Des. Monomers Polym.*, 2007, **10**, 193-205.
240. V. Bellas and M. Rehahn, *Macromol. Rapid Commun.*, 2007, **28**, 1415-1421.
241. A. P. Soto and I. Manners, *Macromolecules*, 2009, **42**, 40-42.
242. H. R. Allcock, J. M. Nelson, S. D. Reeves, C. H. Honeyman and I. Manners, *Macromolecules*, 1997, **30**, 50-56.
243. H. R. Allcock, S. D. Reeves, J. M. Nelson, C. A. Crane and I. Manners, *Macromolecules*, 1997, **30**, 2213-2215.
244. B. Wang, E. Rivard and I. Manners, *Inorg. Chem.*, 2002, **41**, 1690-1691.
245. R. K. Iha, K. L. Wooley, A. M. Nyström, D. J. Burke, M. J. Kade and C. J. Hawker, *Chem. Rev.*, 2009, **109**, 5620-5686.
246. A. Nunns, C. A. Ross and I. Manners, *Macromolecules*, 2013, **46**, 2628-2635.
247. M. Tanabe, G. W. Vandermeulen, W. Y. Chan, P. W. Cyr, L. Vanderark, D. A. Rider and I. Manners, *Nature Mater.*, 2006, **5**, 467-470.
248. D. E. Herbert, U. F. Mayer, J. B. Gilroy, M. J. Lopez-Gomez, A. J. Lough, J. P. Charmant and I. Manners, *Chem. Eur. J.*, 2009, **15**, 12234-12246.
249. S. K. Patra, G. R. Whittell, S. Nagiah, C. L. Ho, W. Y. Wong and I. Manners, *Chem. Eur. J.*, 2010, **16**, 3240-3250.
250. R. Ahmed, S. K. Patra, I. W. Hamley, I. Manners and C. F. Faul, *J. Am. Chem. Soc.*, 2013, **135**, 2455-2458.
251. J. B. Gilroy, S. K. Patra, J. M. Mitchels, M. A. Winnik and I. Manners, *Angew. Chem., Int. Ed.*, 2011, **50**, 5851-5855.
252. L. Chabanne, I. Matas, S. K. Patra and I. Manners, *Polym. Chem.*, 2011, **2**, 2651.

253. D. J. Lunn, C. E. Boott, K. E. Bass, T. A. Shuttleworth, N. G. McCreanor, S. Papadouli and I. Manners, *Macromol. Chem. Phys.*, 2013, **214**, 2813-2820.
254. F. Wurm, S. Hilf and H. Frey, *Chem. Eur. J.*, 2009, **15**, 9068-9077.
255. J. A. Massey, K. N. Power, M. A. Winnik and I. Manners, *Adv. Mater.*, 1998, **10**, 1559-1562.
256. C. Kloninger and M. Rehahn, *Macromolecules*, 2004, **37**, 8319-8324.
257. R. G. H. Lammertink, M. A. Hempenius, J. E. van den Enk, V. Z. H. Chan, E. L. Thomas and G. J. Vancso, *Adv. Mater.*, 2000, **12**, 98-103.
258. R. G. H. Lammertink, M. A. Hempenius, E. L. Thomas and G. J. Vancso, *J. Polym. Sci., Part B: Polym. Phys.*, 1999, **37**, 1009-1021.
259. K. Temple, K. Kulbaba, K. N. Power-Billard, I. Manners, K. A. Leach, T. Xu, T. P. Russell and C. J. Hawker, *Adv. Mater.*, 2003, **15**, 297-300.
260. J. Gwyther, G. Lotze, I. Hamley and I. Manners, *Macromol. Chem. Phys.*, 2011, **212**, 198-201.
261. J. D. Wilbur, Z. Fang, B. A. Garetz, M. C. Newstein and N. P. Balsara, *Macromolecules*, 2008, **41**, 4464-4470.
262. R. G. H. Lammertink, M. A. Hempenius and G. J. Vancso, *Langmuir*, 2000, **16**, 6245-6252.
263. J. Xu, V. Bellas, B. Jungnickel, B. Stühn and M. Rehahn, *Macromol. Chem. Phys.*, 2010, **211**, 2276-2285.
264. H. B. Eitouni and N. P. Balsara, *J. Am. Chem. Soc.*, 2004, **126**, 7446-7447.
265. H. B. Eitouni, N. P. Balsara, H. Hahn, J. A. Pople and M. A. Hempenius, *Macromolecules*, 2002, **35**, 7765-7772.
266. K. Aissou, H. K. Choi, A. Nunns, I. Manners and C. A. Ross, *Nano Lett.*, 2013, **13**, 835-839.
267. M. Ramanathan, E. Nettleton and S. B. Darling, *Thin Solid Films*, 2009, **517**, 4474-4478.
268. M. Ramanathan and S. B. Darling, *Soft Matter*, 2009, **5**, 4665.
269. W. I. Park, Y. Kim, J. W. Jeong, K. Kim, J. K. Yoo, Y. H. Hur, J. M. Kim, E. L. Thomas, A. Alexander-Katz and Y. S. Jung, *Sci. Rep.*, 2013, **3**, 3190.
270. J. Y. Cheng, C. A. Ross, E. L. Thomas, H. I. Smith and G. J. Vancso, *Adv. Mater.*, 2003, **15**, 1599-1602.
271. J. Y. Cheng, A. M. Mayes and C. A. Ross, *Nature Mater.*, 2004, **3**, 823-828.
272. J. Y. Cheng, F. Zhang, H. I. Smith, G. J. Vancso and C. A. Ross, *Adv. Mater.*, 2006, **18**, 597-601.
273. J. Y. Cheng, F. Zhang, V. P. Chuang, A. M. Mayes and C. A. Ross, *Nano Lett.*, 2006, **6**, 2099-2103.
274. V. P. Chuang, J. Y. Cheng, T. A. Savas and C. A. Ross, *Nano Lett.*, 2006, **6**, 2332-2337.
275. M. Roerdink, M. A. Hempenius, U. Gunst, H. F. Arlinghaus and G. J. Vancso, *Small*, 2007, **3**, 1415-1423.
276. A. C. Arsenault, D. A. Rider, N. Tétreault, J. I. L. Chen, N. Coombs, G. A. Ozin and I. Manners, *J. Am. Chem. Soc.*, 2005, **127**, 9954-9955.
277. D. A. Rider, J. I. L. Chen, J.-C. Eloi, A. C. Arsenault, T. P. Russell, G. A. Ozin and I. Manners, *Macromolecules*, 2008, **41**, 2250-2259.
278. W. Zheng and Z.-G. Wang, *Macromolecules*, 1995, **28**, 7215-7223.
279. Y. Bohbot-Raviv and Z.-G. Wang, *Phys. Rev. Lett.*, 2000, **85**, 3428-3431.
280. V. P. Chuang, J. Gwyther, R. A. Mickiewicz, I. Manners and C. A. Ross, *Nano Lett.*, 2009, **9**, 4364-4369.

281. J. G. Son, J. Gwyther, J. B. Chang, K. K. Berggren, I. Manners and C. A. Ross, *Nano Lett.*, 2011, **11**, 2849-2855.
282. T. Gemma, A. Hatano and T. Dotera, *Macromolecules*, 2002, **35**, 3225-3237.
283. A. S. Abd-El-Aziz, *Macromol. Rapid Commun.*, 2002, **23**, 995-1031.
284. I. Manners, *Science*, 2001, **294**, 1664-1666.
285. U. S. Schubert and C. Eschbaumer, *Angew. Chem., Int. Ed.*, 2002, **41**, 2892-2926.
286. G. R. Whittell and I. Manners, *Adv. Mater.*, 2007, **19**, 3439-3468.
287. A. Nunns, J. Gwyther and I. Manners, *Polymer*, 2013, **54**, 1269-1284.
288. J. Zhang, K. Cao, X. S. Wang and B. Cui, *Chem. Commun.*, 2015, **51**, 17592-17595.
289. M. Ramanathan, Y.-C. Tseng, K. Ariga and S. B. Darling, *J. Mater. Chem. C*, 2013, **1**, 2080.
290. I. Korczagin, R. G. H. Lammertink, M. A. Hempenius, S. Golze and G. J. Vancso, *Adv. Polym. Sci.*, 2005, **200**, 91-117.
291. C. Hinderling, Y. Keles, T. Stöckli, H. F. Knapp, T. de los Arcos, P. Oelhafen, I. Korczagin, M. A. Hempenius, G. J. Vancso, R. Pugin and H. Heinzelmann, *Adv. Mater.*, 2004, **16**, 876-879.
292. S. Lastella, Y. J. Jung, H. Yang, R. Vajtai, P. M. Ajayan, C. Y. Ryu, D. A. Rider and I. Manners, *J. Mater. Chem.*, 2004, **14**, 1791.
293. J. Q. Lu, T. E. Kopley, N. Moll, D. Roitman, D. Chamberlin, Q. Fu, J. Liu, T. P. Russell, D. A. Rider and I. Manners, *Chem. Mater.*, 2005, **17**, 2227-2231.
294. J. Q. Lu, D. A. Rider, E. Onyegam, H. Wang, M. A. Winnik, I. Manners, Q. Cheng, Q. Fu and J. Liu, *Langmuir*, 2006, **22**, 5174-5179.
295. S. Lastella, H. Yang, D. Rider, I. Manners, P. M. Ajayan and C. Y. Ryu, *J. Polym. Sci., Part B: Polym. Phys.*, 2007, **45**, 758-765.
296. S. Lastella, G. Mallick, R. Woo, S. P. Karna, D. A. Rider, I. Manners, Y. J. Jung, C. Y. Ryu and P. M. Ajayan, *J. Appl. Phys.*, 2006, **99**, 024302.
297. J. Lu, T. Kopley, D. Dutton, J. Liu, C. Qian, H. Son, M. Dresselhaus and J. Kong, *J. Phys. Chem. B*, 2006, **110**, 10585-10589.
298. I. W. Hamley, *Nanotechnology*, 2003, **14**, R39.
299. C. J. Hawker and T. P. Russell, *MRS Bull.*, 2005, **30**, 952-966.
300. M. P. Stoykovich and P. F. Nealey, *Mater. Today*, 2006, **9**, 20-29.
301. J. Y. Cheng, C. A. Ross, H. I. Smith and E. L. Thomas, *Adv. Mater.*, 2006, **18**, 2505-2521.
302. J. Bang, U. Jeong, D. Y. Ryu, T. P. Russell and C. J. Hawker, *Adv. Mater.*, 2009, **21**, 4769-4792.
303. C. M. Bates, M. J. Maher, D. W. Janes, C. J. Ellison and C. G. Willson, *Macromolecules*, 2014, **47**, 2-12.
304. C. Cummins, T. Ghoshal, J. D. Holmes and M. A. Morris, *Adv. Mater.*, 2016, In Press.
305. J. Y. Cheng, C. A. Ross, V. Z. H. Chan, E. L. Thomas, R. G. H. Lammertink and G. J. Vancso, *Adv. Mater.*, 2001, **13**, 1174-1178.
306. S.-W. Chang, V. P. Chuang, S. T. Boles, C. A. Ross and C. V. Thompson, *Adv. Funct. Mater.*, 2009, **19**, 2495-2500.
307. J. Lu, D. Chamberlin, D. A. Rider, M. Liu, I. Manners and T. P. Russell, *Nanotechnology*, 2006, **17**, 5792-5797.
308. D. A. Rider, K. Liu, J.-C. Eloi, L. Vanderark, L. Yang, J.-Y. Wang, D. Grozea, Z.-H. Lu, T. P. Russell and I. Manners, *ACS Nano*, 2008, **2**, 263-270.
309. S. Y. Kim, J. Gwyther, I. Manners, P. M. Chaikin and R. A. Register, *Adv. Mater.*, 2014, **26**, 791-795.

310. S. Y. Kim, A. Nunns, J. Gwyther, R. L. Davis, I. Manners, P. M. Chaikin and R. A. Register, *Nano Lett.*, 2014, **14**, 5698-5705.
311. W. I. Park, J. M. Kim, J. W. Jeong, Y. H. Hur, Y. J. Choi, S.-H. Kwon, S. Hong, Y. Yin, Y. S. Jung and K. H. Kim, *Chem. Mater.*, 2015, **27**, 2673-2677.
312. H. K. Choi, J. Gwyther, I. Manners and C. A. Ross, *ACS Nano*, 2012, **6**, 8342-8348.
313. H. K. Choi, N. M. Aimon, D. H. Kim, X. Y. Sun, J. Gwyther, I. Manners and C. A. Ross, *ACS Nano*, 2014, **8**, 9248-9254.
314. K. Aissou, A. Nunns, I. Manners and C. A. Ross, *Small*, 2013, **9**, 4077-4084.
315. H. K. Choi, A. Nunns, X. Y. Sun, I. Manners and C. A. Ross, *Adv. Mater.*, 2014, **26**, 2474-2479.
316. R. Ahmed, A. Priimagi, C. F. Faul and I. Manners, *Adv. Mater.*, 2012, **24**, 926-931.
317. J.-C. Eloi, S. E. W. Jones, V. Poór, M. Okuda, J. Gwyther and W. Schwarzacher, *Adv. Funct. Mater.*, 2012, **22**, 3273-3278.
318. I. W. Hamley, *Block Copolymers in Solution: Fundamentals and Applications*, John Wiley & Sons, Ltd., Chichester, 2005.
319. J. Qian, M. Zhang, I. Manners and M. A. Winnik, *Trends Biotechnol.*, 2010, **28**, 84-92.
320. R. C. Hayward and D. J. Pochan, *Macromolecules*, 2010, **43**, 3577-3584.
321. J. C. Eloi, D. A. Rider, G. Cambridge, G. R. Whittell, M. A. Winnik and I. Manners, *J. Am. Chem. Soc.*, 2011, **133**, 8903-8913.
322. K. N. Power-Billard, R. J. Spontak and I. Manners, *Angew. Chem., Int. Ed.*, 2004, **43**, 1260-1264.
323. X. Wang, G. Guerin, H. Wang, Y. Wang, I. Manners and M. A. Winnik, *Science*, 2007, **317**, 644-647.
324. J. B. Gilroy, T. Gadt, G. R. Whittell, L. Chabanne, J. M. Mitchels, R. M. Richardson, M. A. Winnik and I. Manners, *Nature Chem.*, 2010, **2**, 566-570.
325. J. Massey, K. N. Power, I. Manners and M. A. Winnik, *J. Am. Chem. Soc.*, 1998, **120**, 9533-9540.
326. J. Raez, I. Manners and M. A. Winnik, *J. Am. Chem. Soc.*, 2002, **124**, 10381-10395.
327. D. J. Frankowski, J. Raez, I. Manners, M. A. Winnik, S. A. Khan and R. J. Spontak, *Langmuir*, 2004, **20**, 9304-9314.
328. X. Wang, H. Wang, D. J. Frankowski, P. G. Lam, P. M. Welch, M. A. Winnik, J. Hartmann, I. Manners and R. J. Spontak, *Adv. Mater.*, 2007, **19**, 2279-2285.
329. J. Raez, I. Manners and M. A. Winnik, *Langmuir*, 2002, **18**, 7229-7239.
330. I. Korczagin, M. A. Hempenius, R. G. Fokkink, M. A. Cohen Stuart, M. Al-Hussein, P. H. H. Bomans, P. M. Frederik and G. J. Vancso, *Macromolecules*, 2006, **39**, 2306-2315.
331. J. B. Gilroy, P. A. Rupar, G. R. Whittell, L. Chabanne, N. J. Terrill, M. A. Winnik, I. Manners and R. M. Richardson, *J. Am. Chem. Soc.*, 2011, **133**, 17056-17062.
332. P. Cai, C. Wang, J. Ye, Z. Xie and C. Wu, *Macromolecules*, 2004, **37**, 3438-3443.
333. T. Chen, L. Wang, G. Jiang, J. Wang, J. Wang and J. Zhou, *Polymer*, 2005, **46**, 5773-5777.
334. D. A. Rider, M. A. Winnik and I. Manners, *Chem. Commun.*, 2007, 4483-4485.
335. L. Shen, H. Wang, G. Guerin, C. Wu, I. Manners and M. A. Winnik, *Macromolecules*, 2008, **41**, 4380-4389.
336. M.-S. Hsiao, S. F. M. Yusoff, M. A. Winnik and I. Manners, *Macromolecules*, 2014, **47**, 2361-2372.
337. B. V. K. J. Schmidt, J. Elbert, D. Scheid, C. J. Hawker, D. Klinger and M. Gallei, *ACS Macro Lett.*, 2015, **4**, 731-735.

338. J. F. Gohy, B. G. Lohmeijer, A. Alexeev, X. S. Wang, I. Manners, M. A. Winnik and U. S. Schubert, *Chem. Eur. J.*, 2004, **10**, 4315-4323.
339. X. Wang, M. A. Winnik and I. Manners, *Macromolecules*, 2005, **38**, 1928-1935.
340. K. B. Thurmond, T. Kowalewski and K. L. Wooley, *J. Am. Chem. Soc.*, 1996, **118**, 7239-7240.
341. K. B. Thurmond, T. Kowalewski and K. L. Wooley, *J. Am. Chem. Soc.*, 1997, **119**, 6656-6665.
342. V. Bütün, A. B. Lowe, N. C. Billingham and S. P. Armes, *J. Am. Chem. Soc.*, 1999, **121**, 4288-4289.
343. X.-S. Wang, A. Arsenault, G. A. Ozin, M. A. Winnik and I. Manners, *J. Am. Chem. Soc.*, 2003, **125**, 12686-12687.
344. X.-S. Wang, H. Wang, N. Coombs, M. A. Winnik and I. Manners, *J. Am. Chem. Soc.*, 2005, **127**, 8924-8925.
345. X. Wang, K. Liu, A. C. Arsenault, D. A. Rider, G. A. Ozin, M. A. Winnik and I. Manners, *J. Am. Chem. Soc.*, 2007, **129**, 5630-5639.
346. H. Wang, X. Wang, M. A. Winnik and I. Manners, *J. Am. Chem. Soc.*, 2008, **130**, 12921-12930.
347. Z. M. Hudson, D. J. Lunn, M. A. Winnik and I. Manners, *Nat. Commun.*, 2014, **5**, 3372.
348. P. A. Rupar, G. Cambridge, M. A. Winnik and I. Manners, *J. Am. Chem. Soc.*, 2011, **133**, 16947-16957.
349. S. F. Mohd Yusoff, J. B. Gilroy, G. Cambridge, M. A. Winnik and I. Manners, *J. Am. Chem. Soc.*, 2011, **133**, 11220-11230.
350. J. Qian, G. Guerin, G. Cambridge, I. Manners and M. A. Winnik, *Macromol. Rapid Commun.*, 2010, **31**, 928-933.
351. J. Qian, G. Guerin, Y. Lu, G. Cambridge, I. Manners and M. A. Winnik, *Angew. Chem., Int. Ed.*, 2011, **50**, 1622-1625.
352. J. Qian, Y. Lu, G. Cambridge, G. Guerin, I. Manners and M. A. Winnik, *Macromolecules*, 2012, **45**, 8363-8372.
353. J. Qian, Y. Lu, A. Chia, M. Zhang, P. A. Rupar, N. Gunari, G. C. Walker, G. Cambridge, F. He, G. Guerin, I. Manners and M. A. Winnik, *ACS Nano*, 2013, **7**, 3754-3766.
354. H. Qiu, Y. Gao, V. A. Du, R. Harniman, M. A. Winnik and I. Manners, *J. Am. Chem. Soc.*, 2015, **137**, 2375-2385.
355. H. Wang, W. Lin, K. P. Fritz, G. D. Scholes, M. A. Winnik and I. Manners, *J. Am. Chem. Soc.*, 2007, **129**, 12924-12925.
356. T. Gädt, N. S. Ieong, G. Cambridge, M. A. Winnik and I. Manners, *Nature Mater.*, 2009, **8**, 144-150.
357. H. Qiu, G. Cambridge, M. A. Winnik and I. Manners, *J. Am. Chem. Soc.*, 2013, **135**, 12180-12183.
358. J. C. Wittmann and B. Lotz, *J. Polym. Sci., Polym. Phys.*, 1981, **19**, 1837-1851.
359. J. C. Wittmann, A. M. Hodge and B. Lotz, *J. Polym. Sci., Polym. Phys.*, 1983, **21**, 2495-2509.
360. T. J. Peckham, J. A. Massey, M. Edwards, I. Manners and D. A. Foucher, *Macromolecules*, 1996, **29**, 2396-2403.
361. F. He, T. Gadt, I. Manners and M. A. Winnik, *J. Am. Chem. Soc.*, 2011, **133**, 9095-9103.
362. H. Wang, A. J. Patil, K. Liu, S. Petrov, S. Mann, M. A. Winnik and I. Manners, *Adv. Mater.*, 2009, **21**, 1805-1808.

363. Y. Gao, H. Qiu, H. Zhou, X. Li, R. Harniman, M. A. Winnik and I. Manners, *J. Am. Chem. Soc.*, 2015, **137**, 2203-2206.
364. J. R. Finnegan, D. J. Lunn, O. E. Gould, Z. M. Hudson, G. R. Whittell, M. A. Winnik and I. Manners, *J. Am. Chem. Soc.*, 2014, **136**, 13835-13844.
365. Z. M. Hudson, J. Qian, C. E. Boott, M. A. Winnik and I. Manners, *ACS Macro Lett.*, 2015, **4**, 187-191.
366. H. Qiu, V. A. Du, M. A. Winnik and I. Manners, *J. Am. Chem. Soc.*, 2013, **135**, 17739-17742.
367. H. Zhou, Y. Lu, H. Qiu, G. Guerin, I. Manners and M. A. Winnik, *Macromolecules*, 2015, **48**, 2254-2262.
368. G. Cambridge, G. Guerin, I. Manners and M. A. Winnik, *Macromol. Rapid Commun.*, 2010, **31**, 934-938.
369. A. Nunns, G. R. Whittell, M. A. Winnik and I. Manners, *Macromolecules*, 2014, **47**, 8420-8428.
370. P. A. Rupar, L. Chabanne, M. A. Winnik and I. Manners, *Science*, 2012, **337**, 559-562.
371. Z. Nie, D. Fava, E. Kumacheva, S. Zou, G. C. Walker and M. Rubinstein, *Nature Mater.*, 2007, **6**, 609-614.
372. P. Y. Keng, B. Y. Kim, I.-B. Shim, R. Sahoo, P. E. Veneman, N. R. Armstrong, H. Yoo, J. E. Pemberton, M. M. Bull, J. J. Griebel, E. L. Ratcliff, K. G. Nebesny and J. Pyun, *ACS Nano*, 2009, **3**, 3143-3157.
373. Q. Chen, S. C. Bae and S. Granick, *Nature*, 2011, **469**, 381-384.
374. A. H. Gröschel, F. H. Schacher, H. Schmalz, O. V. Borisov, E. B. Zhulina, A. Walther and A. H. E. Müller, *Nat. Commun.*, 2012, **3**, 710.
375. Y. Wang, A. D. Hollingsworth, S. K. Yang, S. Patel, D. J. Pine and M. Weck, *J. Am. Chem. Soc.*, 2013, **135**, 14064-14067.
376. H. Cui, Z. Chen, S. Zhong, K. L. Wooley and D. J. Pochan, *Science*, 2007, **317**, 647-650.
377. H. Qiu, G. Russo, P. A. Rupar, L. Chabanne, M. A. Winnik and I. Manners, *Angew. Chem., Int. Ed.*, 2012, **51**, 11882-11885.
378. H. Qiu, Z. M. Hudson, M. A. Winnik and I. Manners, *Science*, 2015, **347**, 1329-1332.
379. O. E. Gould, H. Qiu, D. J. Lunn, J. Rowden, R. L. Harniman, Z. M. Hudson, M. A. Winnik, M. J. Miles and I. Manners, *Nat. Commun.*, 2015, **6**, 10009.
380. X. Li, Y. Gao, C. E. Boott, M. A. Winnik and I. Manners, *Nat. Commun.*, 2015, **6**, 8127.
381. S. F. Mohd Yusoff, M.-S. Hsiao, F. H. Schacher, M. A. Winnik and I. Manners, *Macromolecules*, 2012, **45**, 3883-3891.
382. A. P. Soto, J. B. Gilroy, M. A. Winnik and I. Manners, *Angew. Chem., Int. Ed.*, 2010, **49**, 8220-8223.
383. Z. M. Hudson, C. E. Boott, M. E. Robinson, P. A. Rupar, M. A. Winnik and I. Manners, *Nature Chem.*, 2014, **6**, 893-898.
384. G. Cambridge, M. J. Gonzalez-Alvarez, G. Guerin, I. Manners and M. A. Winnik, *Macromolecules*, 2015, **48**, 707-716.
385. H. Qiu, Y. Gao, C. E. Boott, O. E. C. Gould, R. L. Harniman, M. J. Miles, S. E. D. Webb, M. A. Winnik and I. Manners, *Science*, 2016, **352**, 697-701.
386. J. Ge, J. Lei and R. N. Zare, *Nature Nanotech.*, 2012, **7**, 428-432.
387. R. Shrestha, M. Elsabahy, H. Luehmann, S. Samarajeewa, S. Florez-Malaver, N. S. Lee, M. J. Welch, Y. Liu and K. L. Wooley, *J. Am. Chem. Soc.*, 2012, **134**, 17362-17365.

388. J. Zhu, S. Zhang, F. Zhang, K. L. Wooley and D. J. Pochan, *Adv. Funct. Mater.*, 2013, **23**, 1767-1773.
389. L. Jia, G. Zhao, W. Shi, N. Coombs, I. Gourevich, G. C. Walker, G. Guerin, I. Manners and M. A. Winnik, *Nat. Commun.*, 2014, **5**, 3882.
390. L. Jia, L. Tong, Y. Liang, A. Petretic, G. Guerin, I. Manners and M. A. Winnik, *J. Am. Chem. Soc.*, 2014, **136**, 16676-16682.
391. L. Jia, A. Petretic, G. Molev, G. Guerin, I. Manners and M. A. Winnik, *ACS Nano*, 2015, **9**, 10673-10685.
392. L. Cao, J. A. Massey, M. A. Winnik, I. Manners, S. Riethmüller, F. Banhart, J. P. Spatz and M. Möller, *Adv. Funct. Mater.*, 2003, **13**, 271-276.
393. K. T. Kim, C. Park, G. W. Vandermeulen, D. A. Rider, C. Kim, M. A. Winnik and I. Manners, *Angew. Chem., Int. Ed.*, 2005, **44**, 7964-7968.
394. J. Lee, H. Ahn, I. Choi, M. Boese and M. J. Park, *Macromolecules*, 2012, **45**, 3121-3128.
395. J. Schmelz, A. E. Schedl, C. Steinlein, I. Manners and H. Schmalz, *J. Am. Chem. Soc.*, 2012, **134**, 14217-14225.
396. J. Qian, X. Li, D. J. Lunn, J. Gwyther, Z. M. Hudson, E. Kynaston, P. A. Rupar, M. A. Winnik and I. Manners, *J. Am. Chem. Soc.*, 2014, **136**, 4121-4124.
397. L. Sun, A. Pitto-Barry, N. Kirby, T. L. Schiller, A. M. Sanchez, M. A. Dyson, J. Sloan, N. R. Wilson, R. K. O'Reilly and A. P. Dove, *Nat. Commun.*, 2014, **5**, 5746.
398. Y. Ni, I. Manners, J. B. Sheridan and R. T. Oakley, *J. Chem. Ed.*, 1998, **75**, 766.
399. C. H. Honeyman, D. A. Foucher, F. Y. Dahmen, R. Rulkens, A. J. Lough and I. Manners, *Organometallics*, 1995, **14**, 5503-5512.
400. M. Tamm, A. Kunst, T. Bannenberg, E. Herdtweck, P. Sirsch, C. J. Elsevier and J. M. Ernsting, *Angew. Chem., Int. Ed.*, 2004, **43**, 5530-5534.
401. U. F. J. Mayer, J. B. Gilroy, D. O'Hare and I. Manners, *J. Am. Chem. Soc.*, 2009, **131**, 10382-10383.
402. H. Braunschweig and T. Kupfer, *Acc. Chem. Res.*, 2010, **43**, 455-465.
403. S. Baljak, A. D. Russell, S. C. Binding, M. F. Haddow, D. O'Hare and I. Manners, *J. Am. Chem. Soc.*, 2014, **136**, 5864-5867.
404. H. Bhattacharjee and J. Müller, *Coord. Chem. Rev.*, 2016, **314**, 114-133.
405. D. E. Herbert, U. F. J. Mayer and I. Manners, *Angew. Chem., Int. Ed.*, 2007, **46**, 5060-5081.
406. M. Gallei, *Macromol. Chem. Phys.*, 2014, **215**, 699-704.
407. A. Alkan, L. Thomi, T. Gleede and F. R. Wurm, *Polym. Chem.*, 2015, **6**, 3617-3624.
408. Y. Yan, P. Pageni, M. P. Kabir and C. Tang, *Synlett*, 2016, **27**, 984-1005.

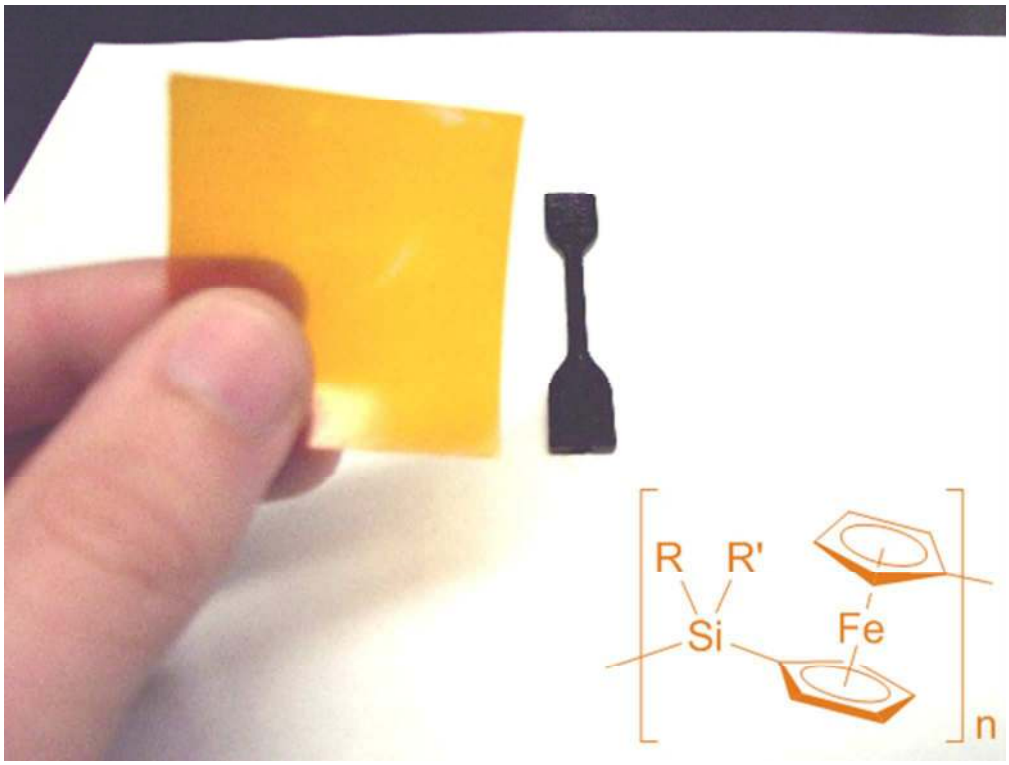
R
R'
Si
Fe
n

This comprehensive review covers polyferrocenylsilanes (PFSs), a well-established, readily accessible class of main chain organosilicon metallopolymer. The focus in on the recent advances involving PFS homopolymers and block copolymers and the article covers the synthesis, properties, and applications of these fascinating materials.